Gallagher, S.J., Fulthorpe, C.S., Bogus, K., and the Expedition 356 Scientists
Proceedings of the International Ocean Discovery Program Volume 356
publications.iodp.org

doi:10.14379/iodp.proc.356.104.2017

Site U1459[1]

S.J. Gallagher, C.S. Fulthorpe, K. Bogus, G. Auer, S. Baranwal, I.S. Castañeda, B.A. Christensen, D. De Vleeschouwer, D.R. Franco, J. Groeneveld, M. Gurnis, C. Haller, Y. He, J. Henderiks, T. Himmler, T. Ishiwa, H. Iwatani, R.S. Jatiningrum, M.A. Kominz, C.A. Korpanty, E.Y. Lee, E. Levin, B.L. Mamo, H.V. McGregor, C.M. McHugh, B.F. Petrick, D.C. Potts, A. Rastegar Lari, W. Renema, L. Reuning, H. Takayanagi, and W. Zhang[2]

Keywords: International Ocean Discovery Program, IODP, Expedition 356, *JOIDES Resolution*, Site U1459, Perth Basin, Indonesian Throughflow, Eocene, Oligocene, Miocene, Pliocene, Pleistocene, Leeuwin Current, West Australian Current, subsidence, Australian winter-dominated rainfall regime, Houtman-Abrolhos Reef, subtropical carbonates

Contents

Background and objectives

International Ocean Discovery Program (IODP) Site U1459 lies in the northern part of the Perth Basin, about 1 nmi seaward of Site U1458 and the Houtman-1 industry well on the northern Rottnest shelf (James et al., 1999; Collins et al., 2014). Site U1459 was originally intended as an alternate to IODP Site U1458. The ship moved to Site U1459 after having difficulty coring the uppermost sediments at Site U1458. Like U1458, Site U1459 is directly seaward of and downdip from the Houtman Abrolhos main reef complex, which contains the most southerly tropical reefs in the Indian Ocean. Sites U1458 and U1459 represent the southernmost sites of our latitudinal transect (Figures **F1**, **F2**, **F3**).

The objectives for Site U1459 were the same as those for Site U1458. The evolution of the Houtman Abrolhos reef complex is directly related to the path of the Leeuwin Current. Dating of sediments cored at Site U1459, coupled with seismic correlation, will provide insight into the pre-Quaternary history of these reefs and a long-term perspective on Leeuwin Current evolution at the tropical/subtropical boundary off Western Australia. In addition, it has been suggested that subsidence rates over the last 140 ky were low compared to those of the Carnarvon Basin reefs (Collins and Testa, 2010). Subsidence analyses of the shelf wedge drilled at this site will extend this record and allow more precise modeling of dynamic subsidence along the western margin of Australia. An additional objective was to use any finer grained facies in this section to yield a Pliocene–Pleistocene record of the onset and variability of the southern Australian winter-dominated rainfall regime.

Operations

Transit to Site U1459

After a 1.25 h (1 nmi; average speed = 0.8 kt) transit in dynamic positioning mode from Site U1458, the vessel arrived at Site U1459 at 1540 h on 5 August 2015. The vessel was offset 75 m to the west of the site coordinates and an acoustic beacon was deployed (1553 h on 5 August). After offsetting the vessel from the beacon, drill floor activities commenced.

Site U1459

Site U1459 consisted of three holes (Tables **T1**, **T2**). The original plan called for three advanced piston corer (APC) holes to refusal with the last two holes being extended by the extended core barrel (XCB) system to 330 meters below seafloor. It became immediately apparent in Hole U1459A that the APC system would not penetrate the surface formation. After breaking the first APC core barrel, the half-length APC (HLAPC) core barrel was run and recovered 0.1 m of core. Fourteen cores were subsequently recovered from Hole U1459A using both the HLAPC and XCB systems (70.3 m cored with 30.59 m recovered). The first hole was challenging, with multiple hard layers interspersed through the upper 55 m, and resulted in 44% overall recovery for the entire hole. After a stuck core barrel forced the abandonment of Hole U1459A at 70.3 m drilling depth below seafloor (DSF), a detailed coring plan for Hole U1459B was developed using information gained from Hole U1459A. The alternating use of the HLAPC (for soft intervals) and XCB (for harder intervals) systems in Hole U1459B greatly increased core recovery

[1] Gallagher, S.J., Fulthorpe, C.S., Bogus, K., Auer, G., Baranwal, S., Castañeda, I.S., Christensen, B.A., De Vleeschouwer, D., Franco, D.R., Groeneveld, J., Gurnis, M., Haller, C., He, Y., Henderiks, J., Himmler, T., Ishiwa, T., Iwatani, H., Jatiningrum, R.S., Kominz, M.A., Korpanty, C.A., Lee, E.Y., Levin, E., Mamo, B.L., McGregor, H.V., McHugh, C.M., Petrick, B.F., Potts, D.C., Rastegar Lari, A., Renema, W., Reuning, L., Takayanagi, H., and Zhang, W., 2017. Site U1459. *In* Gallagher, S.J., Fulthorpe, C.S., Bogus, K., and the Expedition 356 Scientists, *Indonesian Throughflow*. Proceedings of the International Ocean Discovery Program, 356: College Station, TX (International Ocean Discovery Program). http://dx.doi.org/10.14379/iodp.proc.356.104.2017

[2] **Expedition 356 Scientists' addresses.**

MS 356-104: Published 26 February 2017

Figure F1. Map of the northwest shelf showing major basins and location of modern and "fossil" reefs. Stars = Expedition 356 sites, green circles = Deep Sea Drilling Project/Ocean Drilling Program sites and other core locations referred to in text, yellow circles = industry well locations (Angel = Angel-1; G2/6/7 = Goodwyn-2, Goodwyn-6, Goodwyn-7; A1 = Austin-1; M/MN1 = Maitland/Maitland North-1; TR1 = West Tryal Rocks-1). WA = Western Australia, NT = Northern Territory, SA = South Australia, QLD = Queensland, NSW = New South Wales.

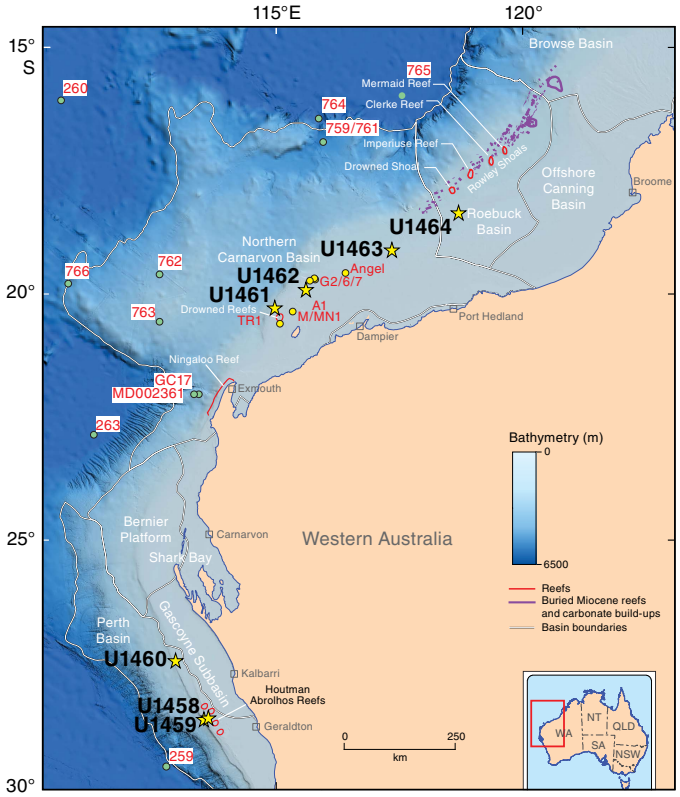

(78%). Deeper than ~55 m DSF, HLAPC coring encountered no resistance and continued to 218.9 m DSF. The third hole became necessary when the XCB system failed at 233.0 m DSF, destroying an XCB cutting shoe in the process. The drill string was recovered and a rotary core barrel (RCB) bottom-hole assembly (BHA) was assembled with a C-4 coring bit and a mechanical bit release. Hole U1459C was started and drilled without coring to 205.8 m DSF. The center bit was pulled and RCB coring began at 205.8 m DSF, terminating at 400.0 m DSF (194.2 m cored with 22.6 m recovered [11%]). Two separate logging tool runs were completed with the triple combination (combo) and Formation MicroScanner (FMS)-sonic.

The total time spent on Site U1459 was 6.9 days. Overall, 484 m were cored with 224.96 m recovered, resulting in a core recovery of 46.5% for Site U1459, which utilized the HLAPC, XCB, and RCB systems.

Hole U1459A

Hole U1459A (28°40.2606′S, 113°33.5376′E) began on 5 August 2015 with preparations for coring. A full-length nonmagnetic core barrel was picked up and run into the hole to spud Hole U1459A. On the first core barrel run to establish the mudline, the core barrel came back empty. The bit depth was repositioned, and the second core barrel made contact with the seafloor but failed at the center threaded connection. The HLAPC nonmagnetic core barrel was then prepared, the bit was lowered to tag the bottom, and a water depth of 192.3 meters below sea level (mbsl) was recorded. Hole

Figure F2. Bathymetric map showing the seafloor around Sites U1458 and U1459. Bathymetric data are derived from the Geoscience Australia Australian bathymetry and topography grid, June 2009. Positions of multichannel seismic profiles are shown. The Houtman Abrolhos reef complex is the most southerly reef system in the Indian Ocean. Red circles = locations of preexisting industry wells.

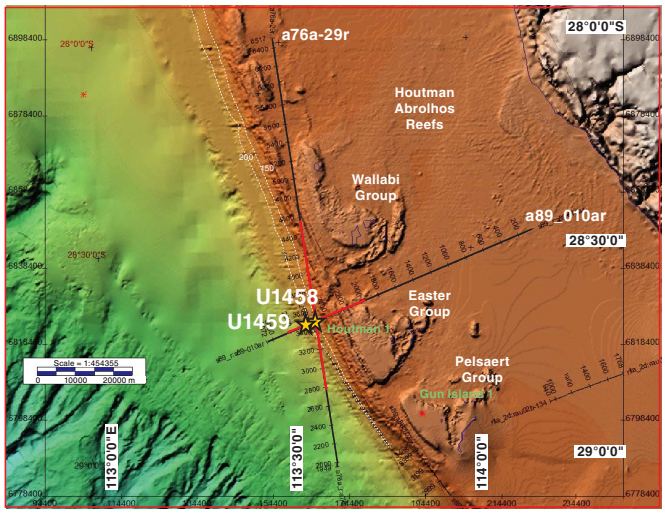

U1459A was started at 1920 h on 5 August. Only 0.01 m was recovered in Core 356-U1459A-1F. After determining that the seafloor was too firm for either the APC or HLAPC system, the XCB system was picked up and deployed. A 9.6 m interval was cored and recovered only 0.63 m of core in 120 rotating minutes (Core 2X). Unfortunately, in order to make a connection with poor hole conditions, the bit had to clear the seafloor. After redrilling and coring an additional 3.7 m to ~13.5 m DSF, hole conditions once again forced us to pull above the seafloor. Coring continued with the XCB system to 32.1 m DSF (Core 5X) with poor recovery (2%). An increased penetration rate indicated that the hard formation had given way to something amenable to the HLAPC. The HLAPC was picked up and Cores 6F and 7F recovered (103% and 10% recovery, respectively). While shooting Core 7F, another hard formation was encountered at 34.9 m DSF. The XCB core barrel was again deployed and advanced 2.5 m without recovery. With the change in penetration rate, the HLAPC was again deployed, recovering Cores 9F through 14F to 70.3 m DSF. The core barrel containing Core 14F became stuck in the BHA, and after attempting to free it for more than 1 h, the BHA was pulled to the rig floor to recover the core barrel. Hole U1459A ended at 2135 h on 6 August. The total time spent on Hole U1459A was 29.75 h.

Hole U1459B

After offsetting the vessel 20 m north of Hole U1459A, a coring plan was prepared for Hole U1459B (28°40.2519′S, 113°33.5375′E) based on the recovery and penetration rates from Hole U1459A. Hole U1459B was started at 0025 h on 7 August 2015. After drilling down 13.5 m, the center bit was pulled and an XCB core barrel was dropped. Core 356-U1459B-2X was cut to 22.5 m DSF. The HLAPC system was then deployed for three cores. The XCB system was again deployed at 34.8 m DSF to core (6X) through another hard layer. The HLAPC system was deployed and recovered three additional cores, after which the XCB was used to core to 55 m DSF and through the last known hard layer. HLAPC coring began again and recovered Cores 11F through 46F (average recovery = 97%) to 218.9 m DSF where HLAPC refusal was called. The XCB system

Figure F3. Multichannel seismic profile across Sites U1458 and U1459. Top of green shading = intended depth of penetration and is of Eocene age. SP = shotpoint.

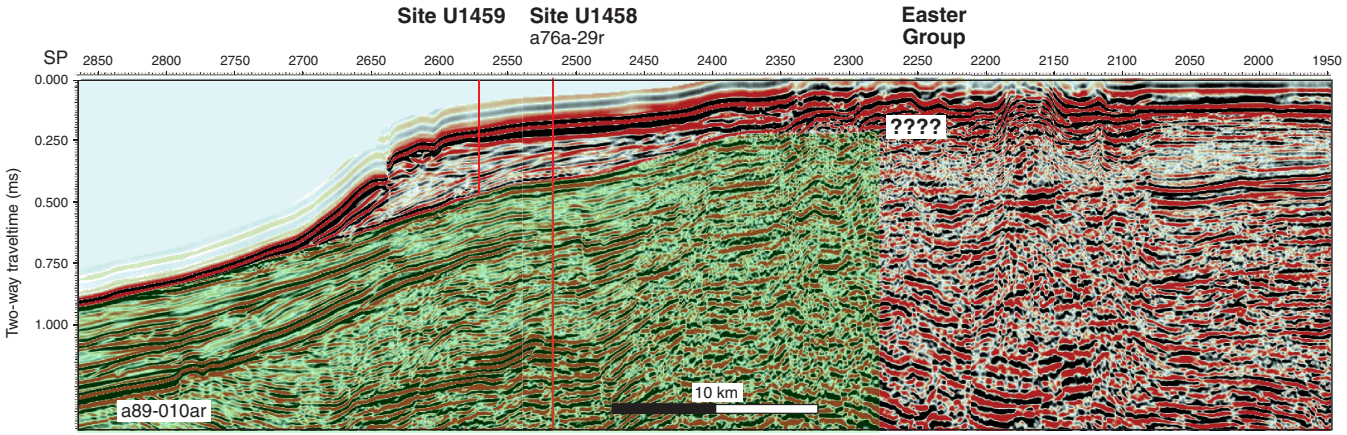

Table T1. Operations summary, Site U1459. mbsl = meters below sea level. **Download table in .csv format.**

Hole	Latitude	Longitude	Water depth (mbsl)	Penetration DSF (m)	Cored interval (m)	Recovered length (m)	Recovery (%)	Drilled interval (m)	Drilled interval (*N*)	Total cores (*N*)	APC cores (*N*)	HLAPC cores (*N*)	XCB cores (*N*)	RCB cores (*N*)	Time on hole (days)
U1459A	28°40.2606′S	113°33.5376′E	192.27	70.30	70.30	30.59	44		0	14	0	9	5	0	1.25
U1459B	28°40.2519′S	113°33.5375′E	192.32	233.00	219.50	171.77	78	13.50	1	49	0	42	7	0	1.8
U1459C	28°40.2398′S	113°33.5365′E	192.35	400.00	194.20	22.60	12	205.80	1	41	0	0	0	41	3.84
		Totals:		703.30	484.00	224.96		219.30	2	104	0	51	12	41	

Table T2. Site U1459 core summary. * = drilled interval. DSF = drilling depth below seafloor, CSF = core depth below seafloor. F = half-length advanced piston corer, X = extended core barrel, R = rotary core barrel, numeric core type = drilled interval. (Continued on next two pages.) **Download table in .csv format.**

Core	Top depth drilled DSF (m)	Bottom depth drilled DSF (m)	Advanced (m)	Recovered length (m)	Curated length (m)	Top depth cored CSF (m)	Bottom depth recovered CSF (m)	Recovery (%)	Date (2015)	Time on deck UTC (h)
356-U1459A-										
1F	0.00	0.10	0.1	0.10	0.10	0.00	0.10	100	5 Aug	1130
2X	0.10	9.70	9.6	0.63	0.63	0.10	0.73	7	5 Aug	1450
3X	9.70	13.40	3.7	0.00	0.00	9.70	9.70	0	5 Aug	2055
4X	13.40	22.40	9.0	0.56	0.56	13.40	13.96	6	5 Aug	2255
5X	22.40	32.10	9.7	0.10	0.10	22.40	22.50	1	6 Aug	0020
6F	32.10	34.90	2.8	2.89	2.89	32.10	34.99	103	6 Aug	0210
7F	34.90	39.60	4.7	0.46	0.46	34.90	35.36	10	6 Aug	0300
8X	39.60	42.10	2.5	0.00	0.00	39.60	39.60	0	6 Aug	0455
9F	42.10	46.80	4.7	4.41	4.41	42.10	46.51	94	6 Aug	5020
10F	46.80	51.50	4.7	4.67	4.67	46.80	51.47	99	6 Aug	0545
11F	51.50	56.20	4.7	2.46	2.46	51.50	53.96	52	6 Aug	0610
12F	56.20	60.90	4.7	4.52	4.52	56.20	60.72	96	6 Aug	0635
13F	60.90	65.60	4.7	4.64	4.64	60.90	65.54	99	6 Aug	0700
14F	65.60	70.30	4.7	5.15	5.15	65.60	70.75	110	6 Aug	1240
356-U1459B-										
11*			***** Drilled interval from 0.00 to 13.50 m DSF *****						6 Aug	2015
2X	13.50	22.50	9.0	0.24	0.24	13.50	13.74	3	6 Aug	2155
3F	22.50	27.20	4.7	4.55	4.55	22.50	27.05	97	6 Aug	2215
4F	27.20	31.90	4.7	4.40	4.40	27.20	31.60	94	7 Aug	0010
5F	31.90	34.80	2.9	2.95	2.95	31.90	34.85	102	7 Aug	0040
6X	34.80	40.00	5.2	0.04	0.04	34.80	34.84	1	7 Aug	0125
7F	40.00	44.70	4.7	4.36	4.36	40.00	44.36	93	7 Aug	0140
8F	44.70	49.40	4.7	4.52	4.52	44.70	49.22	96	7 Aug	0215
9F	49.40	53.50	4.1	3.96	3.96	49.40	53.36	97	7 Aug	0240
10X	53.50	55.00	1.5	0.07	0.07	53.50	53.57	5	7 Aug	0310
11F	55.00	59.70	4.7	4.36	4.36	55.00	59.36	93	7 Aug	0330
12F	59.70	64.40	4.7	4.55	4.55	59.70	64.25	97	7 Aug	0355
13F	64.40	69.10	4.7	4.50	4.50	64.40	68.90	96	7 Aug	0430
14F	69.10	73.80	4.7	4.51	4.51	69.10	73.61	96	7 Aug	0505
15F	73.80	78.50	4.7	4.59	4.59	73.80	78.39	98	7 Aug	0530
16F	78.50	83.20	4.7	4.70	4.70	78.50	83.20	100	7 Aug	0550

Table T2 (continued). (Continued on next page.)

Core	Top depth drilled DSF (m)	Bottom depth drilled DSF (m)	Advanced (m)	Recovered length (m)	Curated length (m)	Top depth cored CSF (m)	Bottom depth recovered CSF (m)	Recovery (%)	Date (2015)	Time on deck UTC (h)
17F	83.20	87.90	4.7	4.87	4.87	83.20	88.07	104	7 Aug	0605
18F	87.90	92.60	4.7	4.66	4.66	87.90	92.56	99	7 Aug	0625
19F	92.60	97.30	4.7	4.93	4.93	92.60	97.53	105	7 Aug	0640
20F	97.30	102.00	4.7	4.94	4.94	97.30	102.24	105	7 Aug	0700
21F	102.00	106.70	4.7	4.65	4.65	102.00	106.65	99	7 Aug	0725
22F	106.70	111.40	4.7	4.92	4.92	106.70	111.62	105	7 Aug	0820
23F	111.40	116.10	4.7	4.47	4.47	111.40	115.87	95	7 Aug	0845
24F	116.10	120.80	4.7	4.80	4.80	116.10	120.90	102	7 Aug	0910
25F	120.80	122.90	2.1	2.10	2.10	120.80	122.90	100	7 Aug	0930
26F	122.90	127.60	4.7	4.47	4.47	122.90	127.37	95	7 Aug	0950
27F	127.60	132.30	4.7	3.04	3.04	127.60	130.64	65	7 Aug	1035
28F	132.30	137.00	4.7	4.73	4.73	132.30	137.03	101	7 Aug	1100
29F	137.00	141.70	4.7	4.83	4.83	137.00	141.83	103	7 Aug	1135
30F	141.70	146.40	4.7	4.89	4.89	141.70	146.59	104	7 Aug	1200
31F	146.40	151.10	4.7	4.86	4.86	146.40	151.26	103	7 Aug	1225
32F	151.10	155.80	4.7	4.92	4.92	151.10	156.02	105	7 Aug	1240
33F	155.80	160.50	4.7	4.80	4.80	155.80	160.60	102	7 Aug	1300
34F	160.50	165.20	4.7	4.76	4.76	160.50	165.26	101	7 Aug	1330
35F	165.20	169.90	4.7	4.72	4.72	165.20	169.92	100	7 Aug	1355
36F	169.90	174.60	4.7	3.89	3.89	169.90	173.79	83	7 Aug	1415
37F	174.60	179.30	4.7	4.95	4.95	174.60	179.55	105	7 Aug	1435
38F	179.30	184.00	4.7	4.80	4.80	179.30	184.10	102	7 Aug	1455
39F	184.00	188.70	4.7	2.92	2.92	184.00	186.92	62	7 Aug	1535
40F	188.70	193.40	4.7	1.88	1.88	188.70	190.58	40	7 Aug	1555
41F	193.40	198.10	4.7	4.62	4.62	193.40	198.02	98	7 Aug	1750
42F	198.10	202.80	4.7	3.09	3.09	198.10	201.19	66	7 Aug	1810
43F	202.80	207.50	4.7	2.09	2.09	202.80	204.89	44	7 Aug	2000
44F	207.50	212.20	4.7	2.34	2.34	207.50	209.84	50	7 Aug	2045
45F	212.20	216.90	4.7	0.00	2.34	212.20	212.20	0	7 Aug	2115
46F	216.90	218.90	2.0	2.04	2.04	216.90	218.94	102	7 Aug	2255
47X	218.90	223.90	5.0	0.35	0.35	218.90	219.25	7	8 Aug	0015
48X	223.90	228.90	5.0	0.02	0.02	223.90	223.92	0	8 Aug	0100
49X	228.90	232.90	4.0	0.12	0.12	228.90	229.02	3	8 Aug	0140
50X	232.90	233.00	0.1		0.12	232.90	233.02		8 Aug	0300
356-U1459C-										
11*	0.00	205.80	205.8	2.65	2.65	0.00	2.65		9 Aug	0030
2R	205.80	210.30	4.5	0.66	0.66	205.80	206.46	15	9 Aug	0130
3R	210.30	214.80	4.5	0.41	0.41	210.30	210.71	9	9 Aug	0215
4R	214.80	219.60	4.8	1.05	1.05	214.80	215.85	22	9 Aug	0310
5R	219.60	224.40	4.8	0.53	0.53	219.60	220.13	11	10 Aug	0455
6R	224.40	229.20	4.8	0.05	0.05	224.40	224.45	1	10 Aug	0530
7R	229.20	234.00	4.8	0.10	0.10	229.20	229.30	2	10 Aug	0605
8R	234.00	238.80	4.8	0.18	0.18	234.00	234.18	4	10 Aug	0650
9R	238.80	243.60	4.8	0.05	0.05	238.80	238.85	1	10 Aug	0725
10R	243.60	248.40	4.8	0.25	0.25	243.60	243.85	5	10 Aug	0910
11R	248.40	253.20	4.8	1.03	1.03	248.40	249.43	21	10 Aug	0955
12R	253.20	258.00	4.8	0.73	0.73	253.20	253.93	15	10 Aug	1035
13R	258.00	262.80	4.8	0.35	0.35	258.00	258.35	7	10 Aug	1125
14R	262.80	267.60	4.8	2.47	2.47	262.80	265.27	51	10 Aug	1210
15R	267.60	272.40	4.8	1.46	1.46	267.60	269.06	30	10 Aug	1305
16R	272.40	277.20	4.8	1.44	1.44	272.40	273.84	30	10 Aug	1400
17R	277.20	282.00	4.8	1.42	1.42	277.20	278.62	30	10 Aug	1500
18R	282.00	286.80	4.8	1.28	1.28	282.00	283.28	27	10 Aug	1540
19R	286.80	291.60	4.8	0.30	0.30	286.80	287.10	6	10 Aug	1630
20R	291.60	296.40	4.8	1.54	1.54	291.60	293.14	32	10 Aug	1715
21R	296.40	301.20	4.8	0.08	0.08	296.40	296.48	2	10 Aug	1750
22R	301.20	306.00	4.8	0.12	0.12	301.20	301.32	3	10 Aug	1835
23R	306.00	310.80	4.8	0.22	0.22	306.00	306.22	5	10 Aug	1920
24R	310.80	315.60	4.8	0.17	0.17	310.80	310.97	4	10 Aug	2005
25R	315.60	320.40	4.8	0.04	0.04	315.60	315.64	1	10 Aug	2055
26R	320.40	325.20	4.8	0.79	0.79	320.40	321.19	16	10 Aug	2140
27R	325.20	330.00	4.8	0.53	0.53	325.20	325.73	11	10 Aug	2220
28R	330.00	334.80	4.8	0.40	0.40	330.00	330.40	8	10 Aug	2305
29R	334.80	339.60	4.8	0.93	0.93	334.80	335.73	19	10 Aug	2350
30R	339.60	344.40	4.8	0.18	0.18	339.60	339.78	4	11 Aug	0035
31R	344.40	349.20	4.8	0.17	0.17	344.40	344.57	4	11 Aug	0120

Table T2 (continued).

Core	Top depth drilled DSF (m)	Bottom depth drilled DSF (m)	Advanced (m)	Recovered length (m)	Curated length (m)	Top depth cored CSF (m)	Bottom depth recovered CSF (m)	Recovery (%)	Date (2015)	Time on deck UTC (h)
32R	349.20	354.00	4.8	0.49	0.49	349.20	349.69	10	11 Aug	0200
33R	354.00	358.80	4.8	0.21	0.21	354.00	354.21	4	11 Aug	0245
34R	358.80	363.60	4.8	0.24	0.24	358.80	359.04	5	11 Aug	0330
35R	363.60	368.40	4.8	0.32	0.32	363.60	363.92	7	11 Aug	0410
36R	368.40	373.20	4.8	0.36	0.36	368.40	368.76	8	11 Aug	0450
37R	373.20	378.00	4.8	0.46	0.46	373.20	373.66	10	11 Aug	0535
38R	378.00	382.80	4.8	0.17	0.17	378.00	378.17	4	11 Aug	0615
39R	382.80	387.60	4.8	0.20	0.20	382.80	383.00	4	11 Aug	0655
40R	387.60	392.40	4.8	0.39	0.39	387.60	387.99	8	11 Aug	0735
41R	392.40	397.20	4.8	0.31	0.31	392.40	392.71	6	11 Aug	0820
42R	397.20	400.00	2.8	0.52	0.52	397.20	397.72	19	11 Aug	0920

was deployed, and coring continued through to Core 50X. After trying to advance with Core 50X for 1 h, the core barrel was pulled and the XCB cutting shoe was determined to have reached refusal depth. Hole U1459B was completed at a final depth of 233.0 m DSF. The drill string was recovered with the top drive still installed and cleared the seafloor at 1345 h on 8 August. Hole U1459B ended at 1640 h. The total time spent on Hole U1459B was 43.25 h. Overall, 219.5 m was cored and 171.77 m recovered (78.3%); however, 189.7 m of this hole was cored with the HLAPC with 170.93 m recovered (90.1%), whereas the XCB system cored 29.8 m with 0.84 m recovered (2.8%).

Hole U1459C

After offsetting the vessel 20 m north of Hole U1459B, preparations were made for RCB coring. A drilling/coring plan was prepared for Hole U1459C based on the total depth of Hole U1459B and the recovery toward the end of the hole with the APC/XCB system. Hole U1459C (28°40.2398′S, 113°33.5365′E) was started at 2225 h on 8 August 2015. After a 205.8 m drilled interval, the center bit was pulled. Two sections (~300 cm) of material were found in the core liner and curated (as Core 356-U1459C-11) with the drilled interval. RCB coring began with Core 2R and continued through Core 4R to 219.6 m DSF. A nonmagnetic core barrel was dropped, but the increasing amplitude of the ship's heave made it difficult to keep the bit on the bottom for coring. Coring was suspended with the vessel heave increasing to >4 m. The bit was pulled up off the bottom to 212 m DSF while the driller maintained circulation and rotation and worked the pipe up and down. At 1515 h on 9 August, the torque began increasing and rotation stopped. After working the stuck pipe for almost 1 h with circulation, rotation, and overpull, the pipe came free. In order to avoid a possible repeat of this event, the drill string was pulled back to 115.5 m DSF and the driller continued to circulate, rotate, and work the pipe up and down. Heave continued to increase, peaking at ~5.8 m before gradually diminishing over the next 12 h. The following day (10 August), heave had reduced to the point where it was possible to pull the empty core barrel back to the surface. A center bit was dropped and the hole was washed back to the bottom without difficulty. With good hole conditions, a mud sweep was pumped to clean the hole, the center bit was retrieved, and a core barrel was dropped. Coring resumed at 1215 h on 10 August with recovery of Core 5R from 219.6 m DSF. Coring continued for another 3.25 h, when the drill string became stuck again. After 1.25 h of working the stuck drill pipe, it came free and coring resumed. Cores 6R through 42R were recovered to a final depth of 400.0 m DSF at ~1730 h on 11 August. In total, 194.2 m was cored with 22.6 m recovered (11.6%).

High-viscosity mud was circulated to clean the hole of cuttings. The hole was displaced with 120 barrels of +11 lb/gal mud. The drill string was pulled up to logging depth (72.2 m DSF), and the logging tool strings were rigged up at 2330 h on 11 August. The first tool string contained the following: magnetic susceptibility sonde (MSS), Hostile Environment Natural Gamma Ray Sonde (HNGS) (caliper only, no source), Hostile Environment Litho-Density Tool (HLDT), Enhanced Digital Telemetry Cartridge (EDTC), and logging equipment head-q tension (LEH-QT). The tools were assembled, tested, and run into the hole at 0030 h on 12 August. After the tool string exited the drill pipe, the active heave compensator was turned on. The initialization of the unit normally shocks the wireline system slightly, but because of the shallow water and the shortness of the logging string, the fluctuation in the wireline tension was excessive and resulted in the wireline coming off the sheaves of the compensator. The logging tool string was hung off with a T-bar while the wireline was put back into the sheaves and tested. The compensator software was modified slightly to be less reactive to the high heave conditions. A downlog was performed from just above the seafloor to the full hole depth of 389.0 m wireline log depth below seafloor (WSF). The hole was logged up with the triple combo tool string to 278 m WSF. A second uplog was made from 389.0 to ~139 m WSF. There was a problem with the caliper on the second pass that caused the arm to stick at ~10 inches (bit size). Eventually, it was powered up and a third pass was made from ~317 m WSF with a better caliper response. The second and third passes were spliced together into a complete log. The tools were pulled from the hole and were at the surface at 0445 h. The FMS-sonic logging tool string was then assembled with the following tools: FMS, Dipole Sonic Imager (DSI), HNGS, EDTC, and LEH-QT. At 0630 h, the tool string was lowered without difficulty through the drill pipe and to ~180 mbsl (just above the seafloor). The logging tools were turned on and the hole was logged down to 300 m WSF. After trying unsuccessfully to make it past an apparent bridge, the hole was logged upward. The calipers for the FMS tool were opened at 287 m WSF, and the hole was logged up to just below the end of pipe. The tool string was lowered back to the bottom of the hole, where infill was present to 292 m WSF. A second pass was made over the total length of the open hole. The tool string was pulled back into the drill pipe and logging continued to the seafloor. The tool string was pulled back to the surface and rigged down by 1030 h on 12 August, successfully completing logging operations.

The drill string was pulled from the hole, the thrusters and hydrophones were pulled and secured, and Site U1459 ended at 1254 h on 12 August. The total time spent on Hole U1459C was 92.25 h.

Lithostratigraphy

Lithostratigraphic units and their boundaries are defined by changes in lithology (using visual core description and smear slide observations), physical properties, color reflectance (L*, a*, and b*), X-ray diffraction (XRD), X-ray fluorescence (XRF), and petrographic thin section analyses. Site U1459 consists of seven lithostratigraphic units (Table **T3**; Figures **F4**, **F5**). The major lithologic differences between units are in texture, degree of lithification, fossil content, diagenetic changes, and mineralogical components. Unit boundaries are defined based on the first occurrence of a new lithology downhole. All smear slide samples are listed in Table **T4**, thin section samples are listed in Table **T5**, XRD samples are listed in Table **T6**, and XRF samples and bulk elemental concentrations are listed in Table **T7**.

The lithologic descriptions are based primarily on sediments recovered from Hole U1459B for 0–233.02 m core depth below seafloor (CSF-A) (i.e., to bottom of Hole U1459B), augmented with observations from Holes U1459A and U1459C. Descriptions for lithologic units deeper than 233.02 m CSF-A come exclusively from Hole U1459C.

Hole alignment

Holes U1459A and U1459B were aligned based on drilling depth and confirmed by the similar lithologies in the two holes. The top of Sample 356-U1459C-2R-1A, 0 cm, was aligned with Sample 356-U1459B-46F-1A, 105 cm, based on the presence of the same rock type at these depths. Although Sample 356-U1459C-2R-1A, 0 cm, must align with a location in Subunit Vb in Hole U1459B between Samples 356-U1459B-44F-3A, 55 cm, and 46F-1A, 105 cm, such correlation was not attempted for this interval because cores from Hole U1459B were disturbed by drilling or were not recovered.

Unit I

Intervals: 356-U1459A-2X-1A, 0 cm, through 6F-2A, 10 cm; 356-U1459B-2X-CC, 0 cm, through 3F-1A, 56 cm
Depths: Hole U1459A = 0–32.78 m CSF-A (32.78 m thick); Hole U1459B = 0–23.06 m CSF-A (23.06 m thick)
Age: recent–Middle Pleistocene
Lithology: lithified skeletal packstone to floatstone
Core quality: this unit is poorly represented because of low recovery of material in Holes U1459A and U1459B and is moderately to severely affected by drilling disturbances

Unit I is beige to greenish-gray skeletal packstone to floatstone (Figure **F4**) that is primarily present in Hole U1459A but also occurs in the uppermost parts of Hole U1459B. This unit is lithified at the top and becomes increasingly less lithified with depth. The bioclastic components comprise a diverse assemblage dominated by small and large benthic foraminifers, planktonic foraminifers, bryozoans, bivalves, and gastropods, with some molds of unidentified macrofossils (Figures **F5A**, **F6**). Glauconite is intermittently abundant and is most readily recognized macroscopically by the occurrence of green-colored intervals (Figure **F4**). Based on the abundance of skeletal material (Figure **F6**), especially macrofossils, and grain size, this unit is interpreted as a neritic facies.

Smear slides

One smear slide from Unit I in Hole U1459A shows micrite with rare nannofossils (Table **T4**; Figure **F5A**).

Thin sections

Four thin sections were prepared from well-lithified limestone intervals of Unit I (Table **T5**). The limestones have similar textures and compositions, consisting mainly of moderately to strongly bioturbated skeletal packstones with abundant planktonic (*Globigerina* spp. and *Orbulina* spp.) and benthic (*Cibicides* spp.) foraminifers, coralline red algae fragments (*Lithophyllum*?), bryozoa, echinoderms, and mollusks. Glauconite, phosphatized miliolid foraminifers, and finely disseminated pyrite framboids are common (Figure **F6**). Skeletal grains show intense bioerosion traces (borings). The primary porosity is low. Pores are coated with thin layers of microcrystalline and fibrous dogtooth cement. Brachiopods and bivalves are present as minor skeletal components.

XRD and XRF

No XRD or XRF analyses were performed for Unit I.

Table T3. Lithostratigraphic unit summary, Site U1459. **Download table in .csv format.**

Lith. unit	Hole U1459A				Hole U1459B				Hole U1459C			
	Core, section, interval (cm)		Depth CSF-A (m)		Core, section, interval (cm)		Depth CSF-A (m)		Core, section, interval (cm)		Depth CSF-A (m)	
	Top	Bottom	Top	Bottom	Top	Bottom	Top	Bottom	Top	Bottom	Top	Bottom
	356-U1459A-	356-U1459A-			356-U1459B-	356-U1459B-			356-U1459C-	356-U1459C-		
I	2X-1, 0	6F-2, 10	0.00	32.78	2X-CC, 0	3F-1, 56	0.00	23.06				
II	6F-2, 10	9F-1, 83	32.78	42.93	3F-1, 56	7F-1, 65	23.06	40.65				
III	9F-1, 83	14F-CC, 34	42.93	70.75	7F-1, 65	19F-3, 0	40.65	95.60				
IV					19F-3, 0	29F-2, 70	95.60	139.20				
Va					29F-2, 70	38F-3, 0	139.20	182.30				
Vb					38F-3, 0	50X-CC, 13	182.30	233.02	2R-1, 0	13R-1, 25	205.80	258.25
VI									13R-1, 25	21R-CC, 0	258.25	296.40
VII									21R-CC, 0	42R-CC, 52	296.40	397.72

Figure F4. Lithostratigraphic summary, Site U1459. Lithification, core image, graphic lithology, texture, lithostratigraphic units, age, structures and diagenesis, and facies show composite record from Holes U1459B and U1459C. See Figures **F6** and **F7** in the Expedition 356 methods chapter (Gallagher et al., 2017) for lithology, structure, diagenesis, and facies keys. b*, MSP, and NGR: red = Hole U1459A, black = Hole U1459B, blue = Hole U1459C. cps = counts per second. Age boundaries are based on biostratigraphy depths listed in Table **T8**.

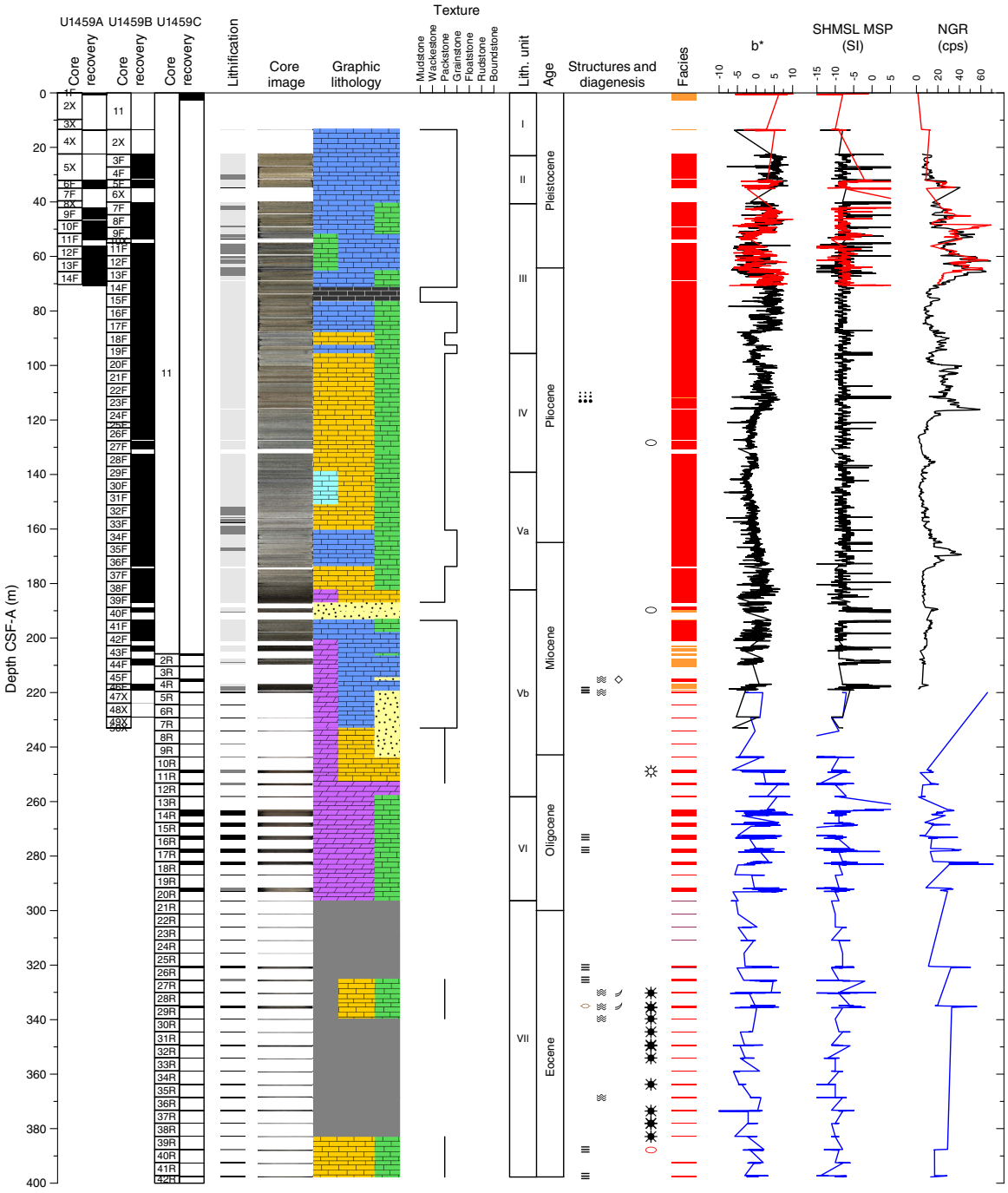

Unit II

Intervals: 356-U1459A-6F-2A, 10 cm, through 9F-1A, 83 cm; 356-U1459B-3F-1A, 56 cm, through 7F-1A, 65 cm
Depths: Hole U1459A = 32.78–42.93 m CSF-A (10.15 m thick); Hole U1459B = 23.06–40.65 m CSF-A (17.59 m thick)
Age: Middle Pleistocene–early Pleistocene

Lithology: unlithified mudstone to packstone with intercalated layers of skeletal grainstone
Core quality: drilling disturbance is moderate to very severe at the top of each core (both holes), with occasional suspected fall-in material (sand to gravel sized) and artificial grading (an artifact of the core recovery processes on the catwalk)

Figure F5. Smear slide summary, Site U1459. See Figure **F7** in the Expedition 356 methods chapter (Gallagher et al., 2017) for lithology key. A. Hole U1459A. (Continued on next two pages.)

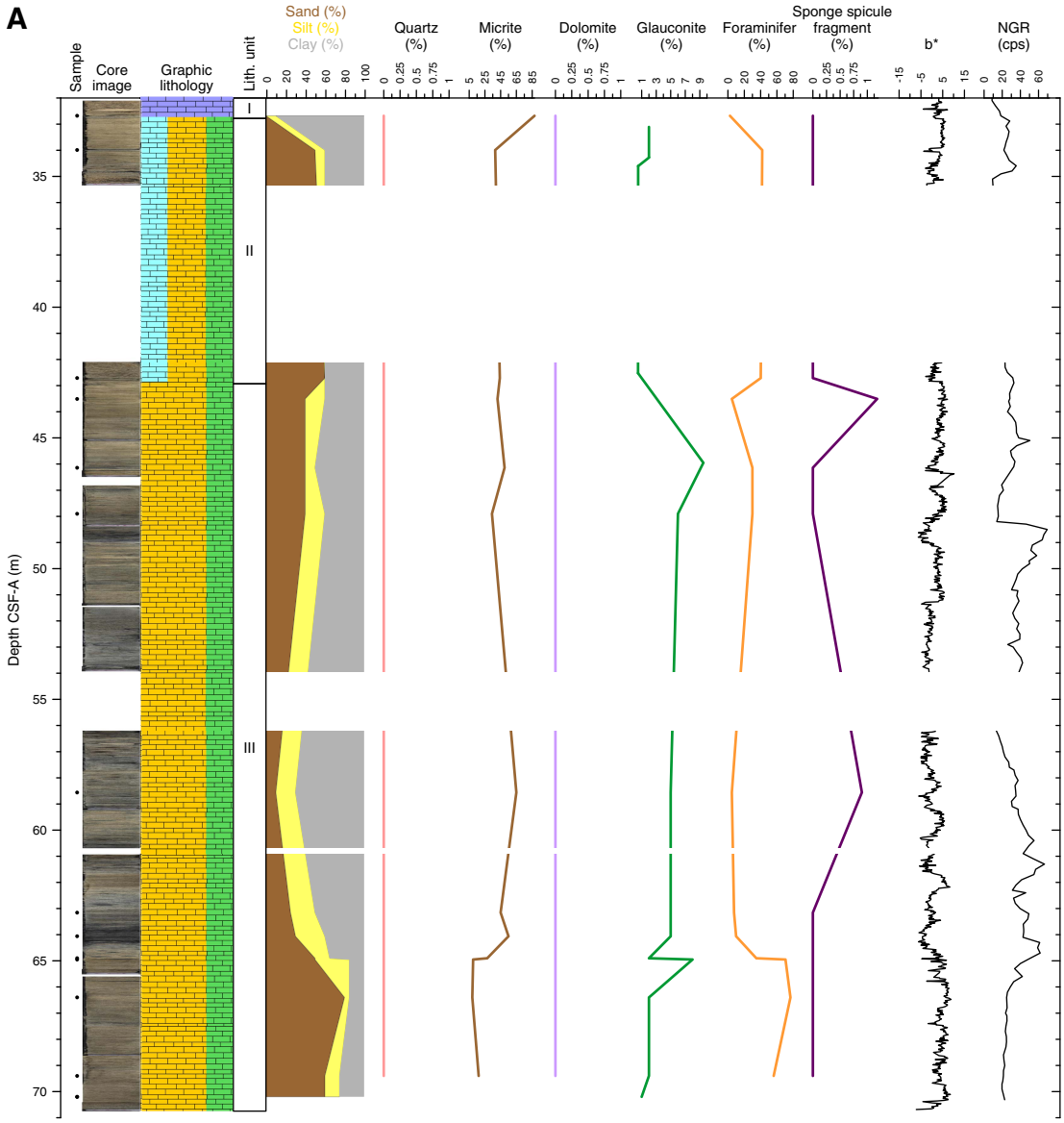

Unit II is beige to light greenish-gray mudstone to packstone with intermittent centimeter-scale layers of skeletal grainstone (Figure **F4**). This texture and the fact that Unit II is mostly unlithified distinguishes Unit II from Unit I. Unit II is present in both Holes U1459A and U1459B and is primarily unlithified with partially lithified sections in the lower half of Unit II in Hole U1459B. Identifiable macrofossils are less abundant in the finer grained sediments, but where present, they include bivalves, gastropods, bryozoans, and scaphopods. Small benthic foraminifers (particularly in the top of Unit II in Hole U1459A) and sponge spicules are abundant in the finer grained intervals (Figure **F5**). Bioclastic components in the skeletal packstones are dominated by small benthic foraminifers, bivalves, bryozoans, and sponge spicules with lesser amounts of echinoderm and gastropod fragments. Glauconite content is variable throughout Unit II but is relatively low compared to other units described from Site U1459 (Figures **F4**, **F5**). The stratigraphic variability of glauconite is recognized macroscopically by slight variations in sediment color (e.g., shades of green). Unit II is interpreted as a hemipelagic facies because of the higher abundance of finer grained material and finer scale bioclasts.

Smear slides

Sponge spicule–rich grainstones dominate smear slide samples near the upper part of Unit II (from Samples 356-U1459B-3F-1, 115 cm, through 4F-2, 60 cm; Figures **F5**, **F7**). Deeper than this interval, spicules are rare (Samples 356-U1459B-4F-2, 136 cm, through 5F-3, 36 cm). Smear slides show that the mudstones to packstones in the lower part of the unit are increasingly dominated by foraminifers, mollusk fragments, and bryozoans.

Thin sections

Two thin sections prepared from Unit II are moderately to strongly bioturbated skeletal packstones with abundant planktonic and benthic foraminifers, bryozoans, echinoderm fragments, and

Figure F5 (continued). B. Hole U1459B. (Continued on next page.)

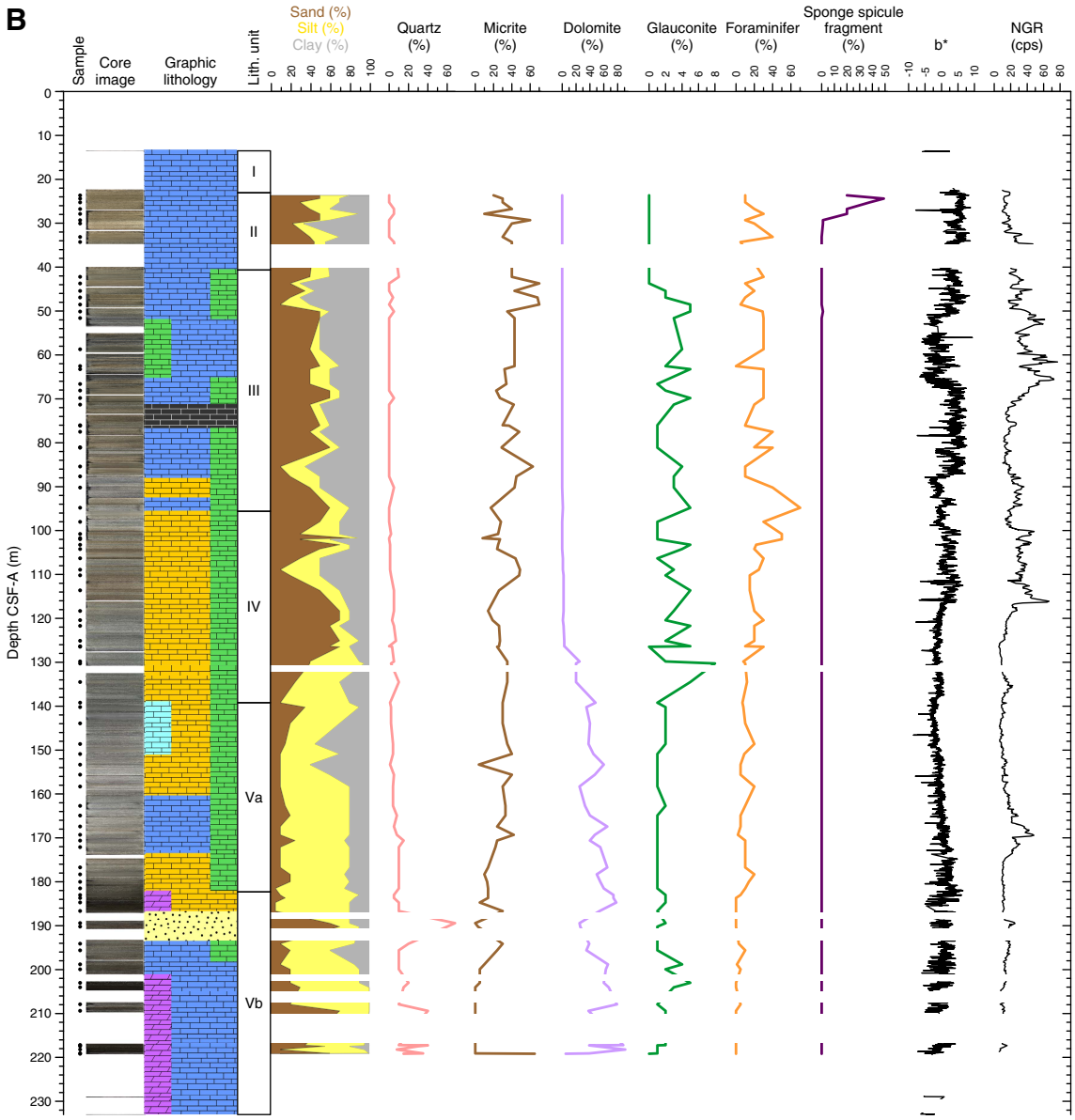

mollusks. The foraminifer tests are partly dissolved. Overall porosity is low, and pores are often filled with a thin layer of microcrystalline sparitic calcite cement (Figure **F8**).

XRD and XRF

Mineral composition of two XRD samples from Hole U1459B were analyzed semiquantitatively (Table **T6**). Low-Mg calcite is the dominant mineral phase, followed by quartz, aragonite, and dolomite. The dolomite is Ca rich with a $MgCO_3$ content of ~42.5 mol%.

There were no XRF measurements for this unit.

Unit III

Intervals: 356-U1459A-9F-1A, 83 cm, through 14F-CC, 34 cm (end of hole); 356-U1459B-7F-1A, 65 cm, through 19F-3A, 0 cm

Depths: Hole U1459A = 42.93–70.75 m CSF-A (end of hole; 27.82 m thick); Hole U1459B = 40.65–95.60 m CSF-A (54.95 m thick)

Age: early Pleistocene–late Pliocene

Lithology: glauconitized unlithified to partially lithified packstone to grainstone with macrofossils

Core quality: fill-in material in core tops but overall slight to moderate drilling disturbance

Unit III is defined by a marked increase in glauconite content compared to Unit II and is characterized by packstones to grainstones, alternating between light gray and greenish gray and containing various macrofossils (Figure **F4**). In both Holes U1459A and U1459B, Unit III is primarily unlithified with some partially lithified intervals near the middle of the unit. Macroscopic and microscopic (see below) analyses indicate bioclastic occurrences are similar in

Figure F5 (continued). C. Hole U1459C.

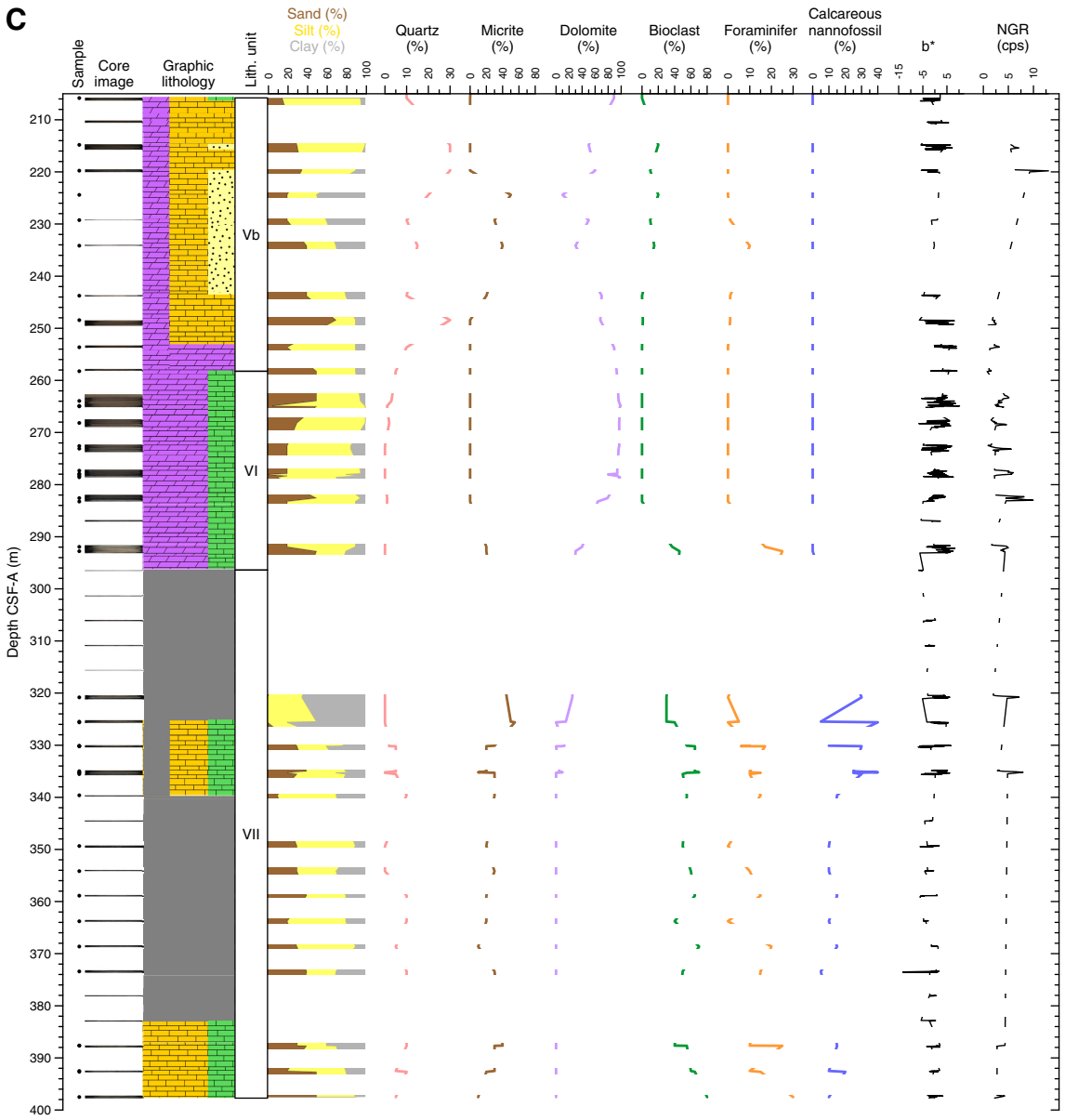

both the gray and green-gray intervals. Bioclasts are dominated by small benthic foraminifers, bivalves, echinoderms, bryozoans, and gastropods, with isolated occurrences of coralline algae, a brachiopod, a solitary coral, and serpulids. Glauconite is discernible macroscopically by color (green), and it occurs as scattered lenses and as glauconite-rich intervals. Particularly dark green (i.e., glauconite rich) intervals with sharp bases and more gradational upper parts are correlated with peaks in natural gamma radiation (NGR) and tend to be more lithified than intervals with less glauconite. The lower part of Unit III (interval 356-U1459A-14F-1, 40 cm, through 14F-CC, 34 cm) is more homogeneous, based on macroscopic analysis (color, composition, and constituents), NGR, and Section Half Multisensor Logger (SHMSL) color reflectance. The Unit III facies is hemipelagic, based on sediment composition, texture, and bioclastic components.

Smear slides

Unit III is rich in sand- and silt-sized foraminifers, with varying amounts of other bioclasts (mainly mollusk and bryozoan fragments, with rare sponge spicules) (Figure **F5A**). Micrite and loose glauconite grains are present in smear slides throughout the unit, and foraminiferal tests are often glauconitized (Figure **F7**).

Thin sections

Five thin sections were prepared from well-lithified limestones within Unit III. In general, the limestones are foraminifer-rich packstones with abundant mollusks and echinoderm fragments (Figure **F9**). Silt-sized glauconite and quartz grains are present. Foraminifers are generally medium sand sized and occasionally have geopetal infills. Microsparitic cement is present throughout the unit. Porosity is moderate and mostly moldic.

Table T4. Site U1459 smear slide samples. **Download table in .csv format.**

Lith. unit	Core, section, interval (cm)	Top depth CSF-A (m)
	356-U1459A-	
I	6F-2A, 5	32.73
II	6F-3A, 4	34.03
II	9F-1A, 141	43.51
II	9F-1W, 61	42.71
III	9F-3W, 104	46.14
III	10F-1W, 110	47.90
III	12F-2W, 86	58.56
III	13F-2W, 76	63.155
III	13F-3W, 16	64.22
III	13F-3W, 100	65.06
III	13F-3W, 105	65.11
III	14F-1W, 80	66.40
III	14F-3W, 80	69.40
	356-U1459B-	
II	3F-1W, 115	23.65
II	3F-2W, 40	24.40
II	3F-2W, 124	25.24
II	3F-3W, 125	26.75
II	4F-1W, 67	27.87
II	4F-2W, 60	29.30
II	4F-2W, 136	30.06
II	5F-2W, 71	33.13
II	5F-3W, 36	34.28
III	7F-2W, 71	42.21
III	7F-3W, 71	43.71
III	8F-1W, 71	45.41
III	8F-2W, 71	46.91
III	8F-3W, 80	48.51
III	9F-1W, 71	50.11
III	9F-2W, 71	51.61
III	11F-3W, 71	58.71
III	12F-2W, 134	62.54
III	12F-3W, 54	63.24
III	13F-2W, 71	66.61
III	13F-3W, 71	68.11
III	14F-1W, 71	69.81
III	14F-2W, 71	71.31
III	15F-2W, 71	76.01
III	15F-2W, 81	76.11
III	15F-3W, 71	77.51
III	16F-2W, 102	81.02
III	16F-2W, 113	81.13
III	17F-2W, 71	85.41
III	17F-4W, 46	87.67
III	18F-2W, 80	90.20
III	19F-2W, 71	94.81
IV	20F-1W, 71	98.01
IV	20F-3W, 48	100.78
IV	20F-4W, 33	101.74
IV	20F-4W, 57	101.98
IV	21F-1W, 124	103.24
IV	21F-2W, 71	104.21
IV	21F-4W, 30	106.32
IV	22F-2W, 71	108.91
IV	22F-3W, 50	110.20
IV	23F-2W, 71	113.62
IV	24F-2W, 71	118.31
IV	24F-4W, 30	120.42
IV	25F-1W, 90	121.70
IV	26F-2W, 71	125.11
IV	26F-3W, 45	126.35
IV	26F-3W, 57	126.47
IV	27F-2W, 71	129.81
IV	27F-2W, 118	130.28
IV	28F-2W, 71	134.51
Va	29F-2W, 71	139.21
Va	29F-3W, 21	140.21
Va	30F-2W, 71	143.91
Va	31F-2W, 2	148.61
Va	31F-4W, 40	150.90
Va	32F-2W, 71	153.31
Va	32F-4W, 40	155.60
Va	33F-2W, 100	158.30
Va	34F-2W, 71	162.71
Va	34F-4W, 30	164.90
Va	35F-2W, 71	167.41
Va	35F-3W, 110	169.30
Va	36F-1W, 71	170.61
Va	36F-2W, 71	172.11
Va	37F-2W, 63	176.73
Va	37F-3W, 71	178.31
Va	38F-1W, 71	180.01
Va	38F-2W, 71	181.51
Vb	38F-3W, 71	183.01
Vb	38F-4W, 30	183.70
Vb	39F-1W, 71	184.71
Vb	39F-2W, 115	186.65
Vb	40F-1W, 71	189.41
Vb	40F-2W, 50	190.21
Vb	41F-1W, 71	194.11
Vb	41F-2W, 71	195.61
Vb	42F-1W, 71	198.81
Vb	42F-2W, 71	199.94
Vb	43F-1W, 21	203.01
Vb	43F-2W, 71	204.04
Vb	44F-1W, 41	207.91
Vb	44F-3W, 18	209.39
Vb	46F-1W, 35	217.25
Vb	46F-1W, 56	217.46
Vb	47X-CCW, 18	219.08
Vb	47X-CCW, 27	219.17
	356-U1459C-	
Vb	2R-1A, 3	205.83
Vb	4R-1W, 1	214.81
Vb	5R-1W, 16	219.76
Vb	6R-CCW, 0–5	224.40
Vb	7R-CCA, 5	229.25
Vb	8R-CCW, 16	234.16
Vb	10R-CCW, 16	243.76
Vb	11R-1A, 4	248.44
Vb	12R-1A, 45	253.65
Vb	13R-1W, 24	258.24
VI	14R-1W, 116	263.955
VI	14R-2W, 60	264.90
VI	14R-2W, 69	264.985
VI	15R-1W, 57	268.17
VI	16R-1W, 19	272.59
VI	16R-1W, 71	273.11
VI	17R-1W, 113	278.33
VI	17R-1W, 12	277.32
VI	17R-1W, 71	277.91
VI	17R-1W, 85	278.05
VI	17R-CCW, 22	278.59
VI	18R-1W, 59	282.59
VI	18R-CCW, 18	283.25
VI	20R-1W, 118	292.78
VI	20R-1W, 34	291.94
VII	26R-1A, 43	320.83
VII	27R-1A, 28	325.48
VII	27R-CCW, 6	325.61
VII	28R-1W, 10	330.10
VII	28R-1W, 18	330.18
VII	28R-1W, 21	330.21
VII	29R-1W, 20	335.00
VII	29R-1W, 40	335.20
VII	29R-1W, 50	335.30
VII	29R-1W, 75	335.55
VII	30R-CCW, 1	339.61
VII	32R-1W, 15	349.35
VII	33R-CCW, 18	354.18
VII	34R-CCW, 7	358.87
VII	35R-CCW, 18	363.78
VII	36R-CCW, 24	368.64
VII	37R-CCW, 20	373.40
VII	40R-CCW, 3	387.63
VII	40R-CCW, 8	387.68
VII	41R-CCW, 11	392.51
VII	41R-CCW, 28	392.68
VII	42R-CCW, 32	397.52

Table T5. Thin section samples, Site U1459 Units I–VII. All thin sections are from working-half sections. **Download table in .csv format.**

Lith. unit	Core, section, interval (cm)
	356-
I	U1459A-2X-1, 33–36
I	U1459A-2X-CC, 6–9.5
I	U1459A-4X-1, 19–21
I	U1459A-4X-CC, 1.5–4.5
II	U1459A-6X-CC, 13–15
II	U1459B-3F-1, 20–22
III	U1459A-13F-1, 45–46
III	U1459A-13F-3, 47–49
III	U1459A-14F-1, 16–18
III	U1459A-14F-CC, 7–9
III	U1459B-12F-1, 79–81
IV	U1459B-21F-4, 30–31
IV	U1459B-22F-1, 6–7
IV	U1459B-25F-1, 90–92
IV	U1459B-27F-2, 71–72
IV	U1459B-28F-1, 3–4
Va	U1459B-31F-2, 79–81
Va	U1459B-32F-1, 131–133
Va	U1459B-33F-2, 100–103
Vb	U1459B-50X-CC, 6–12
Vb	U1459C-4R-1, 83–86
VI	U1459C-13R-2, 11–16
VI	U1459C-17R-1, 60–64
VI	U1459C-18R-1, 83–86
VII	U1459C-29R-1, 68–70
VII	U1459C-32F-1, 131–133

XRD and XRF

The mineralogical composition of five samples from Hole U1459A was analyzed semiquantitatively using XRD (Table **T6**). Low-Mg calcite is the dominant mineral phase, followed by dolomite and then quartz. The dolomite is Ca rich with a calculated $MgCO_3$ content of ~44 mol% based on the d-value of the [104] peak (Lumsden, 1979). In four samples, aragonite and pyrite are present in trace amounts.

There were no XRF measurements for this unit.

Unit IV

Interval: 356-U1459B-19F-3A, 0 cm, through 29F-2A, 70 cm
Depth: Hole U1459B = 95.60–139.20 m CSF-A (43.60 m thick)
Age: late–early Pliocene
Lithology: unlithified packstone
Core quality: drilling disturbance is slight to absent

Unit IV is an unlithified, cream to light brown packstone and is distinguished from Unit III by a change in texture to packstone and a lower degree of glauconitization (Figure **F4**). Macrofossils, consisting of bivalves with occasional echinoderm fragments, are rare in this unit and decrease in abundance with depth. Microscopic analyses (see below) indicate the occurrence of planktonic and small benthic foraminifers throughout the unit (Figure **F5**). Glauconite grains are present throughout Unit IV but are less abundant and smaller than in Unit III. Dolomite appears near the base of Unit IV

Table T6. Semiquantitative XRD analysis of dominant mineral phases, Site U1459. $MgCO_3$ content of dolomite was calculated based on the d-value of the [104] peak (Lumsden, 1979). **Download table in .csv format.**

Lith. unit	Hole, core, section, interval (cm)	Depth CSF-A (m)	Relative (%)				Mg content (mol%)
			Aragonite	Quartz	Calcite	Dolomite	
	356-						
II	U1459B-4F-2, 67	29.37	19	8	71	2	42.8
II	U1459B-5F-2, 67	33.09	6	2	86	6	42.2
III	U1459A-10F-1, 75	47.55	3	2	88	7	44.1
III	U1459A-10F-2, 11	48.41	7	1	87	6	44.1
III	U1459A-10F-2, 75	49.05	4	3	84	9	44.5
III	U1459A-14F-1, 16	65.76	5	3	68	24	44.2
III	U1459A-14F-2, 27	67.37	0	1	93	6	44.3
IV	U1459B-21F-1, 124	104.45	0	5	84	11	44.1
IV	U1459B-23F-3, 67	115.08	0	4	91	5	44.2
IV	U1459B-24F-1, 67	116.77	0	7	78	15	44.5
IV	U1459B-26F-3, 21	126.11	0	1	58	41	43.8
Va	U1459B-38F-1, 60	179.90	0	11	22	75	44.6
Vb	U1459B-39F-1, 121	185.21	0	4	0	95	45.2
Vb	U1459C-5R-1, 35	219.95	0	13	0	87	45.6
Vb	U1459B-50X-CC, 6	232.96	0	87	12	1	44.1
Vb	U1459C-8R-CC, 13	234.13	0	10	51	39	44.0
Vb	U1459C-10R-CC, 17	243.77	0	6	3	93	46.2
VI	U1459C-17R-1, 97	278.17	0	0	0	100	46.1
VI	U1459C-18R-1, 75	282.75	0	0	7	93	44.7

Table T7. XRF bulk elemental concentrations, Site U1459. Mining profile results were converted to parts per million for comparison with Soil profile data. NA = not available. **Download table in .csv format.**

XRF profile	Lith. unit	Core, section, interval (cm)	Depth CSF-A (m)	Si (ppm)	Al (ppm)	K (ppm)	Ca (ppm)	Mg (ppm)	Fe (ppm)	Zr (ppm)	Sr (ppm)	Sc (ppm)
		356-U1459B-										
Soil	IV	20F-2, 49	99.29	NA	NA	1,133	136,576	NA	NA	6	229	625
		20F-2, 124	100.04	NA	NA	1,047	125,888	NA	NA	6	269	604
		20F-3, 49	100.79	NA	NA	1,204	156,492	NA	NA	9	281	637
		20F-4, 57	101.98	NA	NA	1,180	217,336	NA	NA	7	279	437
		22F-1, 56	107.26	NA	NA	1,131	153,769	NA	NA	8	269	537
		22F-2, 94	109.14	NA	NA	1,473	198,127	NA	NA	18	274	510
		22F-4, 56	111.98	NA	NA	1,787	215,251	NA	NA	39	337	339
Mining	Vb	47X-CC, 19	219.09	19,250	690	2,140	139,740	2,040	1,890	NA	NA	NA
		47X-CC, 25	219.15	61,890	910	2,060	286,870	2,550	2,490	NA	NA	NA
		49X-CC, 6	228.96	36,140	840	2,020	232,590	6,700	1,060	NA	NA	NA
		50X-CC, 5	232.95	224,680	810	1,990	98,540	470	530	NA	NA	NA

Figure F6. Thin section images in plane-polarized light (PPL), Unit I (left: 356-U1459A-2X-CC, 6–9.5 cm, right: 4X-1, 19–21 cm). Bioturbated skeletal packstones with planktonic and benthic foraminifers, bryozoans, echinoderms, and mollusks. Skeletal grains show intense bioerosion borings. Primary porosity is low. Pores are coated with thin layers of microcrystalline and fibrous dogtooth cement.

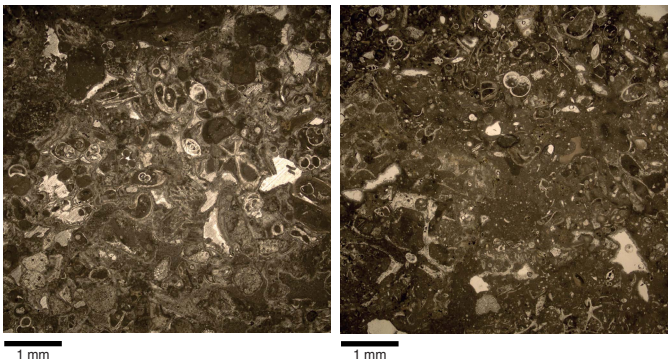

Figure F7. Smear slide photomicrograph, Unit II (356-U1459B-3F-2, 124 cm). Abundant sponge spicules with foraminifer fragments and other calcitic skeletal grains in a fine micrite matrix.

Figure F8. Thin section images, Unit II (356-U1459B-3F-1, 20–22 cm). Moderately to strongly bioturbated foraminifer-rich skeletal packstone. Foraminifer tests are partly dissolved and often filled with a thin layer of microcrystalline sparitic calcite cement. Note that bryozoans are dominant in other parts of the thin section. Porosity is low and moldic. Left: PPL. Right: cross-polarized light (XPL) (pore space appears black).

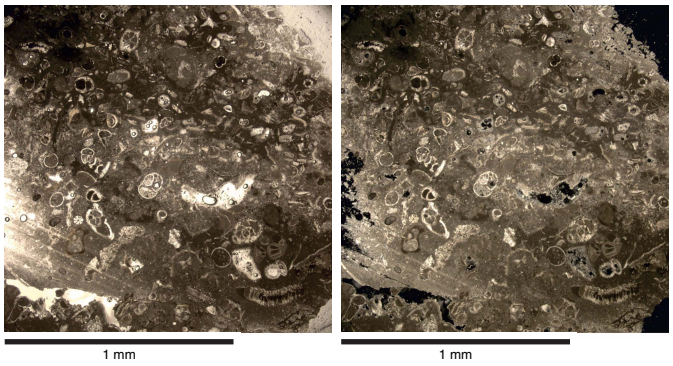

Figure F9. Thin section images, Unit III (356-U1459A-13F-3, 47–49 cm). Foraminifer-rich packstones with echinoderms and small amounts of silt-sized glauconite and quartz grains. Foraminifers are about the size of medium sand grains. Microsparitic cement is present throughout the unit. Porosity is moderate and mostly moldic. Recrystallization of micrite to sparite might have decreased primary porosity. Left: PPL. Right: XPL (geopetal structure in the middle of the image and pore spaces appear black).

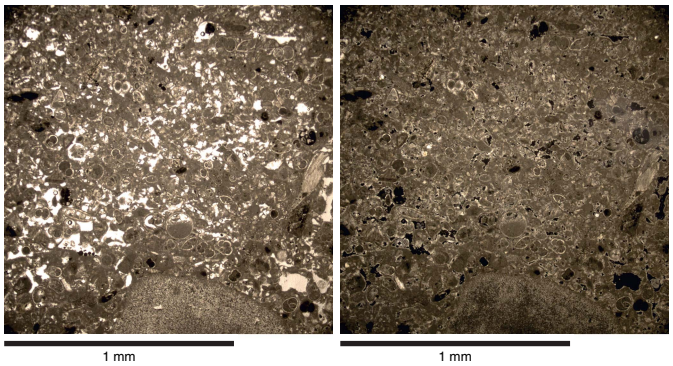

but is detectable only in microscope analyses; its abundance increases slightly with depth. Sediment composition and characteristics suggest Unit IV is a hemipelagic facies.

Smear slides

Planktonic foraminifers, small benthic foraminifers (Figure F10), and other skeletal fragments are present throughout the unit. There is generally less glauconitization than in Unit III, although heavily glauconitized foraminiferal tests and glauconite grains are common. Micrite is present, and isolated crystals of euhedral silt-sized dolomite occur in some samples, particularly in the lower half of the unit. Euhedral dolomite crystals dominate the silt-sized sediment fraction in one sample (356-U1459B-27F-2, 71 cm).

Thin sections

Five thin sections prepared from partly and unlithified limestones within Unit IV show mainly skeletal packstones of abundant planktonic and benthic foraminifers, bryozoans, echinoderm fragments, and mollusks (Figure F11). Coarse angular sand-sized intraclasts are present. The intraclasts consist of fine-grained skeletal fragments in a micrite matrix.

Figure F10. Smear slide photomicrograph, Unit IV (356-U1459B-23F-2, 71 cm). Sand-sized planktonic and benthic foraminifers with other skeletal carbonates embedded in a fine micritic matrix. Note glauconite grains and partial glauconitization of foraminiferal tests.

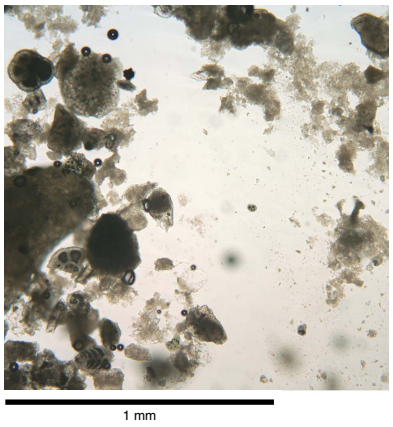

Figure F11. Representative thin section images, Unit IV (356-U1459B-25F-1, 90–92 cm). Unlithified skeletal packstone with planktonic and benthic foraminifers. Large echinoderm fragments dominate the sediments. Coarse sand–sized angular to irregular intraclasts are present, including fine skeletal fragments in a dark micrite matrix. Left: PPL. Right: XPL.

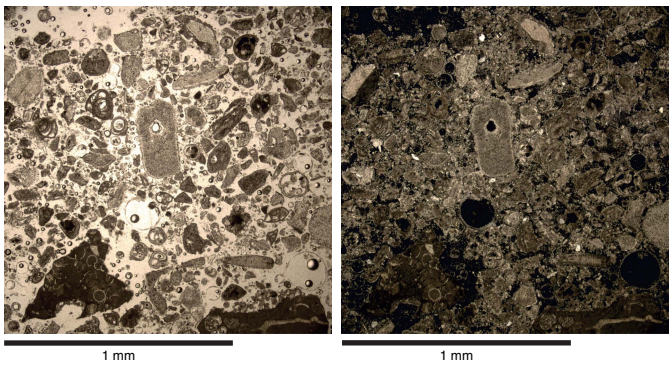

XRD and XRF

Four samples from Hole U1459B were analyzed semiquantitatively using XRD (Table T6). Low-Mg calcite is the dominant mineral phase followed by dolomite and quartz. In contrast to Unit III, aragonite is absent. Trace amounts of pyrite are present. The dolomite is Ca rich with a calculated $MgCO_3$ content of ~44 mol%.

XRF was measured on spot samples in Unit IV (and Subunit Vb) to test methodologies (Table T7). Too few samples were measured to detect trends or changes between units.

Unit V

Intervals: 356-U1459B-29F-2A, 70 cm, through 50X-CC, 13 cm; 356-U1459C-2R-1A, 0 cm, through 13R-1A, 25 cm
Depths: Hole U1459B =139.20–233.02 m CSF-A (93.82 m thick); Hole U1459C = 205.80–258.25 m CSF-A (52.45 m thick)
Age: early Pliocene–Oligocene
Lithology: dolomitic packstone with quartz; Subunit Va, unlithified packstone that includes a partially to fully lithified interval, and Subunit Vb, unlithified packstone with dolomite interbedded with lithified fine quartz sand
Core quality: drilling disturbance is minimal to moderate in Hole U1459B until Core 44F, after which disturbance is com-

mon with intervals of no recovery; drilling disturbance is moderate to severe for Hole U1459C (see subunit description for details)

Unit V consists of packstone with dolomite divided into two subunits based on variations in degree of lithification, color, concentrations of dolomite, and the quartz and fossil content of the sediment. Fossil content decreases markedly from Subunit Va to Vb. Subunit Va is recovered in Hole U1459B only, and the contact between Subunits Va and Vb is toward the base of Hole U1459B. The top of Hole U1459C begins in Subunit Vb (see **Hole alignment** for an explanation).

Subunit Va

Interval: 356-U1459B-29F-2A, 70 cm, through 38F-3A, 0 cm
Depth: Hole U1459B =139.20–182.30 m CSF-A (43.10 m thick)
Age: early Pliocene–late Miocene
Lithology: unlithified packstone with euhedral dolomite crystals and a nonskeletal partially to fully lithified packstone interval
Core quality: drilling disturbance is slight to moderate

Subunit Va is defined by the dominance of euhedral dolomite crystals in smear slide samples (Figure **F5**). Macroscopically, Subunit Va is primarily an unlithified, light gray to creamy gray packstone (Figure **F4**). Bioclasts are rare, but when present include bivalves, sponge spicules, and small benthic foraminifers (particularly in the upper half of the subunit) (Figure **F5**). In microscopic analyses, microfossils decline in abundance as dolomite increases in abundance with depth. Glauconite is present throughout much of Subunit Va, although in relatively small amounts compared to other units at Site U1459. There are no bioclasts in the thin sections from the partially lithified to lithified interval (356-U1459B-32F-1, 80 cm, through 35F-3, 0 cm; 151.9–168.2 m CSF-A) (e.g., Figure **F12**). Sediment composition and rare bioclasts in Subunit Va are indicative of a hemipelagic facies.

Smear slides

Smear slides of samples taken from Subunit Va show decreasing amounts of glauconitization compared to Unit IV (Figure **F5**). Microfossils decline in abundance with increasing depth and are replaced by euhedral dolomite crystals as the dominant component (Figure **F13**). Siliciclastic components also increase, particularly the abundance of sand-sized quartz grains (Figure **F5**).

Thin sections

Three thin sections prepared from the lithified limestones within Subunit Va show mainly nonskeletal packstone with abundant peloids and sparitic cement (e.g., Figure **F14**). Dolomite rhombs suggest early stage dolomitization. Peloidal grains have no signs of compaction. Microspar cement fills pores between the grains. Silt-sized quartz grains are abundant. Echinoderm fragments are the dominant bioclasts, and some are associated with syntaxial cement overgrowth.

XRD and XRF

The single XRD sample from the lowermost part of Subunit Va is dominated by dolomite, followed by calcite and quartz (Table **T6**). The relatively high quartz content reflects the increase in siliciclastic material toward the base of this subunit, which continues to increase through Subunit Vb.

There were no XRF measurements for Subunit Va.

Figure F12. Thin section images, Subunit Va (356-U1459B-33F-2, 100–103 cm). Nonskeletal packstone with abundant peloids. Early stage dolomitization is present. The peloidal grains show no signs of compaction. Occasionally, microspar cement fills pore spaces between grains. Coarse silt–sized quartz grains are abundant. Echinoderm fragments are the dominant bioclast particles. Left: PPL. Right: XPL (pore space appears black).

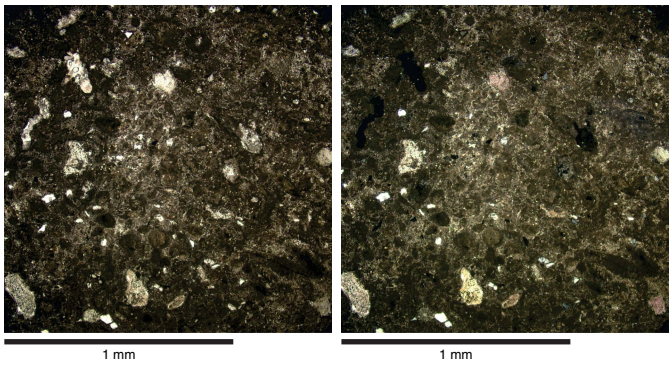

Figure F13. Smear slide photomicrograph of abundant silt-sized euhedral dolomite crystals in the lower part of Hole U1459B Subunit Va (34F-2, 71 cm). Dolomite crystals are frequently the dominant sediment component in this interval. Example of a detrital glauconite grain shown in the upper middle of the image.

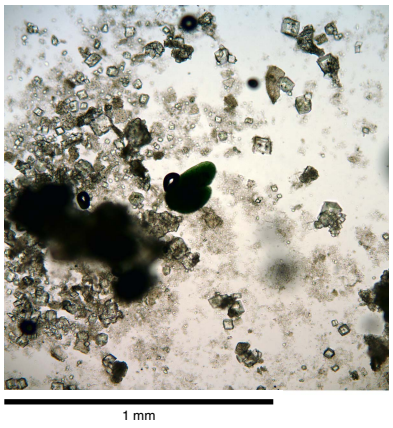

Subunit Vb

Intervals: 356-U1459B-38F-3A, 0 cm, through 50X-CC, 13 cm (end of hole); 356-U1459C-2R-1A, 0 cm, through 13R-1A, 25 cm
Depths: Hole U1459B = 182.30–233.02 m CSF-A (50.72 m thick); Hole U1459C = 205.80–258.25 m CSF-A (52.45 m thick)
Age: late Miocene–Oligocene
Lithology: unlithified dolomitic packstone to grainstone interbedded with lithified fine quartz sand
Core quality: drilling disturbance is moderate and there is no recovery between Samples 356-U1459B-44F-3A, 55 cm, and 50X-CC, 13 cm (end of hole)

Subunit Vb is primarily an unlithified packstone, similar to Subunit Va, but is defined as a subunit by macroscale dolomitization and, a couple of meters below the top of the subunit, the presence of quartz sand in smear slide analyses of Hole U1459B (Figure **F5B**). Subunit Vb is generally unlithified with alternating brown dolomitic grainstone and gray quartz-rich grainstone/sandstone intervals. In Hole U1459C, alternation is similar, changing between cream to

Figure F14. XPL smear slide photomicrograph from a quartz sand–rich interval in the lower part of Hole U1459B (40F-2, 50 cm; Subunit Vb). Quartz dominates the sand-sized fraction. Euhedral dolomite crystals dominate the silt-sized fraction.

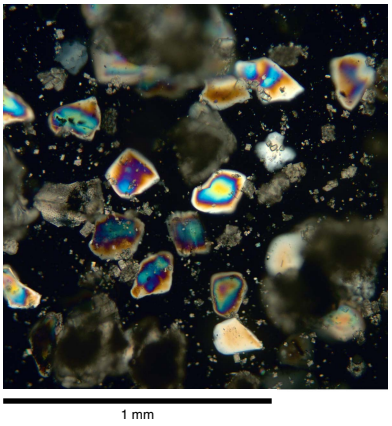

brown dolomitic packstone containing very fine grained, well-sorted quartz sand and light grayish-green packstone with some sand and glauconite (Figure **F5C**). As in Subunit Va, bioclasts are rare but are slightly more diverse, including bivalves, sponge spicules, echinoderms, gastropods, bryozoans, and foraminifers (Figure **F5**). These bioclastics typically occur in enigmatic skeletal quartz grainstones that contain hematite-coated grains and are interbedded with quartz-rich grainstones. Glauconite is slightly more abundant in Subunit Vb in Hole U1459C than in Hole U1459B. Based on compositional changes/alternations throughout, Subunit Vb facies are hemipelagic.

Smear slides

In Hole U1459B, Subunit Vb shows increasing quartz content with depth (Figure **F14**). Larger aggregates of euhedral dolomite crystals in the lowest intervals indicate increased dolomitization. This is consistent with the increasing lithification of the sediment with depth.

Thin sections

Two thin sections of lithified layers from Subunit Vb show partly silicified, medium sand-sized calcilithites (sandstone with carbonate rock fragments [Figure **F15**]). Chalcedony and microcrystalline silica cement fill the pores between carbonate bioclasts and partly replace a relatively older carbonate cement generation. Rare bioclast fragments are present.

XRD and XRF

The mineralogical composition of the five samples of Subunit Vb is variable, but dolomite is always an important component, except for Sample 356-U1459B-50X-CC, 6 cm, which is dominated by quartz and low-Mg calcite (Table **T6**). In four samples, quartz content is higher than calcite content. Trace amounts of pyrite are present in all samples. The dolomite is Ca rich with a calculated $MgCO_3$ content of ~45 mol%.

Four XRF spot samples were measured in Subunit Vb (and Unit IV) to test methodologies (Table **T7**). Too few samples were measured to detect trends or changes between units.

Unit VI

Interval: 356-U1459C-13R-1A, 25 cm, through 21R-CC, 0 cm
Depth: Hole U1459C = 258.25–296.40 m CSF-A (38.15 m thick)

Figure F15. Representative thin section images, Subunit Vb (356-U1459B-50X-CC, 6–12 cm). Medium sand-sized calcilithite (sandstone with carbonate rock fragments), with silica cemented throughout. Porosity is mostly interparticle and rarely intraparticle. Silica cement (chalcedony to quartz) fills the pores between the grains and even inside the grain and in some cases replaces the carbonate cement, which seems to be deposited earlier than silica cements. Bioclast fragments (low percentage) are still recognizable. Rock fragments are carbonate type (mostly fine grained and micritic). Left: PPL. Right: XPL (pore space appears black).

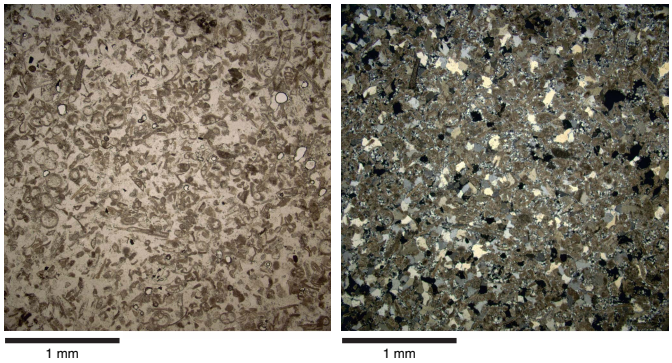

Age: Oligocene
Lithology: lithified beige to light brown/gray to brown dolostone
Core quality: core recovery is low; however, where core was recovered, drilling disturbance is slight to moderate

Unit VI is a lithified dolostone that darkens downcore from beige to light brown to brown and then lightens again near the base of the unit becoming light greenish gray to cream (Figure **F4**). Unit VI is primarily differentiated from Subunit Vb by a sharp decrease in siliciclastic (quartz sand) content (see Site U1459 smear slides in **Core descriptions**) (Figure **F5**). Glauconite is present throughout the unit. Texturally, the dolostone in Unit VI is relatively homogeneous with a few isolated occurrences of parallel laminations (Figure **F4**). The sediment composition and scarcity of bioclasts in Unit VI suggest a hemipelagic facies.

Smear slides

Smear slides show that euhedral fine to medium crystalline dolomite, ranging from 50 to 250 µm, with varying abundances of detrital glauconite, dominate the sediment of Unit VI (Figure **F5**). No microfossils are present in this unit. Quartz is only present in minor amounts and decreases further with depth, with quartz absent deeper than Sample 356-U1459C-15R-1, 57 cm (Figures **F16**, **F17**).

Thin sections

Three thin sections were prepared from lithified intervals within Unit VI, showing highly porous fine to medium crystalline dolostone with medium sand-sized glauconite grains (Figure **F18**). The size and shape of dolomite crystals varies from fine crystalline anhedral to medium crystalline euhedral. No biogenic components were observed. Porosity (estimated at 10%–15%) is secondary and intercrystalline.

XRD and XRF

Two samples from Hole U1459C were analyzed semiquantitatively using XRD (Table **T6**). Dolomite is the dominant mineral phase followed by low-Mg calcite. Quartz is present in one sample. The dolomite is Ca rich with a calculated $MgCO_3$ content of ~45.5 mol%.

There were no XRF measurements for Unit VI.

Figure F16. PPL smear slide photomicrograph showing typical mineralogical composition of Unit VI (356-U1459C-18R-1, 59 cm). Dolomite dominates the sediment with brown glauconite. Bright dark green (likely detrital) glauconite is visible in the center and the lower left of the image. Opaque phases are likely artifacts caused by metal flakes detached during the scraping the lithified rock with a spatula.

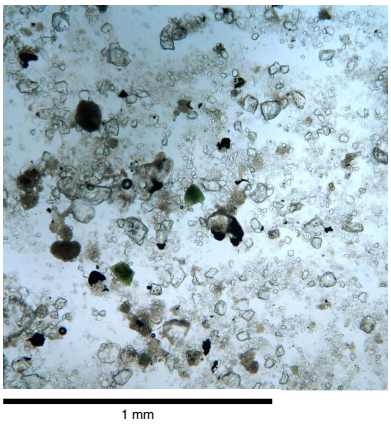

Figure F17. XPL photomicrograph of Figure **F16** showing the absence of quartz or other lithic grains within the sediment in this interval. Brownish to multicolored grains are dolomite, whereas dark greenish-brown grains are glauconite.

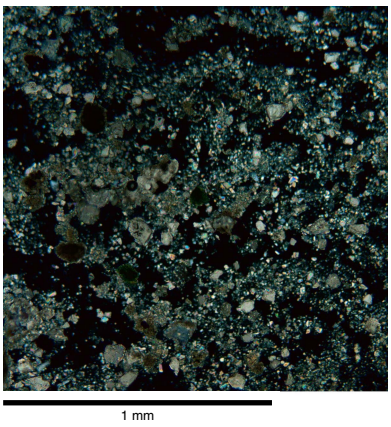

Unit VII

Interval: 356-U1459C-21R-CC, 0 cm, through 42R-CC, 52 cm (end of hole)
Depth: Hole U1459C = 296.40–397.72 m CSF-A (101.32 m thick)
Age: early Oligocene–Eocene
Lithology: lithified, chert-rich packstone and microcrystalline dark gray chert
Core quality: drilling disturbance is severe

Unit VII is primarily lithified, nonskeletal, light greenish-gray, chert-rich packstone and microcrystalline, dark gray chert (Figure **F4**). The first occurrence of chert defines Unit VII. No bioclasts are present, but glauconite, flaser and lenticular bedding, and wavy laminations are common throughout most of the unit (Figure **F5**). The cherts contain bands of veins and cavities filled by either white carbonate or light greenish-gray grainstone containing glauconite. The Unit VII facies is hemipelagic, based on sediment composition and texture.

Figure F18. Thin section images, Unit VI (356-U1459C-17R-1, 60–64 cm). Highly porous fine to medium crystalline dolostone with glauconite. The size and shape of dolomite crystals changes from fine anhedral to medium euhedral. Medium sand–sized glauconite grains make up the noncarbonate component. Secondary intercrystalline porosity is estimated at ~10%–15%. Left: PPL. Right: XPL (pore space appears black).

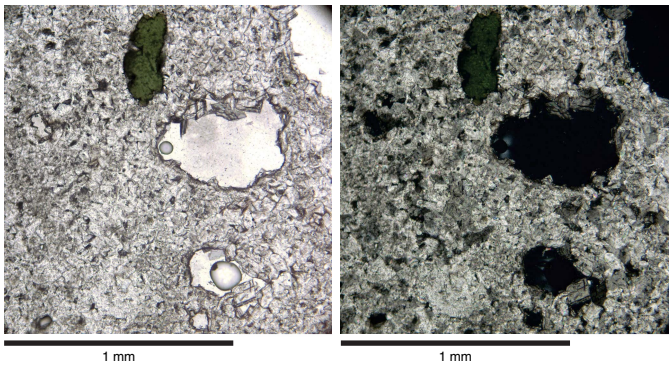

Smear slides

The lithologic change marking the beginning of Unit VII is confirmed by the reappearance of microfossils in smear slide Sample 356-U1459C-20R-1, 34 cm. The slide shows a diverse assemblage of heavily glauconitized foraminifers, together with echinoid spines, minor amounts of sponge spicules, and mollusk fragments, which are entirely overgrown by dolomite in the upper part of the unit and calcite in the lower part (Figure **F5**). Dolomite concentrations decrease between Cores 20R and 29R (Sample 29R-1, 50 cm). From this point downcore rare isolated euhedral dolomite crystals occur in the sediment. Detrital glauconite is relatively rare but present throughout Unit VII. Micrite content is higher on average in this unit compared to Unit VI. Quartz content increases with depth. Deeper than Core 30R-CC, quartz remains a minor component with fairly consistent abundances until the end of Hole U1459C. The skeletal packstones of this unit contain abundant and diverse skeletal fragments, which include, in the larger grain sizes, echinoid spines and mollusks with slightly lower amounts of planktonic and benthic foraminifers and minor amounts of sponge spicules and bryozoan fragments. Echinoderm fragment–rich sediments are found primarily between Cores 36R and 37R. The clay and fine silt (<20 µm) fractions contain calcareous nannofossils throughout Unit VII, where they are a minor to major component of the sediment (Figures **F19**, **F20**). Foraminiferal tests show heavy glauconitization throughout the unit, comparable to the material observed in Units II–IV.

Thin sections

Two thin sections of lithified intervals from Unit VII show partly silicified dolomitic pack- to grainstones (e.g., Figure **F21**). The primary skeletal limestone has been altered by two phases of diagenesis and replacement. In the early phase of diagenesis the sediment was affected by dolomitization, which resulted in the growth of fine crystalline dolomites throughout the sediment. Subsequently in the late diagenetic phase, chertification affected the texture and components of the rock. Part (probably the larger part) of the primary carbonate rock remains unaffected by diagenesis. Fine-grained chert (chalcedony) partially replaces the finer grains of the primary dolomitized carbonate rock.

Figure F19. PPL smear slide photomicrograph of nannofossil-rich clay layer (356-U1459C-29R-1, 40 cm) showing the generally fine, clay- to fine silt–sized clay and micrite grains between abundant nannofossils. The larger (~20 µm) euhedral rhomboidal crystal in the lower left represents an example of the isolated dolomite crystals present throughout Unit VII.

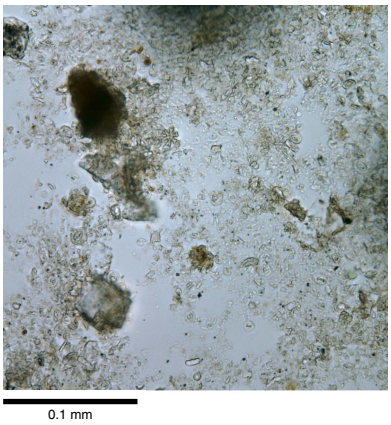

Figure F20. XPL smear slide photomicrograph of Figure **F19** (356-U1459C-29R-1, 40 cm; Unit VII). Abundant nannofossils with their distinctive extinction pattern, also illustrating the minor amounts of both clay and micrite that occurs together with the nannofossils in the clay- and fine silt–sized fraction.

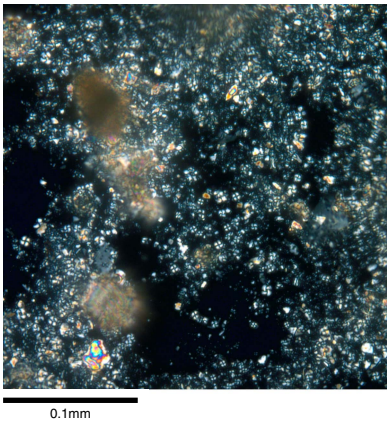

XRD and XRF

No XRD or XRF measurements were made in this unit.

Biostratigraphy and micropaleontology

Calcareous nannofossils were rare to abundant at Site U1459 and showed moderate to very good preservation. Holes U1459A and U1459B contain Pleistocene to late Miocene sediments, whereas the strata in Hole U1459C were determined to be early Miocene to early middle Eocene age. A total of 84 smear slides were examined for biostratigraphic marker species and common taxa.

Biozone Pt1a (0.61–1.93 Ma) can be identified between Cores 356-U1459A-5F and 10F. Deeper (Core 356-U1459B-16F), a Pliocene faunal assemblage was found (Biozone PL4) that dates to an age of at least 3.47 Ma (*Dentoglobigerina altispira*). Between Core 356-U1459B-16F and about Core 356-U1459C-20R, severe dolomitization impeded preservation and made faunal identification difficult. Around Core 356-U1459C-20R, preservation improved with the reappearance of foraminifers, but overall preservation remained (very) poor. The first reappearing species were Oligocene

Figure F21. Thin section images, Unit VII (356-U1459C-32F-1, 131–133 cm). Chertified dolomitic skeletal limestone. The primary skeletal limestone shows two phases of diagenesis and replacement: (1) dolomitization, resulting in growth of fine crystalline dolomite throughout the sediment and replacement of biogenic components; and (2) chertification, which changed the texture and components of the rock. Only the largest components of the dolomitized carbonate rock are unaffected. Smaller components of the dolomitized carbonate rock were partially removed by chert (chalcedony). Left: PPL. Right: XPL (pore space appears black).

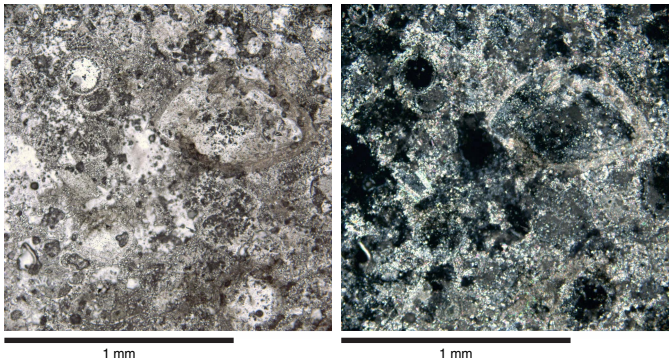

taxa. Deeper than Core 356-U1459C-29R, a distinct Eocene faunal assemblage was present covering Biozones E14–E9 (~38–50 Ma) (i.e., the bottom of Hole U1459C), dating to the latest early Eocene.

The samples contained between 15% and 96% benthic foraminifers, and *Cibicides* spp., and *Cibicidoides* spp. were the most common taxa. Four assemblages defined by abundances of *Textularia* spp., *Uvigerina* spp., *Bolivina* spp., and epifaunal species were present. In each sample, 1–41 species were present. Except for the top three samples, preservation was poor and affected by diagenesis including dolomitization. The estimated paleobathymetry ranged from shallow/neritic environments to ~500 m.

Calcareous nannofossils

Core recovery in Hole U1459A was low from 0 to ~42 m CSF-A (top of Core 356-U1459A-9F), with consolidated sediments in the core catchers. Fragments of these sediments yielded rare and moderately preserved nannofossils after sonification in distilled water. The presence of *Emiliania huxleyi* indicates a recent to Late Pleistocene age for the base of Core 1F (Biozone NN21), and >0.29 Ma for the base of Core 2X (Biozone NN20). The tops of *Pseudoemiliania lacunosa* and nannofossil Biozone NN19 (0.44 Ma) are between Samples 5X-CC and 6F-2, 100 cm. *Gephyrocapsa* spp. >4 µm in size (few) were encountered to Sample 9F-CC (46.48 m CSF-A), adding an additional age datum of 1.73 Ma between this core and the next (Sample 10F-CC; 51.44 m CSF-A).

Good core recovery and the overall good nannofossil preservation in Hole U1459B resulted in several age datums from Core 356-U1459B-3F (27.05 m CSF-A) downhole (Table **T8**). The tops of *P. lacunosa* and Biozone NN19 (0.44 Ma) are between Samples 4F-CC and 5F-CC (31.6 and 34.85 m CSF-A). The abundance of *Discoaster* spp. was very low (Table **T9**), which may have prevented the identification of the Pleistocene Biozone NN18 (top of *Discoaster brouweri*, 1.93 Ma). However, the base of medium (>4 µm) gephyrocapsids is deeper than Sample 9F-CC (53.36 m CSF-A; 1.73 Ma, within Biozone NN19). The top of Biozone NN16, which includes the Pliocene/Pleistocene boundary, was marked by the presence of *Discoaster surculus* in Sample 12F-CC (64.25 m CSF-A; >2.49 Ma). *Sphenolithus* spp. (mainly *Sphenolithus abies*) were present from Sample 18F-CC (92.56 m CSF-A) and further downcore, denoting

Table T8. Calcareous nannofossil (CN) and planktonic foraminifer (PF) datums, Site U1459. Ages are according to Gradstein et al. (2012). **Download table in .csv format.**

Core, section	Depth CSF-A (m)	Marker species	Type (CN/PF)	Zone name	Age (Ma)	Reference
365-U1459A-						
1F-CC	0.10	Base *E. huxleyi*	CN	NN21	0.29	Gradstein et al., 2012
6F-2W	33.68	Top *P. lacunosa*	CN	NN19	0.44	Gradstein et al., 2012
5X-CC	22.45	Top *Globorotalia tosaensis*	PF	PT1a	0.61	Gradstein et al., 2012
9F-CC	46.48	Base *Gephyrocapsa* spp. (>4 µm)	CN	NN19	1.73	Gradstein et al., 2012
10F-CC	51.42	Base *Globorotalia truncatulinoides*	PF	PT1a	1.93	Gradstein et al., 2012
365-U1459B-						
5F-CC	34.85	Top *P. lacunosa*	CN	NN19	0.44	Gradstein et al., 2012
9F-CC	53.36	Base *Gephyrocapsa* spp. (>4 µm)	CN	NN19	1.73	Gradstein et al., 2012
12F-CC	64.25	Top *D. surculus*	CN	NN16	2.49	Gradstein et al., 2012
18F-CC	92.56	Top *Sphenolithus* spp.	CN	NN16 (basal part)	3.54	Gradstein et al., 2012
18F-CC	92.51	Top *Dentoglobigerina altispira*	PF	PL4 (Indo-Pacific)	3.47	Gradstein et al., 2012
23F-CC	115.87	Top *R. pseudoumbilicus*	CN	NN15	3.7	Gradstein et al., 2012
34F-CC	165.26	Top *D. quinqueramus*	CN	NN11	5.59	Gradstein et al., 2012
48X-CC	223.90	Top *Coronocyclus nitescens* (circular)	CN	NN6 (or older)	>11.88	Backman et al., 2012
365-U1459C-						
19R-CC	287.10	Top *E. formosa*	CN	NP21	32.92	Gradstein et al., 2012
26R-CC	321.20	Below base *R. bisecta*, above base *C. reticulatum*	CN	NP16–NN17	38.25–41.66	Gradstein et al., 2012
29R-CC	335.71	Top *Morozovelloides crassatus*	PF	E13	38.25	Gradstein et al., 2012
36R-CC	368.71	*Globigerinatheka kugleri/Morozovella aragonensis*	PF	E9	43.26	Gradstein et al., 2012
40R-CC	387.67	Base *Acarinina cuneicamerata*	PF	E7a	48.31	Gradstein et al., 2012
41R-CC	392.46	Below base *R. umbilicus* (>14 µm), above base *E. formosa*	CN	NP12–NN15	43.32–53.7	Gradstein et al., 2012

the basal part of Biozone NN16. The top of Biozone NN15 was placed between Samples 22F-CC and 23F-CC (111.6 and 115.9 m CSF-A) based on the top occurrence of *Reticulofenestra pseudoumbilicus* (3.7 Ma). Species that define early Pliocene Biozones NN14–NN12 (e.g., *Amaurolithus* spp. and *Ceratolithus* spp.) were absent. The top of the late Miocene Biozone NN11 (5.59 Ma) was identified by the presence of *Discoaster neohamatus* in Sample 33F-CC (160.6 m CSF-A) and *Discoaster quinqueramus* in Sample 34F-CC (165.3 m CSF-A). A barren interval was found in Cores 46F (218.9 m CSF-A) and 47F (219.2 m CSF-A), below which the final sample (48X-CC; 223.9 m CSF-A) investigated for this hole yielded a middle Miocene age.

The Pleistocene and Pliocene assemblages in Holes U1459A and U1459B contain abundant small *Gephyrocapsa* spp. (2 µm) and *Gephyrocapsa caribbeanica* (3–4 µm) with a varying diversity of other reticulofenestrid species (Table **T9**). Other taxa that are present include *Braarudosphaera bigelowii, Calcidiscus* spp., *Coccolithus pelagicus, Helicosphaera carteri, Pontosphaera* spp., *Rhabdosphaera* spp., *Syracosphaera* spp., and *Umbilicosphaera sibogae* (Table **T9**; Figure **F22**).

The core catchers in Hole U1459C contained well-preserved calcareous nannofossils that were rare to abundant within a matrix of micrite with variable amounts of micrometer-scale rhombic dolomite crystals. The few barren intervals (Samples 356-U1459C-12R-CC through 14R-CC [253.9–265.3 m CSF-A] and 16R-CC [273.8 m CSF-A]) were dolomite rich. Samples 2R-CC through 10R-CC (206.4–243.9 m CSF-A) contain typical assemblages of early to late Miocene medium- to large-sized reticulofenestrids (including *Reticulofenestra haqii* and *R. pseudoumbilicus*). However, no biostratigraphic markers were observed. Deeper, core catchers were barren of nannofossils or contained very rare *R. haqii* only.

An earliest Oligocene (or older) age (>32.92 Ma) was inferred based on the presence of *Ericsonia formosa* in Sample 19R-CC (287.1 m CSF-A) and *Reticulofenestra umbilicus* (>14 µm) in Sample 20R-CC (293.1 m CSF-A). The presence of *Cribrocentrum reticulatum* in Sample 26R-CC (321.2 m CSF-A) confirms a late Eocene age (>35.40–41.66 Ma [Gradstein et al., 2012] or >35.24–42.37 Ma in Agnini et al. [2014]), and the base of Hole U1459C was dated to the early middle Eocene based on the presence of *Chiasmolithus grandis* (Biozones NP11–NP17 [Perch-Nielsen, 1985] or CP10–CP12 according to NannoWare Database v. 1.0), *E. formosa* (early Eocene, Ypresian; Biozone NP12, <53.7 Ma), and the absence of *R. umbilicus* (>43.32 Ma) (Figure **F22**).

Table T9. Calcareous nannofossil abundance and range chart, Site U1459. **Download table in .csv format.**

Planktonic foraminifers

A total of 14 core catcher samples were processed for Hole U1459A, 47 for Hole U1459B, and 42 for Hole U1459C.

Core catcher samples were analyzed for their planktonic foraminiferal content from Cores 356-U1459A-1F through 11F (0–70 m CSF-A), 356-U1459B-16F through 46F (70–218 m CSF-A), and 356-U1459C-6R through 40R (224.45–387.68 m CSF-A). The overall species diversity was higher than at Site U1458, with 11–15 different taxa; however, diversity decreased in the dolomitized section (>140 m CSF-A) (see details in **Lithostratigraphy**).

Globorotalia tosaensis was identified in Samples 356-U1459A-5X-CC (22.4 m CSF-A) and 6X-CC (34.9 m CSF-A) with a reported top of ~0.61 Ma (Biozone Pt1a) (Table **T8**). *Globorotalia truncatulinoides* is present down to Sample 10X-CC (51.4 m CSF-A), indicating an age of <1.93 Ma (base of Biozone Pt1a). Additionally, the indicator species *D. altispira* first occurs downhole in Sample 356-U1459B-18F-CC (92.5 m CSF-A) and occurs to Sample 26F-CC (127.3 m CSF-A), suggesting an age of >3.47 Ma for this interval (Biozone PL4; Shackleton et al., 1995). From Cores 356-U1459B-18F (last occurrence of *D. altispira*) through 29F (92.5–141.7 m CSF-A), the fauna includes more typical Pliocene (and early Pleistocene) species such as *Globigerinoides extremus, Globigerinoides obliquus, Globorotalia limbata, Neogloboquadrina humerosa*, and *Globorotalia exilis* (Tables **T10**, **T11**). *G. exilis*, however, has been

Figure F22. Photomicrographs of calcareous nannofossils, Site U1459. A. *Braarudosphaera bigelowii*. B. *Pseudoemiliania lacunosa*. C. *Reticulofenestra pseudoumbilicus*. D. *Helicosphaera intermedia*. E. *Pontosphaera discopora*. F. *Discoaster brouweri*. G. *Discoaster surculus*. H. *Discoaster challengeri*. I. *Discoaster neohamatus*. J. *Discoaster berggrenii*. K. *Sphenolithus abies*. L. *Sphenolithus moriformis*. M. *Cyclicargolithus abisectus*. N. *Reticulofenestra scrippsae*. O. *Cyclicargolithus floridanus*. P. *Ericsonia formosa*. Q. *Reticulofenestra umbilicus*. R. *Isthmolithus recurvus*. S. *Cribrocentrum reticulatum*. T. *Coccolithus eopelagicus*. U. *Discoaster saipanensis*. V. *Chiasmolithus altus*. W. *Chiasmolithus grandis*.

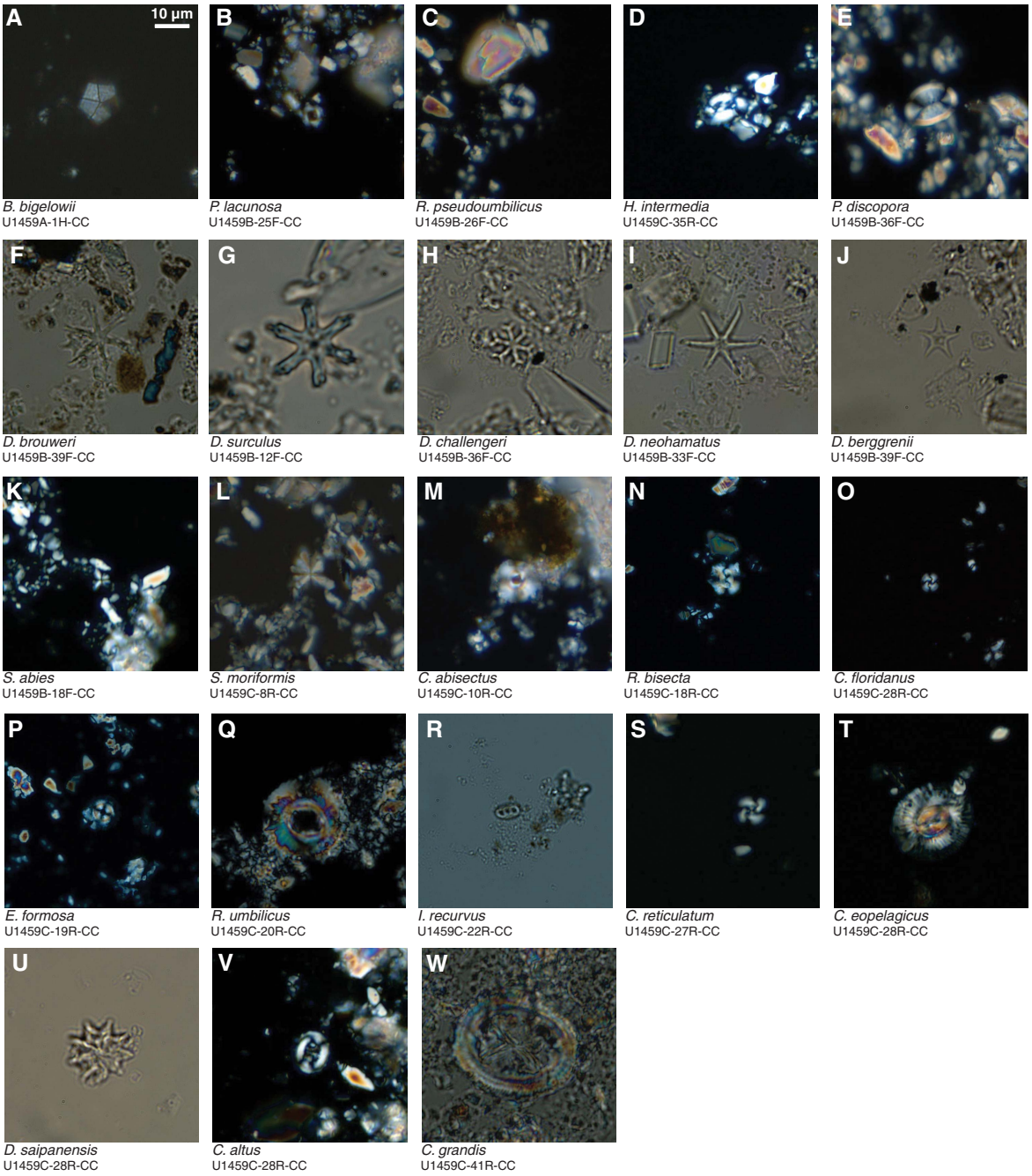

reported as endemic to the tropical Atlantic with Indian/Pacific forms considered morphoforms of *Globorotalia menardii* (Chaisson, 2003).

Deeper than Core 356-U1459B-26F (136.9 m CSF-A), the samples were increasingly affected by dolomite crystallization (see **Lithostratigraphy**). In Cores 40F through 46F (190.5–218.8 m CSF-A), only few unidentifiable planktonic foraminifers were present (Figures **F23**, **F24**).

From Samples 356-U1459C-6R-CC through 10R-CC (224–243 m CSF-A), planktonic foraminifers were rare. From Samples 11R-CC through 17R-CC (249–278 m CSF-A), foraminifers were absent except for Samples 18R-CC (283 m CSF-A) and 19R-CC (287 m CSF-A), with rare planktonic foraminifers along with abundant benthic foraminifers (see details below) (Figures **F23**, **F25**). In Sample 22R-CC (301 m CSF-A), *Dentoglobigerina* sp. and *Paragloborotalia* sp. occurred (Wade et al., 2007), indicating an Oligocene age.

Downcore from Core 356-U1459C-29R (335 m CSF-A), Eocene planktonic foraminiferal species were present (Figure **F26**) including *Subbotina gortanii, Subbotina eoceana, Globigerinatheka index*,

Table T10. Occurrence of main genera and species of benthic and planktonic foraminifers and additional bioclasts and minerals, Site U1459. Preservation: P = poor, M = moderate, G = good. Paleodepth estimates are based on calculations from van Hinsbergen et al. (2005). Bathymetric zones: IS = inner shelf. (Only a portion of this table appears here. The complete table is available in **.csv format**.)

			Benthic foraminifers							Planktonic foraminifers	Other							
Core, section	Top depth CSF-A (m)	Bottom depth CSF-A (m)	Preservation	Benthic foraminifers/total foraminifers (%)	Planktonic foraminifers/total foraminifers (%)	Paleodepth estimate %P (m)	Total number of benthic species	Bathymetric zone	Most abundant benthic foraminifer species (descending order)	Most frequent planktonic foraminifer species	Glauconite	Pyrite	Sponge spicules	Ostracods	Pteropods	Fish teeth	Bryozoans	Comment
356-U1459A-																		
1F-CC	0	0.1	G	60	40	161	41	IS	*Textularia* spp., *Quinqueloculina lamarckiana, Heterolepa bradyi*	*Globigerinoides conglobatus, Globigerinoides ruber* (white), *Globigerinoides sacculifer* (without sac), *Globigerinoides trilobus, Globorotalia cibaoensis, Globorotalia exilis, Globorotalia inflata, Globorotalia truncatulinoides, Globoturborotalita apertura, Neogloboquadrina dutertrei*			X	X	X			Worm casings
2X-CC	0.57	0.59	M	90	10	46	4	IS	*Cibicidoides* spp., *Quinqueloculina lamarckiana*	*Globigerinoides conglobatus, Globorotalia exilis, Globorotalia inflata, Globorotalia truncatulinoides*					X			
5X-CC	22.4	22.5	P	58	42	175	18	IS	*Amphistegina* spp., *Cibicidoides* spp.	*Globigerina bulloides, Globigerinoides immaturus, Globigerinoides ruber* (white), *Globigerinoides sacculifer* (without sac), *Globorotalia inflata, Globorotalia menardii, Globorotalia tosaensis, Globorotalia truncatulinoides, Globorotalia tumida*	X		X	X				
6F-CC	34.94	34.99	P	66	34	125	23	IS	*Cibicidoides* spp., *Amphistegina* spp.	*Globigerina bulloides, Globigerinoides extremus, Globigerinoides ruber* (white), *Globigerinoides sacculifer, Globigerinoides sacculifer* (without sac), *Globorotalia crassaformis, Globorotalia inflata, Globorotalia menardii, Globorotalia truncatulinoides, Globorotalia tumida, Neogloboquadrina dutertrei, Orbulina universa, Pulleniatina obliquiloculata*					X			Heavily encrusted and abraded tests, few bryozoa

and *Acarinina primitiva* (Pearson et al., 2006). These species date Core 29R (335 m CSF-A) to the end of the middle Eocene (Biozone E13; ~38–40 Ma), Core 36R (368 m CSF-A) as middle Eocene (Biozone E9, <43.5 Ma) (e.g., *Globigerinatheka barri, Acarinina collactea*, and *Globorotaloides quadrocameratus*), and Core 40R (387 m CSF-A) to the latest early Eocene (Biozone E7; *Acarinina bullbrooki* and *Acarinina alticonica*; ~50.2 Ma) (Pearson et al., 2006) (Table **T8**).

Benthic foraminifers

A total of 11 core catcher samples were investigated from Hole U1459A, 25 from Hole U1459B, and 26 from Hole U1459C. Overall, the number of species present ranged from 1 (Sample 356-U1459B-38F-CC; 184.1 m CSF-A) to 35 (Sample 356-U1459A-1F-CC; 0.1 m CSF-A), with 13 samples being barren due to alteration such as dolomitization (Samples 356-U1459B-40F-CC through 47F-CC [190.58–218.95 m CSF-A] and 356-U1459C-5R-CC through 17R-CC [220.09–278.47 CSF-A]) (see Tables **T10**, **T12**). With the exception of the two uppermost samples from Hole U1459A (Samples 356-U1459A-1F-CC [0.1 m CSF-A] and 2X-CC [0.59 m CSF-A]), the preservation of benthic foraminiferal tests was poor to very poor throughout Site U1459. Preservational damage ranged from abrasion and fragmentation (breakage) to cementation (coating in secondary crystals), particularly by dolomite (particularly Samples 356-U1459B-35F-CC [169.92 m CSF-A] through 356-U1459C-17R-CC [278.47 m CSF-A]) (Table **T10**) (see **Lithostratigraphy**). Glauc-

Table T11. Planktonic foraminifer presence, abundance, and preservation at Site U1459, including characteristic mineral and other bioclast occurrences. **Download table in .csv format.**

onite was present in varying abundances; it infilled tests downcore from Sample 356-U1459B-5X-CC (22.5 m CSF-A) to the lowest sample (356-U1459C-40R-CC; 387.68 m CSF-A).

Species of *Cibicides* spp. and *Cibicidoides* spp. were present throughout cores from Site U1459, but five specific foraminiferal assemblages (Figure **F25**) were found downcore across Holes U1459A–U1459C. From Samples 356-U1459A-1F-CC through 6F-CC (0.1–34.99 m CSF-A), the first benthic foraminiferal assemblage contains a range of shallow-water temperate to warm-water species. The assemblage is dominated by taxa including *Quinqueloculina lamarckiana, Amphistegina* spp., and *Cibicidoides* spp., with abundant *Discorbinella* spp., *Quinqueloculina* spp., *Textularia agglutinans*, and *Textularia* spp. The taxa found in this assemblage reflect an inner shelf paleodepth.

The next assemblage is present from Samples 356-U1459A-7F-CC (35.36 m CSF-A) through 356-U1459B-18F-CC (92.56 m CSF-A). This assemblage is marked by a dominance of *Heterolepa bradyi* and *Cibicidoides* spp. with abundant *Bolivina* spp., *Brizalina* spp., and *Trifarina* spp. This assemblage contains infaunal shallow-water (50–150 m) species typical of middle and outer shelf depths.

The third assemblage is present from Samples 356-U1459B-20F-CC through 34F-CC (102.24–165.26 m CSF-A). This section contains between 7 and 20 species per sample and is characterized by a dominance of *Uvigerina peregrina* and *H. bradyi* with bolivinids and brizalinids. Additionally, there is evidence of downslope transport with the presence of abundant shallow-water species *Planorbulinella larvata* and *Elphidium* spp. The abundance of infaunal species indicates paleowater depths from the outer shelf to upper bathyal area between 150 and 500 m (Moore et al., 1980).

The fourth assemblage is present from Samples 356-U1459B-35R-CC (169.92 m CSF-A) through 356-U1459C-39F-CC (186.92 m CSF-A) and is dominated by *Bolivina robusta* with abundant *H.*

Figure F23. Planktonic foraminifer abundance, Site U1459. 0 = barren, 1 = very rare, 2 = rare, 3 = few, 4 = common, 5 = abundant (see **Biostratigraphy and micropaleontology** in the Expedition 356 methods chapter [Gallagher et al., 2017] for definitions).

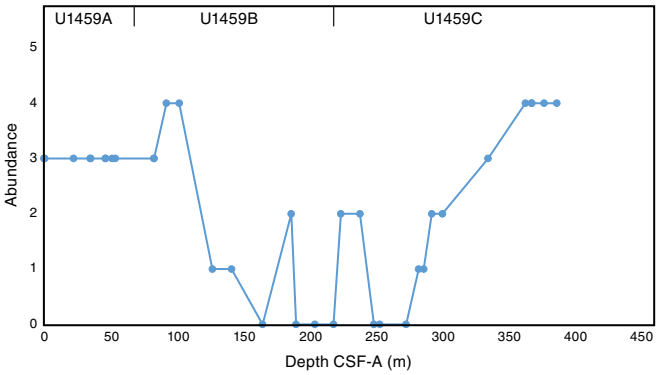

Figure F24. Preservation of planktonic foraminifers, Site U1459. Good (Core 356-U1459A-6F; 34.99 m CSF-A): mostly no dolomitization. Moderate (Core 356-U1459B-18F; 92.56 m CSF-A): small-scale fine dolomitization. Poor (Core 34F; 165.26 m CSF-A): dolomitized. Very poor (Core 39F; 186.92 m CSF-A): heavily dolomitized. See **Biostratigraphy and micropaleontology** in the Expedition 356 methods chapter (Gallagher et al., 2017) for further explanations.

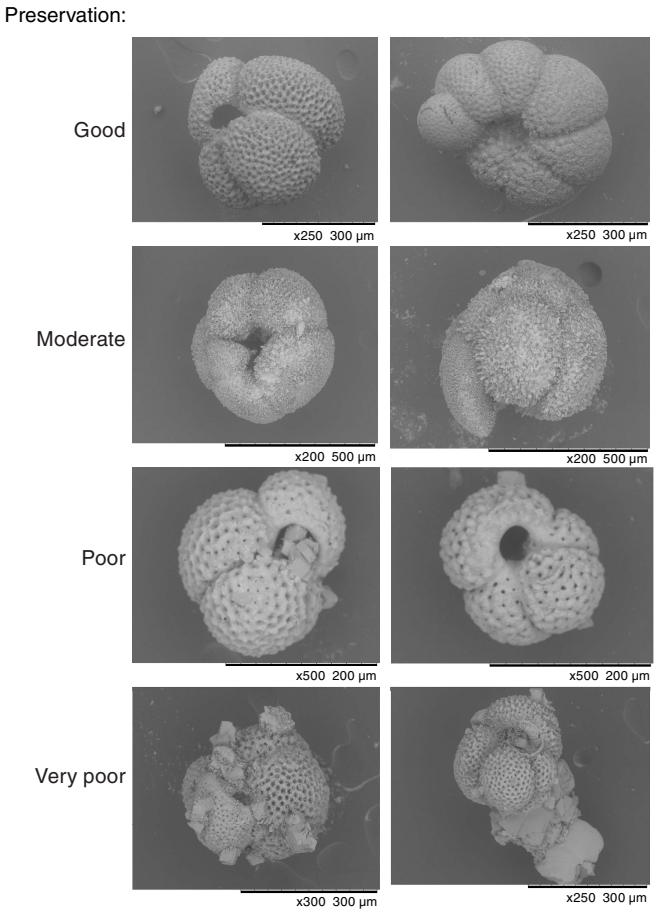

Figure F25. Dominant benthic foraminiferal species and assemblages at Site U1459 with paleodepth based on planktonic/benthic ratio (%P) and bathymetric zone interpretation. Assemblage bathymetric zones were smoothed to generate a synthesis, resulting in slight differences from hole summary data. For raw bathymetric zonation see Table **T10**. This figure is available in an **oversized format**.

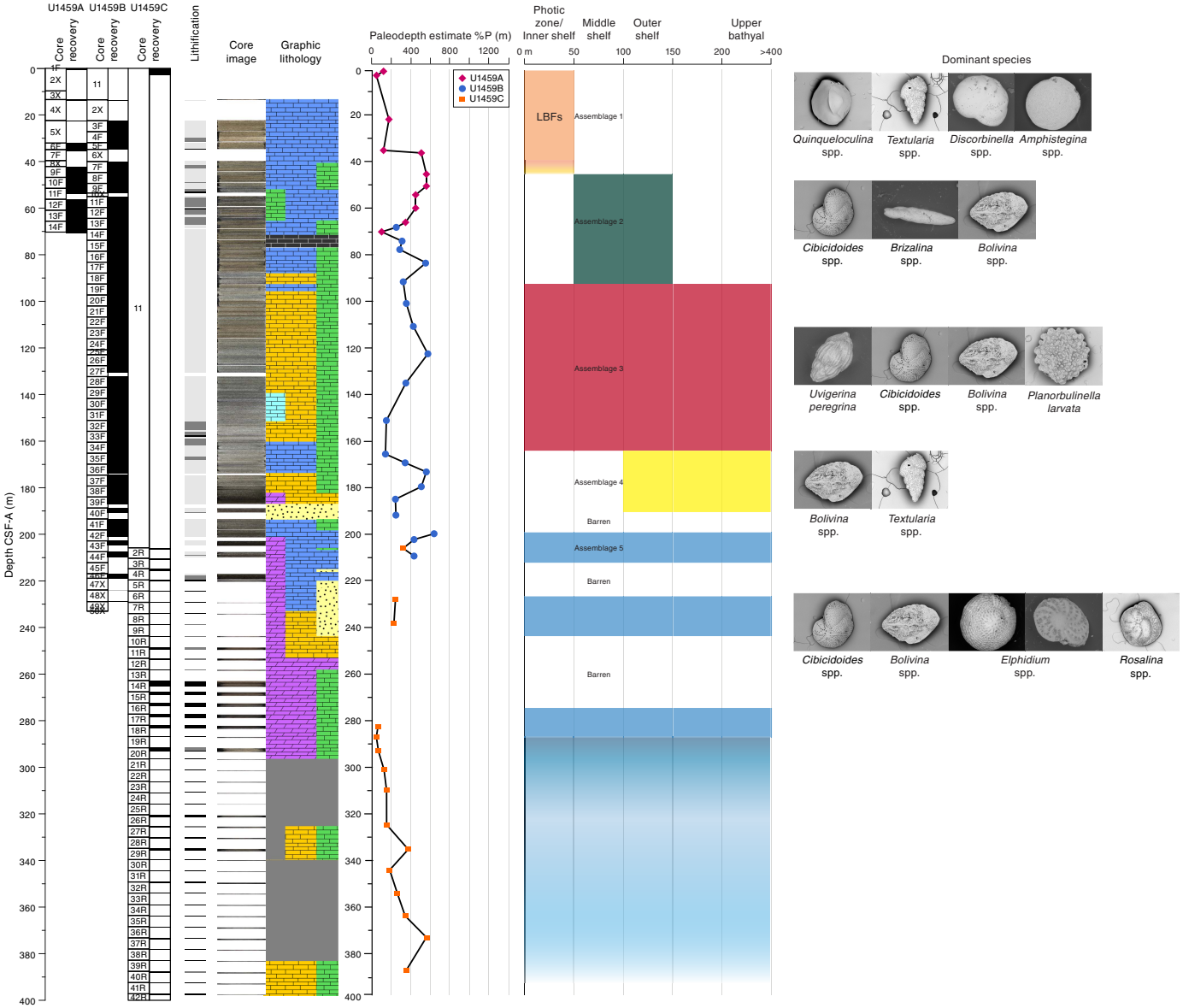

bradyi, *Textularia* spp., and *Melonis* spp. This assemblage has a very low diversity with only 1–11 species per sample, poor preservation, and typifies an outer shelf to upper bathyal paleodepth.

The fifth assemblage is present from Sample 356-U1459C-41R-CC (198.02 m CSF-A) to the base of Hole U1459C (387.68 m CSF-A) and is composed almost entirely of epifaunal species. The assemblage is dominated by *Cibicidoides* spp. and other epifaunal species. Preservation was poor throughout with only 2–11 species per sample due to the heavy dolomitization in this lowermost interval. Here, foraminiferal abundance was substantially reduced and the signal less clear, but dominant taxa would suggest a middle shelf to upper bathyal paleodepth with downslope transport (*Elphidium* spp.).

Overall paleodepth estimates range between 46 m (Core 356-U1459A-2F; 0.59 m CSF-A) and >570 m (Core 356-U1459B-25F; 122.9 m CSF-A) (Table **T10**; Figure **F25**). However, because of poor preservation within many of the samples, a reliable proportion of benthic versus planktonic foraminifers could not always be estimated.

Investigated benthic foraminiferal diversity and percentage for all holes at Site U1459 are illustrated in Figure **F27**.

Other microfossils

Other fossil groups present in the core catcher samples included ostracods, bryozoans, worm casings, and pteropods (Table **T10**).

Figure F26. Typical Eocene planktonic foraminifers in 356-U1459C-29R-CC through 40R-CC, including *Subbotina* sp., *Acarinina* sp., and *Globigerinatheka* sp.

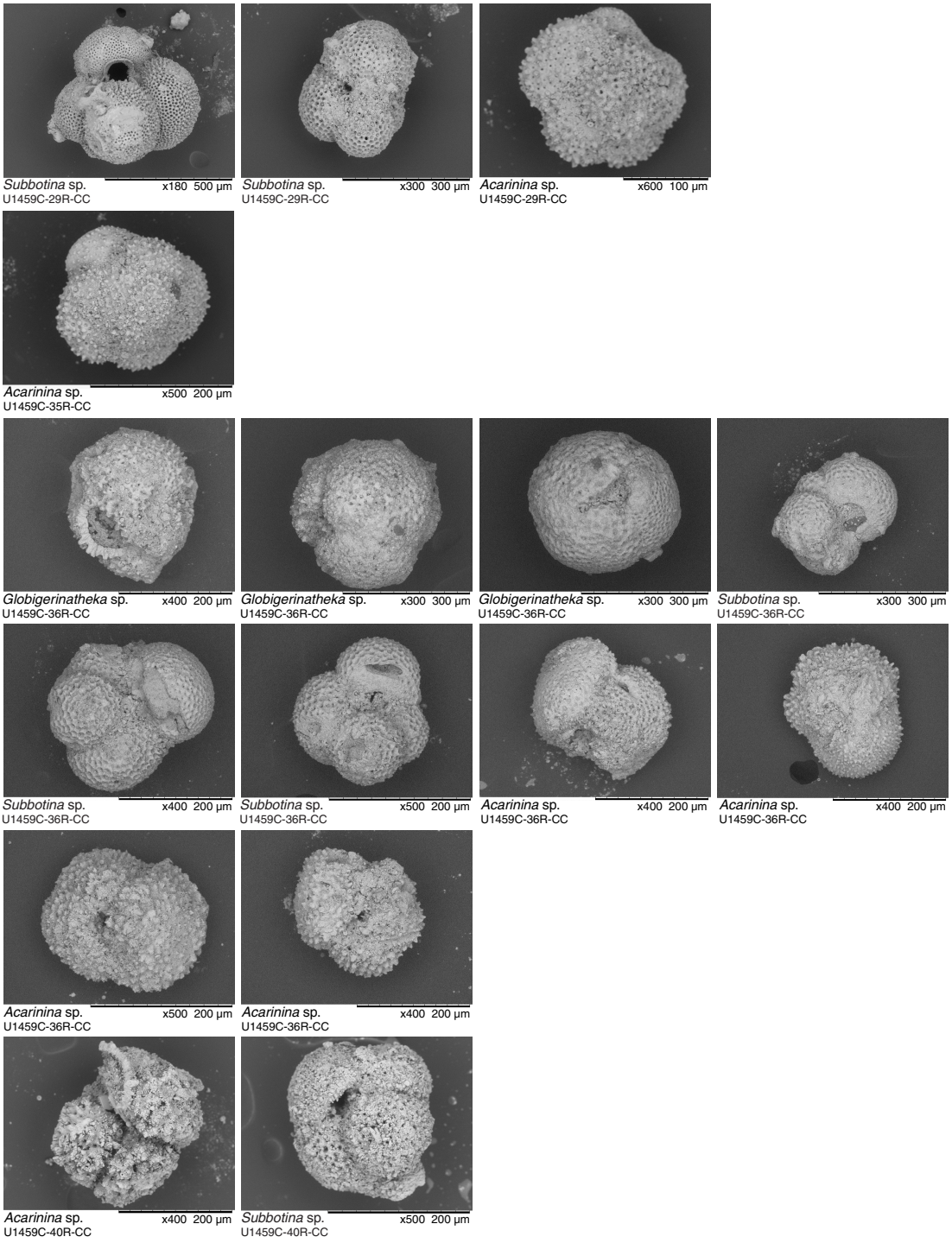

Table T12. Benthic foraminifer abundance, Site U1459. **Download table in .csv format.**

Figure F27. Benthic foraminifer diversity (number of species) and benthic percentage of total foraminifers, Site U1459. Analyzed samples from Holes U1459A–U1459C are combined by CSF-A.

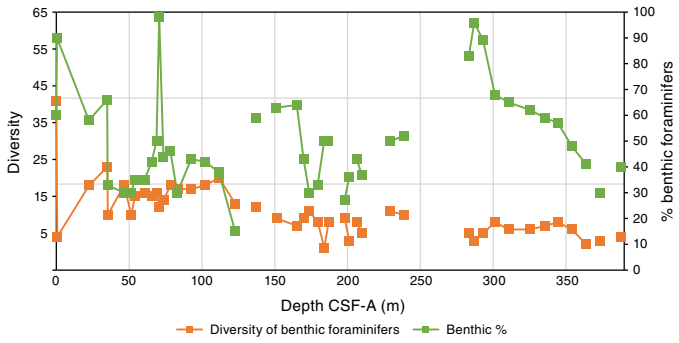

Geochemistry

At Site U1459, 63 samples were analyzed for headspace gas content, 20 samples (5 cm whole rounds) for interstitial water (IW) geochemistry measurements, 24 samples for carbonate, and 20 samples for total organic carbon (TOC) and total nitrogen (TN). Because chert and other lithified materials were recovered in Hole U1459C, no geochemical analyses were performed in this hole except for carbonate and headspace gas measurements, which were made when feasible. In general, the site is characterized by high calcium carbonate (mean = 88 wt%) and low TOC (mean = 0.53 wt%). Elevated salinity also characterizes the site, with values >37 deeper than 45 m CSF-A, reaching maximum values of 50 in the interval from 120 to 195 m CSF-A. Overall, many of the geochemical parameters measured exhibit a change in trend or slope at ~68 or ~120 m CSF-A.

Headspace gases

Headspace gas analysis for routine safety monitoring revealed the presence of methane in very low concentrations, with most samples containing <2 parts per million by volume (ppmv) (Figure **F28**; Table **T13**). One sample at 72 m CSF-A had slightly higher concentrations of ~6 ppmv; this sample was also the only sample that contained ethane (2.77 ppmv). No higher molecular weight hydrocarbons were detected.

Interstitial water geochemistry

Salinity at Site U1459 is 36 near the surface and gradually increases with depth to approximately 120 m CSF-A, where a value of 50 is reached (Figure **F29**). From 120 m CSF-A to the bottom of Hole U1459B, salinity values remain constant at 50. The elevated salinity at this site is notable. Alkalinity at the top of the section is 3.02 mM and displays an overall slight decreasing trend to 120 m CSF-A, where a value of 2.38 mM is noted. Subsequently, alkalinity increases with depth, reaching a maximum 4.65 mM at 183 m CSF-A before finally decreasing to 3.52 mM at the bottom of Hole U1459B. The range of pH values at Site U1459 is relatively small, from 7.5 to 7.7 (Figure **F29**). The highest pH occurs at the top of the hole, and an overall decreasing trend to lower pH values is noted to approximately 154 m CSF-A, which is followed by slightly increasing pH toward the bottom of Hole U1459B.

Bromide, calcium, chloride, magnesium, sulfate, potassium, and sodium all display increasing concentrations with increasing depth, with a change in slope noted at approximately 120 m CSF-A in most (Figure **F30**). Phosphate and ammonium do not follow this pattern; instead, their concentrations are both relatively constant with depth, with mean values of 76.6 and 2.6 µM, respectively (Figure **F30**). Phosphate concentrations were below the detection limit in several samples.

Iron and barium were present in IW samples at Site U1459 in low concentrations (Figure **F31**). In particular, iron concentrations of most samples were not above the detection limit with the excep-

Figure F28. Hydrocarbons in headspace gases, Site U1459.

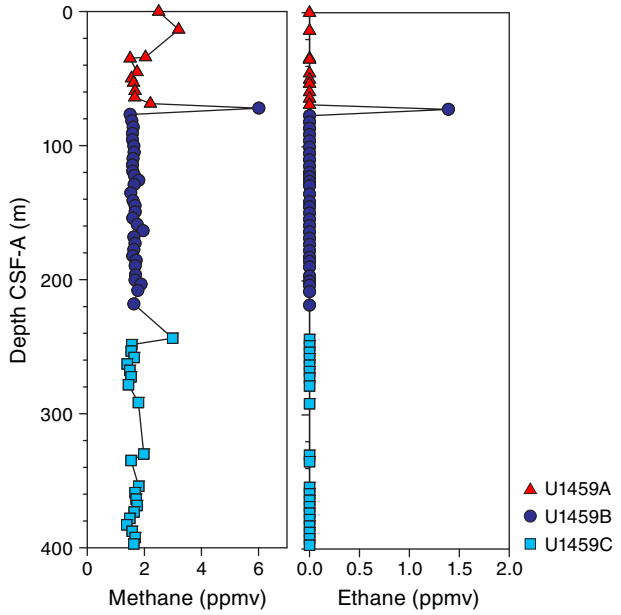

Table T13. Headspace gas contents, Site U1459. **Download table in .csv format.**

Figure F29. Alkalinity, pH, and salinity, Site U1459. Dashed line at 120 m denotes depth at which many of the measured geochemical parameters exhibit a change in trend or slope.

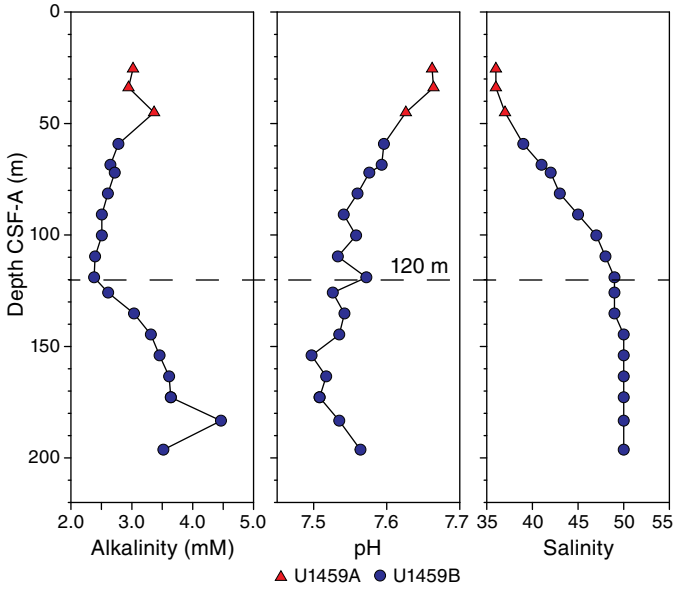

Figure F30. Major element interstitial water geochemistry (bromide, calcium, chloride, magnesium, sulfate, potassium, sodium, phosphate, and ammonium), Site U1459. Dashed line at 120 m denotes depth at which many of the measured geochemical parameters exhibit a change in trend or slope.

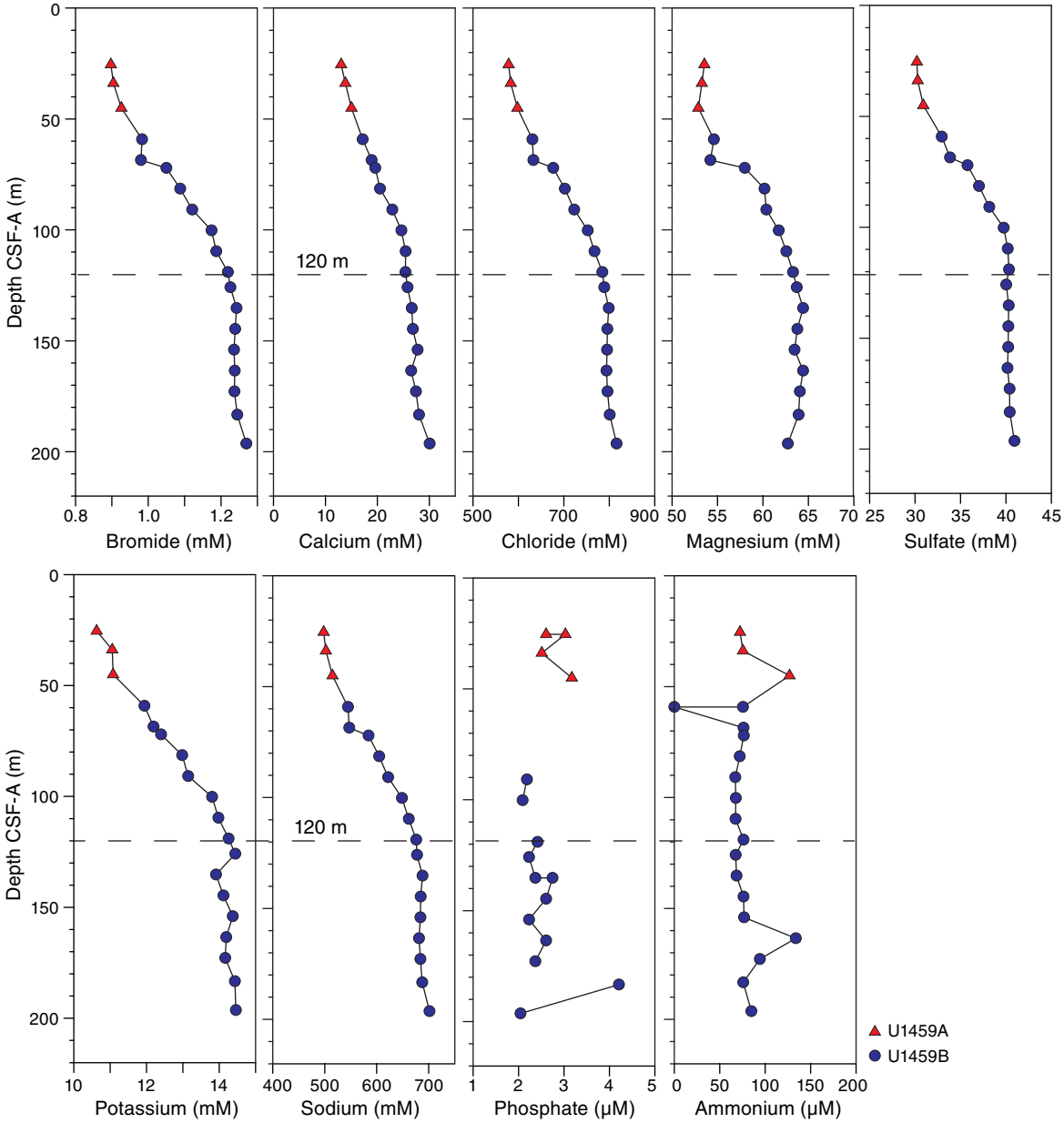

tion of two samples collected at 135 and 145 m CSF-A. This is well correlated with the lithostratigraphic Unit IV/Subunit Va boundary, showing association of increasing dolomite content (see **Lithostratigraphy**). Boron and lithium display similar downcore profiles with relatively rapidly increasing concentrations to approximately 68 m CSF-A, followed by relatively stable or slightly increasing values to the bottom of Hole U1459B. Strontium and silicon display the opposite profile to boron and lithium, with rapidly decreasing values noted in the upper ~68 m CSF-A followed by stable values deeper (Figure **F31**).

Bulk sediment geochemistry

Calcium carbonate content at Site U1459 is high and ranges from 65 to 97 wt% with a mean value of ~90 wt% (Figure **F32**). Generally, sediments in the interval from 150 to 220 m CSF-A contain lower and more variable calcium carbonate values, which are related to Subunits Va and Vb (see **Lithostratigraphy**). TOC ranges from 0.17 to 0.72 wt% with a mean of 0.53 wt% (Figure **F32**); one outlier at 100 m CSF-A was removed because it yielded a negative TOC value. TN is low, ranging from 0.002 to 0.016 wt% with a mean of 0.008 wt%, and was below detection limit in half of the samples analyzed.

Figure F31. Minor element interstitial water geochemistry (boron, barium, iron, lithium, strontium, and silicon), Site U1459. Horizontal dashed line at 68 m denotes depth at which many of the plotted geochemical parameters exhibit a change in trend or slope.

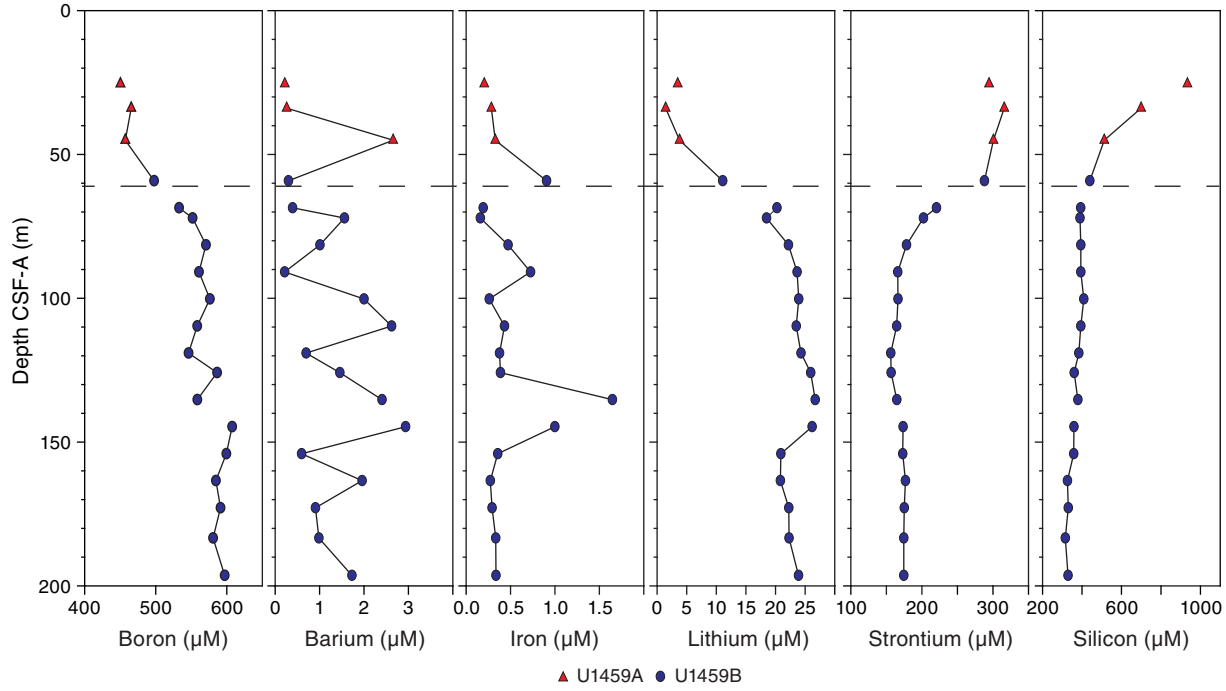

Figure F32. Bulk sediment geochemistry (calcium carbonate, TOC, and TN), Site U1459.

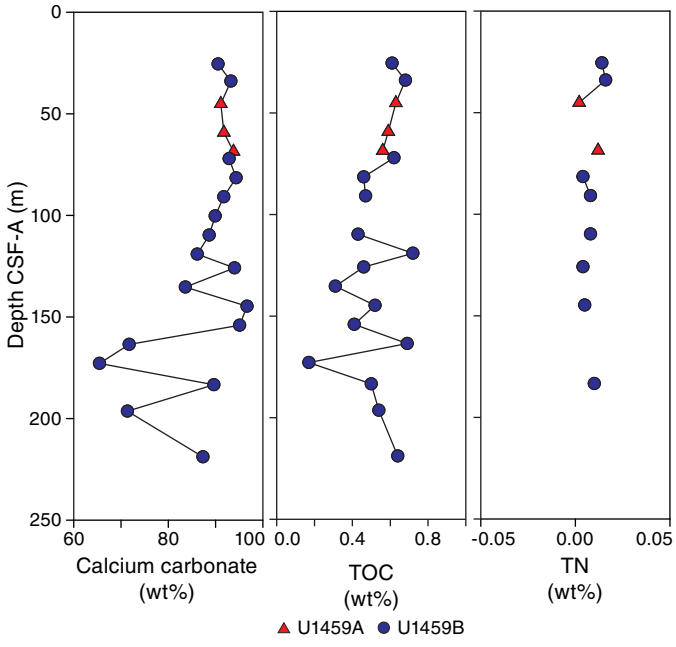

Paleomagnetism

Paleomagnetic investigations at Site U1459 included routine measurements and partial demagnetization of natural remanent magnetization (NRM) of archive-half sections and selected discrete samples from working-half sections. Isothermal remanent magnetization (IRM) acquisition curves were applied for selected samples, and a cumulative log-Gaussian (CLG) curve (Kruiver et al., 2001) was fit with three components for Sample 356-U1459A-2X-CC, which exhibited higher coercivity. Two of the components indicated low magnetic coercivity behavior, indicative of granulometric distribution related to multidomain (MD) magnetite grains.

Although it is not possible to correlate Hole U1459B SRM results reliably with the geomagnetic polarity timescale (GPTS), we found evidence for three peaks of negative magnetic inclination (corresponding to normal polarity) and changes in intensity values around 130 and 140 m CSF-A and a peak of positive magnetic inclination (reversed polarity) around 150 m CSF-A. Intensity values of the sediments from 130 to 150 m CSF-A reached 10^{-2} A/m after alternating field (AF) demagnetization with peak fields of 20 and 30 mT; however, sediments from the rest of the hole were much weaker (~10^{-5} A/m). Based on nannofossil ages at ~110 m CSF-A, the polarity features may be older than 3.7 Ma and may correspond to the three normal polarity intervals from the middle to the top of Chron C3n (C3n.1n, C3n.2n, and C3n.3n) and Subchron C2Ar. However, definitive magnetostratigraphic interpretations cannot be made using this data due to its quality within most of the hole.

Archive-half measurements

NRM measurements on archive-half core sections from the uppermost 81.5 m of Hole U1459B were performed with AF demagnetization steps of 10, 20, and 30 mT at 10 cm resolution. Based on the overall stability of the single magnetic component that was observed by means of principal component analysis (PCA) (Figure **F33**) while accommodating core flow, remaining demagnetization procedures were limited to a peak field of 20 mT. The upper 215 m of Hole U1459B (cored with the HLAPC) was measured (138 sections). Because this section was cored with the HLAPC, the material was unoriented and thus declinations were not used for

Figure F33. AF demagnetization results from archive-half SRM measurements at 3 depths, Hole U1459B. Orthogonal projections (Zijderveld diagram), equal area projections, and demagnetization behavior plots show NRM data measured after each demagnetization treatment. Equal area projection: solid circles = positive inclination, open circles = negative inclination. Orthogonal projection (Zijderveld diagram): solid squares = declination data with *x*- and *y*-axes corresponding to the four cardinal directions, open squares = inclination data with *y*-axis corresponding to up–down and *x*-axis corresponding to north–south. PCA analysis: Horizontal = declination (D), vertical = inclination (I), MAD = maximum angular deviation.

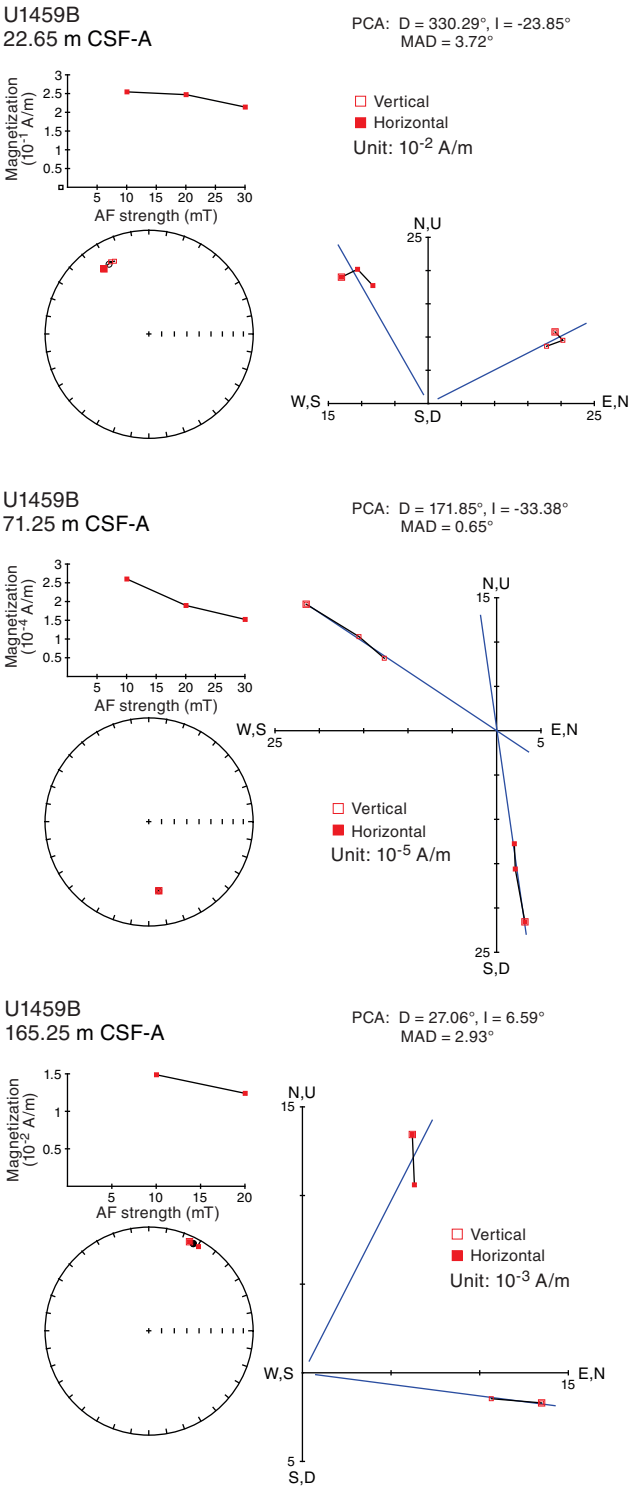

magnetostratigraphic interpretation. As a result of low core recovery and data quality, it was not possible to construct a dependable magnetostratigraphy for Hole U1459A.

Discrete sample measurements

We collected one to three discrete cube samples (see **Paleomagnetism** in the Expedition 356 methods chapter [Gallagher et al., 2017]) per core from Cores 356-U1459A-2X through 14F, depending on recovery and core conditions. Of those taken, samples from Cores 2X, 4X, 7F, 10F, and 14F were measured. Stepwise AF demagnetization on these five discrete samples (Figure **F34**) collected from Hole U1459A was performed at successive peak fields of 0 to 180 mT (steps of 10 mT) using the D-2000 AF demagnetizer (ASC Scientific) to verify the reliability of the split-core measurements and to determine the demagnetization behavior of the recovered sediments. Following each demagnetization step, remanence magnetization was measured with the JR-6A spinner magnetometer and analyzed using Remasoft (version 3.0; Agico, Inc.) software (see **Paleomagnetism** in the Expedition 356 methods chapter [Gallagher et al., 2017]).

One of the samples (356-U1459A-2X-CC, 15–17 cm; 0.62 m CSF-A) exhibited singular behavior with higher coercivity than all other samples. To provide a better constraint on the magnetic coercivity content, which may be present in discrete samples, we generated IRM acquisition curves from representative samples using an IM-10 impulse magnetizer (ASC Scientific). Magnetization was induced in different field steps (0 mT to a field peak of ~1200 mT) along the *z*-axis of discrete samples, which were previously demagnetized at 180 mT. At each step, induced magnetization was measured using the JR-6A spinner magnetometer. Because the grain-size distributions for minerals in natural magnetic assemblages are logarithmic, the IRM curves for individual magnetic phases add linearly, hence yielding a cumulative curve that can be interpreted by a CLG function (Robertson and France, 1994). A CLG curve was fit with three components by the method proposed by Kruiver et al. (2001) for Sample 356-U1459A-2X-CC, 15–17 cm (Figure **F35**). Two of the components exhibit low-magnetic coercivity behavior, with saturation IRM (SIRM) between 100 and 200 mT, and reached ~66% of the highest applied field (~1220 mT), which can be indicative of granulometric distribution related to magnetite. Both components showed dispersion parameter values of ~0.3 that, as discussed by Robertson and France (1994), is often characteristic of MD magnetite grains. Unfortunately, the IM-10 impulse magnetizer cannot induce fields much larger than 1.2 T, so it is not possible to unequivocally identify the presence of hematite. As discussed by Peters and Thompson (1998), natural samples of hematite are difficult to magnetize because hematite resists magnetic induction and does not exhibit saturation even at fields around 1 T.

Magnetostratigraphy

In Hole U1459B, the sediments exhibited residual NRM intensity values ranging from 10^{-2} to 10^{-5} A/m after AF demagnetization with peak fields of 20 and 30 mT (Figure **F36**). Higher intensity peak values (~1 A/m) were observed throughout the whole succession and can be related to a pervasive drilling-induced magnetization that is commonly encountered (e.g., Gee et al., 1989). Because of the nature of the unlithified sediments and the lack of consistent information from rock magnetism measurements, it is not possible to correlate our results reliably with the GPTS for the last 8 My. However, there are two intervals where magnetostratigraphically signifi-

Figure F34. AF demagnetization results for discrete samples at 3 depths, Holes U1459B and Hole U1459A. Orthogonal projection (Zijderveld diagram) and equal area projection of NRM vector measured after each demagnetization treatment. Horizontal = declination, vertical = inclination. Equal area projection: solid circles = positive inclination, open circles = negative inclination. Normalized magnetization behavior plots show highest magnetization intensity (M_{max}) = 1 on *y*-axis with AF demagnetization strengths shown after each measurement on *x*-axis.

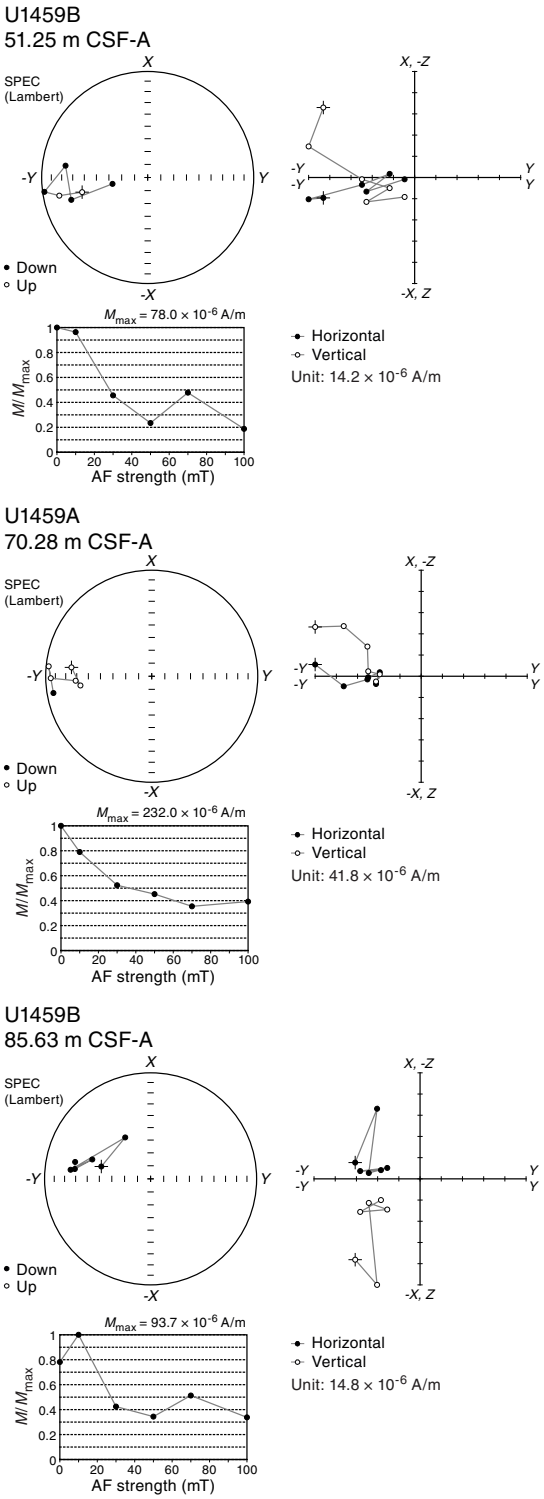

Figure F35. CLG analysis of IRM curve from one discrete sample (356-U1459A-2X-CC). LAP = linear acquisition plot, GAP = gradient acquisition plot, SAP = standardized acquisition plot.

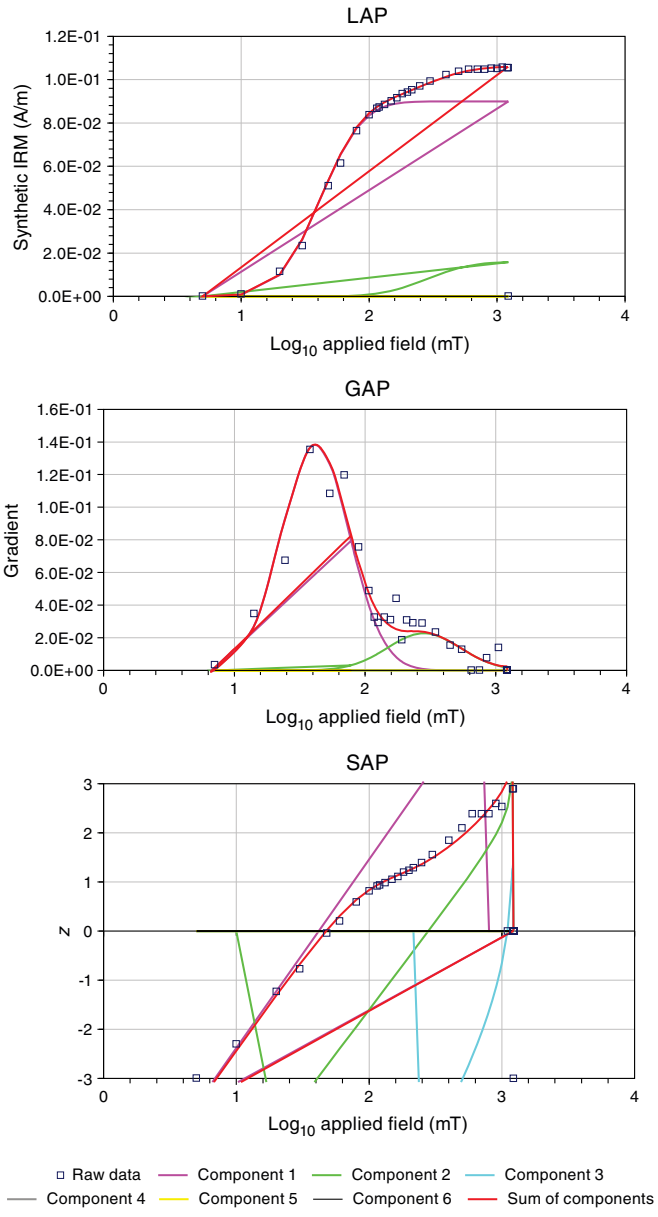

cant patterns may be interpreted: (1) three peaks of negative magnetic inclination (corresponding to normal polarity) and changes of intensity values at around 130 and 140 m CSF-A and (2) peaks of positive magnetic inclination (reversed polarity) at around 150 m CSF-A. Based on identification of the top of calcareous nannofossil *R. pseudoumbilicus* (see **Biostratigraphy and micropaleontology**) at ~110 m CSF-A, the polarity features may be older than 3.7 Ma and correspond to the three normal polarity intervals from the middle to the top of Chron C3n (C3n.1n, C3n.2n, and C3n.3n) and Subchron C2Ar, although further biostratigraphic data are needed to confirm these interpretations.

Figure F36. Magnetostratigraphic data set, Hole U1459B. Magnetic inclination and intensity from AF demagnetization measurements of archive-half sections after background and tray correction with polarity interval correlations (black = normal, white = reversed, gray = unidentified).

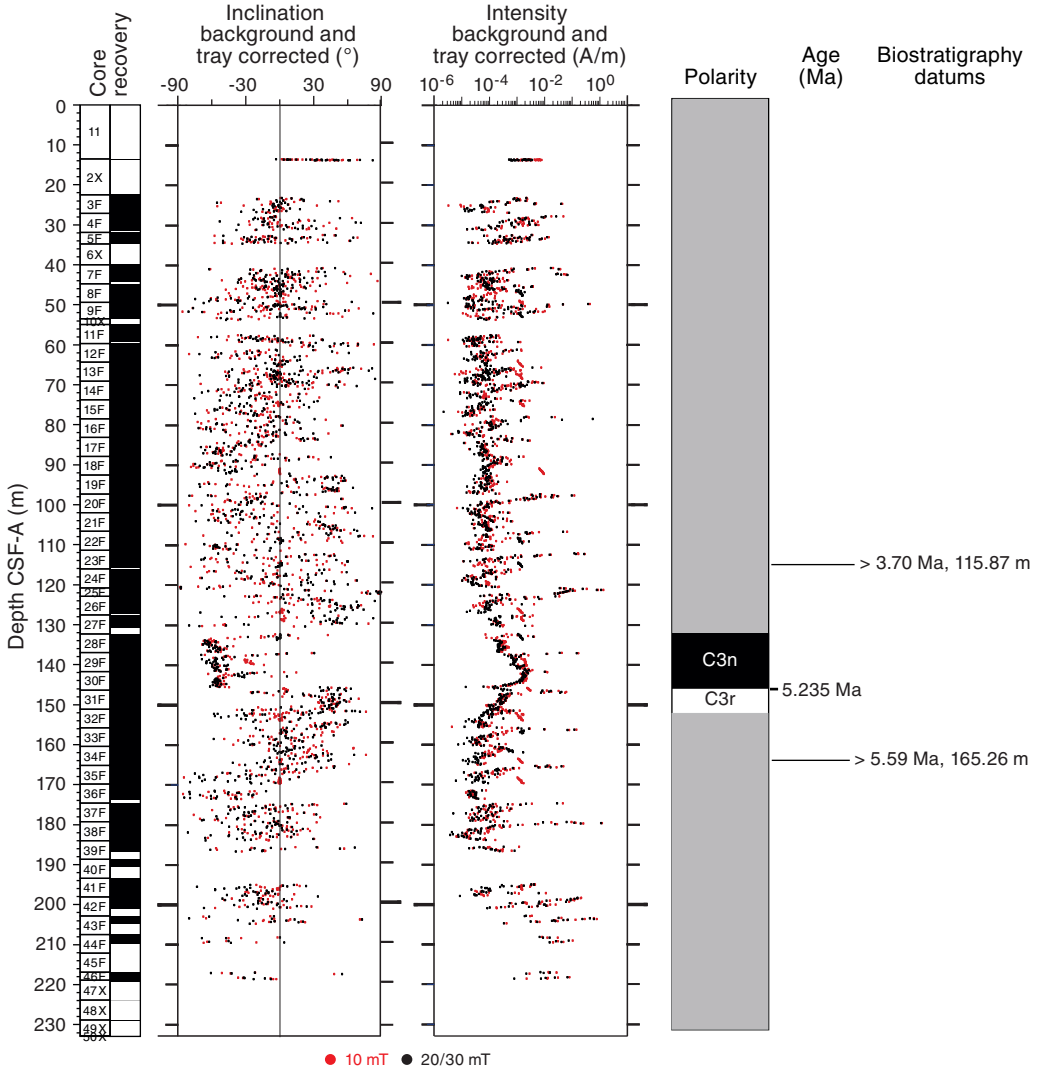

Physical properties

At Site U1459, physical properties measurements were carried out using the Whole-Round Multisensor Logger (WRMSL), NGR Logger, *P*-wave velocity caliper, and discrete sampling. Thermal conductivity was measured in several sections and varied between 1.0 and 1.3 W/(m·K). Bulk density was determined using both gamma ray attenuation (GRA) and moisture and density (MAD). These two methods yielded consistent results. The magnetic susceptibility (MS) of the recovered sediments was low, with most readings ranging between −2 and 4 SI. The MS data showed a rising trend from 80 to 140 m CSF-A corresponding to an overall decrease in NGR. NGR also showed several distinct peaks. These peaks proved to be of value for stratigraphic correlation between different holes. *P*-wave sonic velocities measured at depths shallower than 200 m CSF-A on whole-round cores and discrete samples compare well. In the upper 200 m interval, velocities are typically <2000 m/s. Deeper, *P*-wave velocities show high values, up to 6257 m/s. These high values were obtained from lithified sediment, including cherts and dolomitic cobbles. Reflectance spectroscopy and colorimetry data display high-amplitude variability, consistent with notable color changes in the sediments. Porosity was generally high, ranging between 50% and 60% to 120 m CSF-A. Further downcore, porosity decreased to a minimum of 35% at 208.5 m CSF-A.

Magnetic susceptibility

Recovery from the uppermost section (0–22.5 m CSF-A) was limited. The recovered material consisted of lithified grainstone to rudstone cobbles. Deeper in Holes U1459A and U1459B, MS, as measured by the WRMSL, shows a decreasing trend from ~22 to 35 m CSF-A in Hole U1459B (Figure **F37**). After a coring gap of about 7 m in Hole U1459A and about 5 m in Hole U1459B, MS shows some scatter and an overall decrease to the bottom of Hole U1459A and to ~80 m CSF-A in Hole U1459B. In Hole U1459B, this is followed by a rising trend to ~140 m CSF-A. Deeper, two cycles of rapid increase followed by a slow decrease are noted between 140 and 180 m CSF-A. A third such cycle is suggested by data from 180 to 210 m CSF-A in Hole U1459B, but poor recovery makes this lowermost portion of the core difficult to interpret. In the interval between 210 and 400 m CSF-A in Hole U1459C, MS values remain close to 0 SI, with considerable scatter between −4 and +4 SI. However, the recovered material was only within the most lithified por-

Figure F37. Color reflectance ratios (L*, a*, and b*, see **Physical properties** in the Expedition 356 methods chapter [Gallagher et al., 2017] for definition), MS, and NGR results, Site U1459.

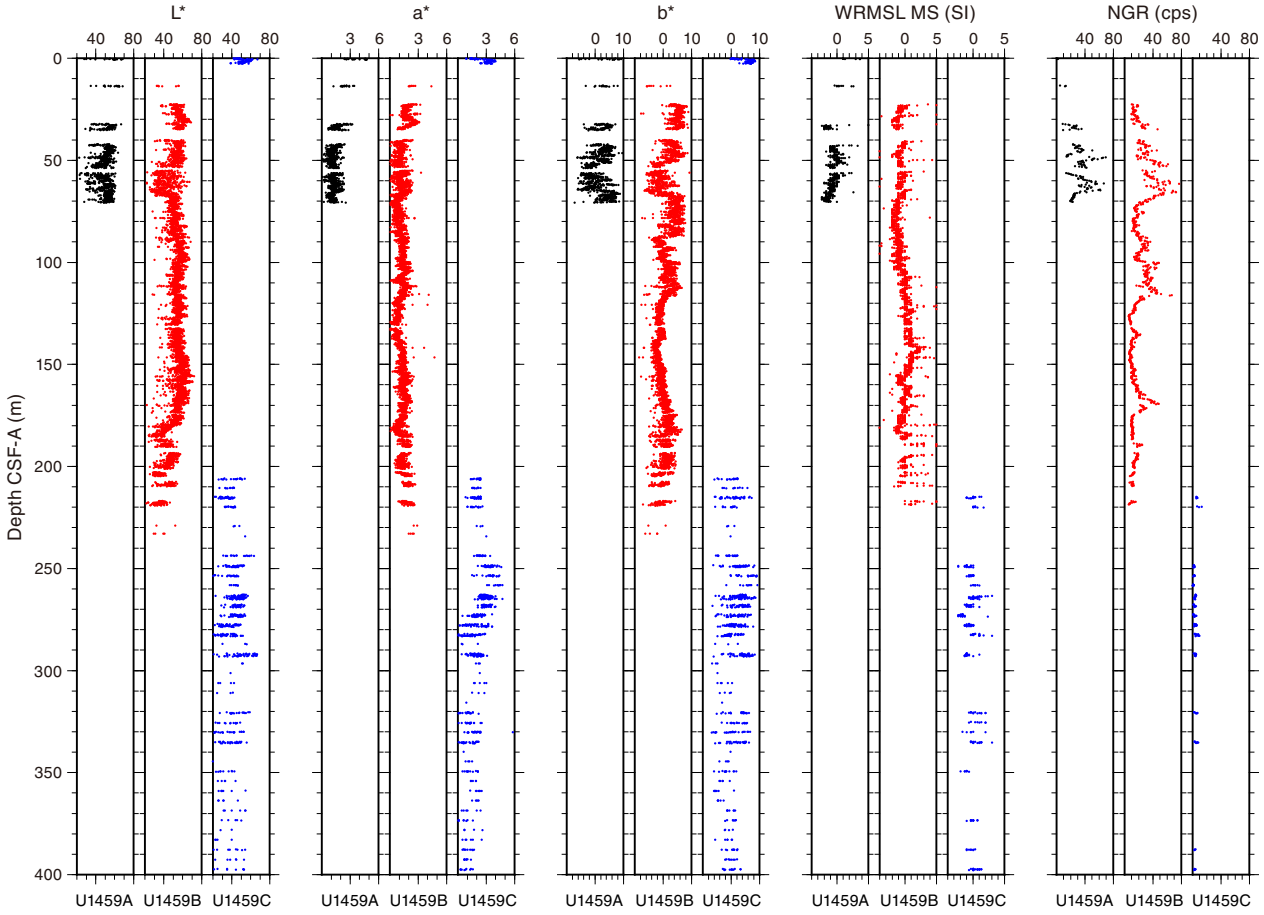

tion of the formation(s), so our data are discontinuous and cannot be considered representative of the entire section.

MS was measured a second time on the archive halves (point magnetic susceptibility [MSP]). These measurements were taken at the fast and low precision (one individual measurement) instrument settings, corresponding to measurement times of about 1 s. This setting resulted in poor data resolution that cannot be compared to the WRMSL data.

Natural gamma radiation

NGR counts obtained from cores showed several distinct peaks that are valuable for correlation between Holes U1459A and U1459B, Hole U1459C downhole logging data, and logs from nearby oil exploration wells. Peaks in NGR occur at 48.5, 61, and 64.5 m CSF-A in Hole U1459A and at 65, 100, and 170 m CSF-A in Hole U1459B (Figure **F37**). These distinct features are used in cross-correlating Hole U1459A with Hole U1459B (see **Stratigraphic correlation**). Between 210 and 400 m CSF-A (Hole U1459C), NGR counts were very low. These low counts were also seen in the limited overlapping sediments in Hole U1459B. However, what was recovered in Hole U1459C was only the most lithified portion of the formations, so our data are discontinuous and cannot be considered representative of the formation(s) drilled in Hole U1459C.

P-wave velocity

P-wave velocities were measured on Hole U1459A using the WRMSL. Whole-core *P*-wave data were not reported for Holes U1459B and U1459C because of instrument malfunction and results that were outside the accepted velocity range. Discrete samples were measured on the split cores and a few MAD samples from each hole. The discrete sampling resolution varied between one per core and one every other core; as we advanced ~5 m with each recovered core, this resulted in a resolution of every ~10 m. Comparison with the whole-round data from Hole U1459A showed excellent agreement between discrete and WRMSL results. Thus, despite the lack of WRMSL *P*-wave data on Holes U1459B and U1459C, we have good data from the discrete measurements. In Hole U1459B, *P*-wave velocities are mostly <2000 m/s throughout the cores (Figure **F38**). However, two discrete sample cubes were taken from indurated cobbles at ~60 and ~49 m CSF-A in Holes U1459B and U1459A, respectively. These cemented samples show considerably higher *P*-wave velocities, in excess of 2000 m/s and as high as 3000 m/s. At the base of Hole U1459B and throughout Hole U1459C, only lithified samples were recovered and measured for their *P*-wave velocities. The result is a bimodal distribution of *P*-wave velocities, with lower velocities of 2000–3000 m/s corresponding to lithified dolomite and calcite cobbles. Higher velocities (up to 6257 m/s) correspond to cherts or completely recrystallized dolomite.

Figure F38. Bulk density, grain density, porosity, and *P*-wave velocity, Site U1459. Dots = WRMSL, squares = discrete samples.

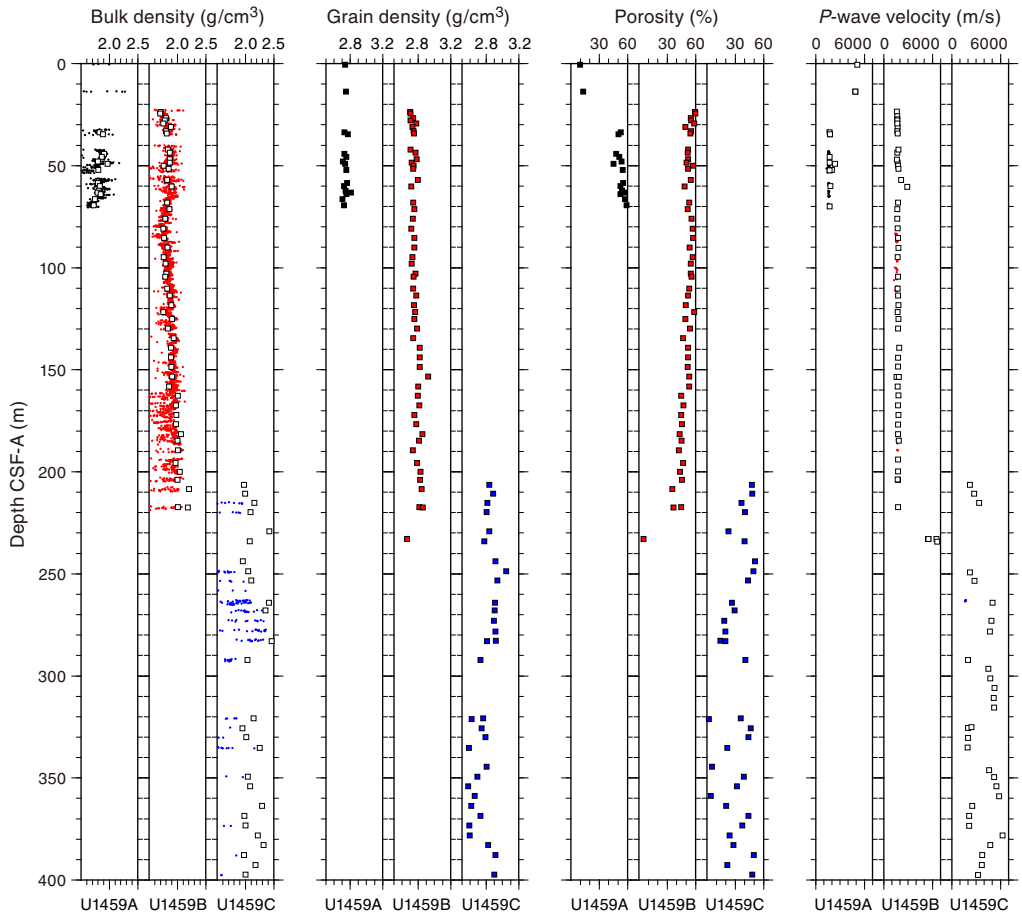

Several experiments were performed on the lithified cube samples from two cores from Holes U1459A and U1459B. A cemented rudstone from Section 356-U1459A-4X-1 and a cemented dolomite from Section 356-U1459B-50X-CC were sampled. Seismic velocity was measured in three directions shortly after sampling and again after sitting in a bath of seawater for 24 h under a vacuum. *P*-wave velocities of the rudstone increased by 0.2%–2% and decreased by 1%, depending on the axis measured (see Table **T14**, not shown on Figure **F38**). *P*-wave velocities of the dolomite decreased slightly in the *x*-direction but increased by 1.2%–3% in the other two axes. If the point of soaking the sample in the seawater bath is to replace any lost water, then we would expect an increase in *P*-wave velocity after soaking for 24 h. However, the velocities generally decrease after soaking but only by a small percentage. These lithified samples show little change in their sonic velocities after drying. The dry velocities decreased in the rudstone by 4.9%–6.5% compared to the soaked wet velocities. An accurate reading of the wet velocities is critical. However, it appears that measurements taken shorty after sampling are at least as accurate as those taken after 24 h immersion under a vacuum.

Table T14. *P*-wave velocity, Site U1459. Impact of soaking lithified samples in a seawater bath. Measurements were made on discrete cubes in 3 states: wet sample = cube sampled from core, SW bath = cube soaked in seawater for 24 h after sampling, dry = cube oven dried at 104°C for at least 24 h before measuring. Ratio shows percent change from the previous state. An increase in velocity is positive. **Download table in .csv format.**

Hole, core, section	State	*x* (m/s)	*y* (m/s)	*z* (m/s)
356-				
U1459A-4X	Wet sample	4867	4746	4564
U1459A-4X	SW bath	4877	4840	4517
U1459A-4X	Ratio	0.21%	1.98%	–1.03%
U1459A-4X	Dry	4563	4585	4294
U1459A-4X	Ratio	–6.44%	–5.27%	–4.94%
U1459B-50X-CC	Wet sample	5523	5225	5628
U1459B-50X-CC	SW bath	5503	5290	5810
U1459B-50X-CC	Ratio	–0.36%	1.24%	3.23%
U1459B-50X-CC	Dry	5312	5078	5422
U1459B-50X-CC	Ratio	–3.47%	–4.01%	–6.68%

Gamma ray attenuation

GRA, measured every 5 cm on the WRMSL, was used to estimate bulk density. GRA increases with depth from 20 to 40 m CSF-A in Hole U1459B (Figure **F38**). Two cycles of decreasing bulk density with depth are seen between 40 and 56 m CSF-A and between 55 and 70 m CSF-A in Holes U1459A and U1459B, respectively. Beginning at 80 m CSF-A in Hole U1459B, there is a slow increase in density with depth to the base of the hole. However, variability in GRA values increases with depth beginning at ~160 m CSF-A. In

Hole U1459C, GRA bulk density values are quite variable. Considering that these measurements were done on cobbles within an air-filled core liner, these measurements cannot be interpreted.

Moisture and density

Discrete samples were obtained from the core at an interval of one or two samples per core. These were generally taken from the middle of the core where evidence of disturbance was low and where smear slides were also taken (see **Lithostratigraphy**). The discrete bulk density measurements compare very well to the GRA estimates of bulk density in both Holes U1459A and U1459B (Figure **F38**). Deeper than ~160 m CSF-A in Hole U1459B, where the GRA bulk densities are variable, the discrete results correspond to the higher GRA bulk density estimates.

In Hole U1459A, discrete bulk densities show the two cycles of decreasing density between 40 and 70 m CSF-A. However, these two cycles are not seen in Hole U1459B.

Discrete measurements of grain densities also show a trend of increasing values with depth beginning at ~80 m CSF-A in Hole U1459B. Because of the high carbonate contents of the sediment, this increase in grain density may reflect increasing diagenesis and generation of dolomite from calcite.

Throughout the cored interval, porosity values have a wide range between 10% and 60%. Porosity decreases with depth beginning at ~50 m CSF-A in Hole U1459B. Porosity drops to 35% at 208.5 m CSF-A. Shallower than 50 m CSF-A, porosity ranges between 50% and 60%. Exceptions are several lithified rocks (rudstones in Hole U1459A and dolomite in Hole U1459B), which have low porosity (<20%). In Hole U1459C, the lithified cobbles result in variable porosity values that range between 50% and <10%. The very low values correspond to chert samples, whereas the higher values reflect different degrees of cobble cementation.

Several experiments were performed on lithified cube samples. A cemented rudstone from Section 356-U1459A-2X-CC and a cemented dolomite from Section 356-U1459B-50X-CC were sampled as cubes. They were weighed shortly after sampling and reweighed after sitting in a bath of seawater for 24 h under a vacuum (Table **T15**). The rudstone decreased in weight by 0.23% after 24 h, whereas the dolomite increased in weight by 0.14%. Since the cube needed to be patted dry before weighing, we suggest that these small differences may be attributed to different amounts of water adhering to the outside of the cube. In short, we did not find that 24 h of soaking significantly changed the weight of lithified samples.

Reflectance spectroscopy and colorimetry

The upper portions of Holes U1459A and U1459B (0–22.5 m CSF-A) display reflectance spectroscopy and colorimetry data that are widely scattered over short stratigraphic intervals (Figure **F37**). Deeper in Holes U1459A and U1459B, reflectance spectroscopy and colorimetry data show well-developed cyclicity, which proved useful for stratigraphic correlation between holes (see **Stratigraphic correlation**). Between 34 and 54 m CSF-A in both Holes U1459A and U1459B, decreasing L* and b* values indicate that sediments become gradually darker with depth. Between 50 and 70 m CSF-A, variability in L* and b* is at a maximum because of the alternation of pronounced dark layers and beige layers. These lithologic alternations are similar and occur close to the same depth in both Holes U1459A and U1459B (see **Lithostratigraphy**). For example, the same dark layer occurs at 64.3 m CSF-A in U1459A and 65.0 m CSF-A in U1459B. In the interval between 70 and 85 m CSF-A in Hole U1459B, the sediment is characterized by high b* and intermediate L* values. At 85 m CSF-A, b* values drop sharply and recover slowly to 115 m CSF-A. This sudden color change is not present in either L* or a*. Between 115 and 125 m CSF-A, b* decreases again, accompanied by a more gradual drop in a*. Deeper, the color indexes are relatively stable until 135 m CSF-A, at which depth all three color indexes show a rising trend to 160 m CSF-A (a* and L*) and 180 m CSF-A (b*). A peak in redness and yellowness (high a* and b*) occurs between 250 and 265 m CSF-A (Hole U1459C). Deeper in the section, these values decrease until 280 m CSF-A, thereafter remaining relatively constant through the deeper portion of Hole U1459C.

Table T15. Impact on sample weight of soaking lithified cube samples in a seawater bath, Site U1459. Measurements were made on discrete cubes in two states: wet sample = sampled directly from core, SW bath = cube soaked in seawater for 24 h after sampling. Ratio shows the percent change in weight. An increase in weight is positive. **Download table in .csv format.**

Hole, core, section	State	Weight (g)
356-		
U1459A-2X-CC	Wet sample	19.851
U1459A-2X-CC	SW bath	19.805
U1459A-2X-CC	Ratio	–0.23%
U1459B-50X-CC	Wet sample	21.385
U1459B-50X-CC	SW bath	21.416
U1459B-50X-CC	Ratio	0.14%

Thermal conductivity

Thermal conductivity measurements were taken on six whole-round core sections from Hole U1459A and 5 from Hole U1459B. Results were variable and ranged from 1.0 to 1.3 W/(m·K) with means of 1.13 W/(m·K) in Hole U1459A and 1.18 W/(m·K) in Hole U1459B (Figure **F39**). Thermal conductivity measurements were not taken deeper than 60 m CSF-A in Hole U1459B because readings became unreliable. Thermal conductivity measurements were not assessed in Hole U1459C.

Discrete stress measurement

Discrete measurements of shear and normal stress were taken in Hole U1459B from Core 356-U1459B-21F onward. The measurements were taken where the sediments were soft enough to use the handheld Torvane and the pocket penetrometer. No stress measurements were conducted on Hole U1459C cores, as the recovered material from this hole was lithified. The penetrometer data were variable with a wider range between 100 and 150 m CSF-A than between 150 m CSF-A and the bottom of Hole U1459B (deepest measurement at 217.4 m CSF-A). Shear strength measurements are also variable throughout Hole U1459B (Figure **F39**). A comparison between these two measures of strength yields a correlation coefficient of 0.45, suggesting that there is some relationship between the two.

Figure F39. Thermal conductivity, penetrometer, and shear strength results, Site U1459.

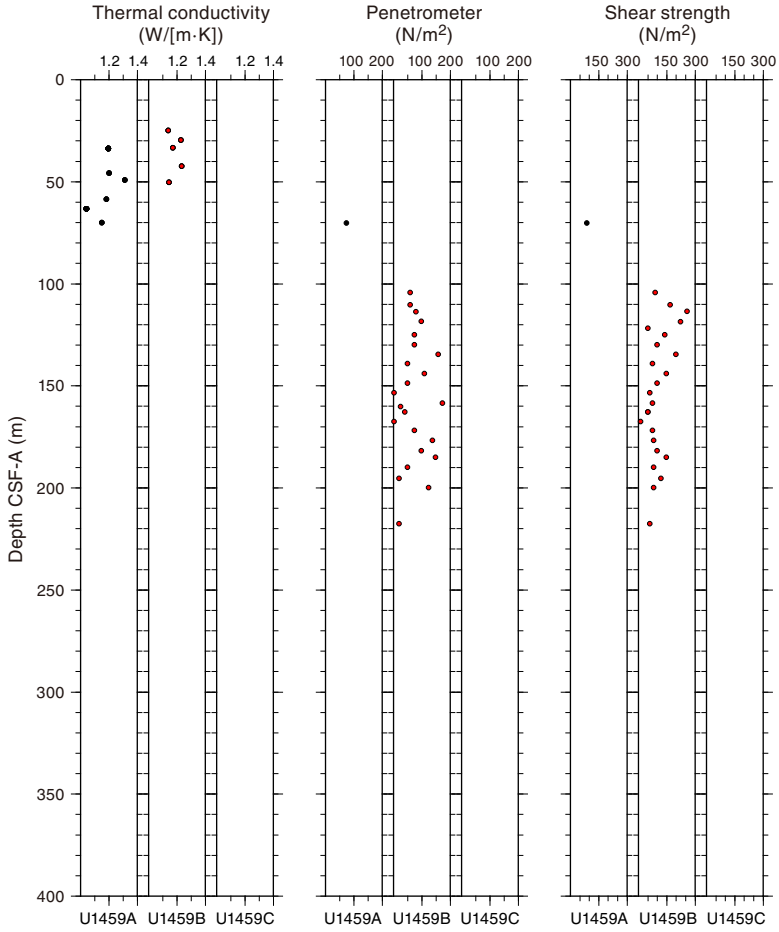

Downhole measurements

Downhole measurements in Hole U1459C were successful and consisted of runs with the triple combo and FMS-sonic tool strings. Because of safety concerns, the triple combo tool string was deployed downhole with a reduced configuration (without the porosity and density tools). Using the triple combo, we measured borehole width, total spectral gamma ray (HSGR), and MS from the seabed to 390 m wireline log matched depth below seafloor (WMSF) (i.e., 10 m above the bottom of the hole) with the drill pipe at 72.2 m WMSF. Two up and down passes were made with this tool (see **Operations**). The FMS-sonic tool failed to deploy deeper than 288 m WMSF. No downhole temperature measurements using the advanced piston corer temperature tool (APCT-3) were attempted at Site U1459.

Depth matching

The preprocessed logs were sent to the Borehole Research Group at Lamont-Doherty Earth Observatory where the logs were processed on shore before sending the processed logs back to the ship during Expedition 356. The wireline logs were depth matched during this processing. The preprocessed logs were first shifted to the seafloor (–205 m), which was determined by the step in gamma ray values observed on the triple combo main run at 205 m. This differed by 2 m from the seafloor depth of 203 meters below rig floor (mbrf) determined by the drillers. The depth-shifted logs were then depth matched to the HSGR log from the main pass of the triple combo. We consider that there is at least a 2 m discrepancy between core depths (CSF-A) and wireline logging depths (WMSF). In the discussion below, we refer to all logs in WMSF and all cores in CSF-A, realizing that the match between the two is only approximate within several meters.

Natural gamma radiation

The HSGR logs obtained with a reduced triple combo tool string showed good agreement with the NGR data obtained on whole-round cores from Hole U1459B. Many NGR peaks and troughs observed in Hole U1459B cores were reproduced in the Hole U1459C downhole log (Figure **F40**), disregarding the uppermost 72.2 m where the HSGR signal is attenuated because of the drill pipe. The five-window spectroscopy of the HSGR tool allows the approximate concentrations of uranium (U), thorium (Th), and potassium (K) to be determined. These data showed that the large peaks in HSGR in the upper 150 m (lithostratigraphic Units III and IV) of Hole U1459C were mainly driven by variations in U content. The HSGR peak in the downhole logging data at 160 m WMSF corresponds to the observed NGR peak in Hole U1459B cores at 168 m CSF-A. This peak was the result of increased concentrations of both U and K, and, to a lesser extent, Th. The HSGR peak in the downhole logging data at 185 m WMSF corresponds to the NGR peak in Hole U1459B cores at 192 m CSF-A, despite the higher amplitude of the peak in the downhole logging HSGR data. This peak was the re-

Figure F40. Hole U1459C diameter (caliper) and HSGR measured by triple combo; NGR from Hole U1459B whole-round cores; and elemental uranium, thorium, and potassium concentrations estimated from Hole U1459C HSGR spectra. gAPI = American Petroleum Institute gamma radiation units.

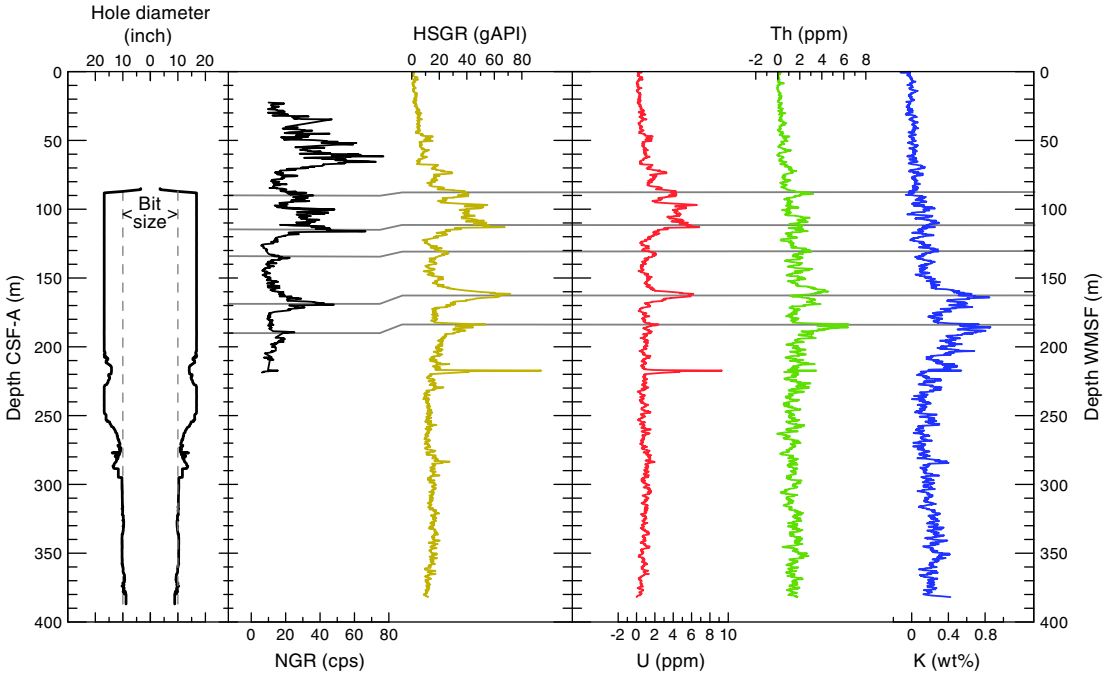

sult of increased concentrations of Th and K and may be consistent with an increase in the input of detrital minerals. These high HSGR values occurred within lithostratigraphic Subunit Vb, which was described as an unlithified dolomitic packstone to grainstone interbedded with lithified fine quartz sand (see **Lithostratigraphy**). In contrast, the prominent narrow HSGR peak at 217 m WMSF was dominated by U and likely indicates a hardground with condensed sedimentation. However, we could not evaluate the sediments that correspond to this peak, as core recovery in this interval (around Cores 356-U1459B-44F and 45F and Cores 356-U1459C-2R, 3R, and 4R) was low.

When distinct peaks and troughs in gamma ray values were correlated between the whole-round core NGR data from Hole U1459B and wireline log HSGR data from Hole U1459C (gray lines on Figure **F40**), the wireline depth was consistently shallower than the cored Hole U1459B CSF-A depth scale. The offset between wireline and coring depth was 2–3 m between 50 and 100 m WMSF, increased slightly to 3–4 m between 100 and 150 m WMSF, and further increased to 7–8 m between 150 and 200 m WMSF.

Magnetic susceptibility

The MS data, as measured during downhole logging with the triple combo, confirmed the increasing trend in susceptibility between 75 and 145 m WMSF, as observed in the data obtained from measuring cores with the WRMSL (Figure **F41**). However, between 145 and 155 m CSF-A, the MS data from Hole U1459B cores show a rapid decrease that is not present in the downhole logging data. In contrast, downhole MS increases gradually with depth between 145 and 210 m WMSF. In this depth interval, there is good correlation in meter- to decimeter-scale variations in the MS data from Hole U1459B cores and wireline logging K concentration data from Hole U1459C. For example, pronounced minima in core-based MS occurred at 158, 182, and 200 m CSF-A and corresponded to minima in K (in weight percent) at 156, 179, and 195 m WMSF in the downhole data. It was unclear why these high-amplitude variations in MS from Hole U1459B cores did not show up in the downhole MS data. In any case, the latter correlations between core-based MS measurements and wireline K estimates are in agreement with the above-reported offset between wireline depth in Hole U1459C and cored depth in Hole U1459B. Between 210 and 275 m WMSF, the downhole logging MS data decrease in two steps. The first step

Figure F41. Hole U1459C diameter (caliper) and MS measured by triple combo, WRMSL MS (blue = Hole U1459A, black = Hole U1459B, red = Hole U1459C), and elemental potassium concentration estimated from Hole U1459C HSGR spectra.

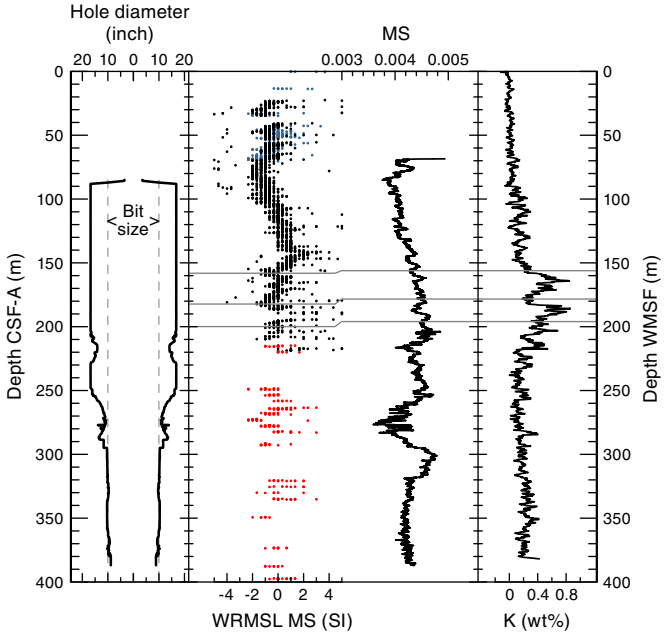

Figure F42. Representative FMS images measured by FMS-sonic, reflecting variations in resistivity through the logged formations, Hole U1459C.

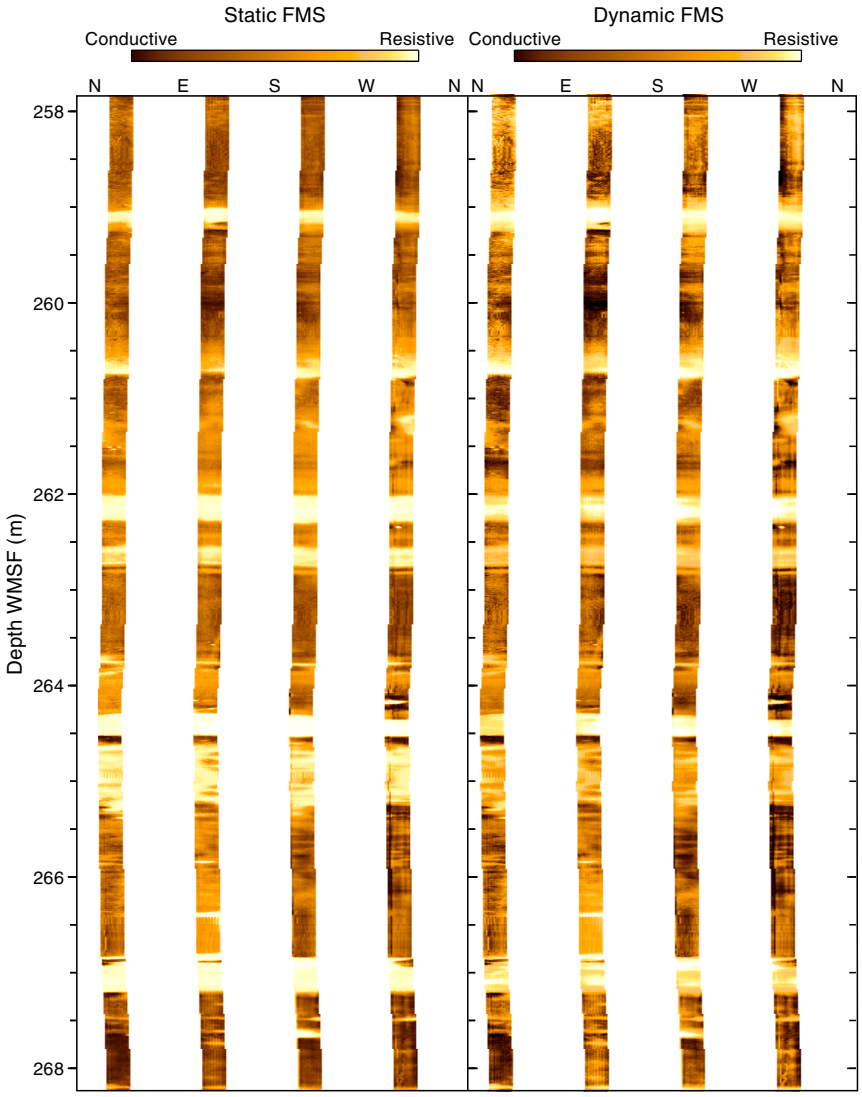

(around 217 m WMSF) corresponds to the prominent thin U peak discussed above (see Figure **F40**). The pronounced minimum in the wireline logging MS data at 276.5 m WMSF corresponds to a minimum in MS data obtained from Section 356-U1459C-16R-1 at 273 m CSF-A. Downhole logging MS values increase between 275 and 300 m WMSF, decrease between 300 and 317 m WMSF, and remain relatively stable between 317 m WMSF and the lowermost data point obtained by wireline logging at 387 m WMSF. The relatively stable MS of sediments in the lowermost ~80 m of Hole U1459C is in agreement with the limited number of data points obtained from cobbles in cores from this interval.

Formation MicroScanner

FMS images reveal differences in textures and lithology through the logged interval of Hole U1459C from about 112 to 286 m WMSF. The FMS images are generally good deeper than about 250 m WMSF, whereas the shallower images are only of intermediate quality. This was true for both the first and second passes, so we relate the differences in quality to the condition of the borehole rather than to the sea state and high heave during logging operations (see **Operations**). Within the small interval of good quality images, we find alternations in resistivity (e.g., Figure **F42**) that may reflect changes in sediment electrical properties related to changes in lithology. The spacing between these alterations ranges from several tens of centimeters to 2 m, with thin (several tens of centimeters) resistive layers embedded within broader, more conductive areas (1–2 m). Often, FMS images are compared against resistivity logs, but no such logs were acquired for this hole. There is no evidence for any dip of the sediment layers, consistent with direct inspection of the cores (see **Lithostratigraphy**).

Sonic imager

Between 100 and 200 m WMSF, sonic velocities measured during downhole wireline logging of Hole U1459C were a few hundred meters per second higher than sonic velocities obtained from discrete measurements with the *P*-wave caliper from Hole U1459B (Figure **F43**). Also, between 175 and 210 m WMSF, the wireline sonic velocities are considerably more variable than the discrete measurements. At 216 m WMSF, wireline sonic velocities peaked at 3228 m/s. This observation is in agreement with the discrete *P*-wave velocity measurements made on a lithified dolomitic cobble from Section 356-U1459C-4R-1 (215.34 m CSF-A). Reported sonic ve-

Figure F43. Hole U1459C diameter (caliper) measured by FMS-sonic and sonic velocities from Hole U1459B discrete measurements and Hole U1459C wireline.

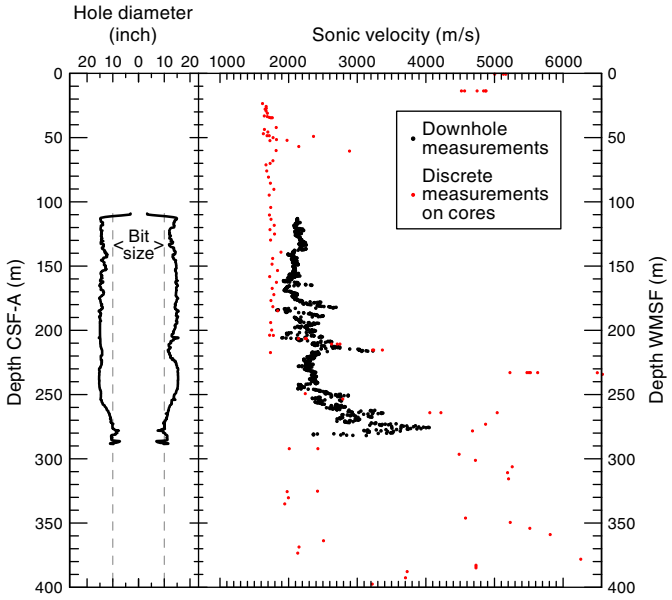

locities for this cobble were 3366, 3224, and 3239 m/s in the *x*-, *y*-, and *z*-directions, respectively (see **Physical properties**). These results suggest that the retrieved dolomitic cobbles can be considered representative of the formation. Between 217 and 245 m WMSF, wireline sonic velocities were relatively constant with values between 2150 and 2400 m/s. In this interval, discrete measurements were only possible on lithified cobbles whose sonic velocities exceeded 5000 m/s. Therefore, these cobbles should not be considered representative of the drilled formations. Between 245 and 275 m WMSF, wireline *P*-wave velocities increase rapidly from 2400 to 4047 m/s and show large variability. Deeper downhole, wireline sonic velocities drop steeply to ~2360 m/s at ~281 m WMSF. Only a handful of discrete *P*-wave measurements from Hole U1459C are available between 245 and 282 m CSF-A, making a detailed comparison impossible. However, the considerable scatter in these discrete measurements is in agreement with the observed variability of wireline sonic velocities.

Stratigraphic correlation

Three holes were cored at Site U1459. The highest recovery occurred in Hole U1459B and the sediments ranged from Late Pleistocene to middle Miocene in age. Unfortunately, recovery in Hole U1459A was not sufficient to allow for either detailed analysis or a high-resolution correlation between Holes U1459A and U1459B. Hole U1459C extended into the Eocene. A natural gamma wireline log was run in Hole U1459C, but the very low recovery did not allow for correlation between Hole U1459C lithology and the wireline log.

Coring at Site U1459 was complicated by the presence of hard intervals within softer lithologies. Penetration of these sediments required the use of the XCB system (see **Operations**). This combination of lithologies was a particular problem in the upper 55 m (Hole U1459A) and lower 200 m (Hole U1459C) and resulted in discontinuous recovery with significant gaps in Holes U1459A and U1459C. Hole U1459B recovery was more successful because the

Table T16. Affine table, Holes U1459A and U1459B and the top of Hole U1459C. **Download table in .csv format.**

Figure F44. Correlation between Holes U1459A and U1459B based on color reflectance b*. Dashed arrows = tie points between cores, black boxes = core recovery, gray boxes = shift required to create as complete a sequence as possible. Gaps in cores limit certainty in correlation; however, the suggested shift (small arrows) may yield continuous sampling. Refer to Table **T16** for a detailed table of correlative depths.

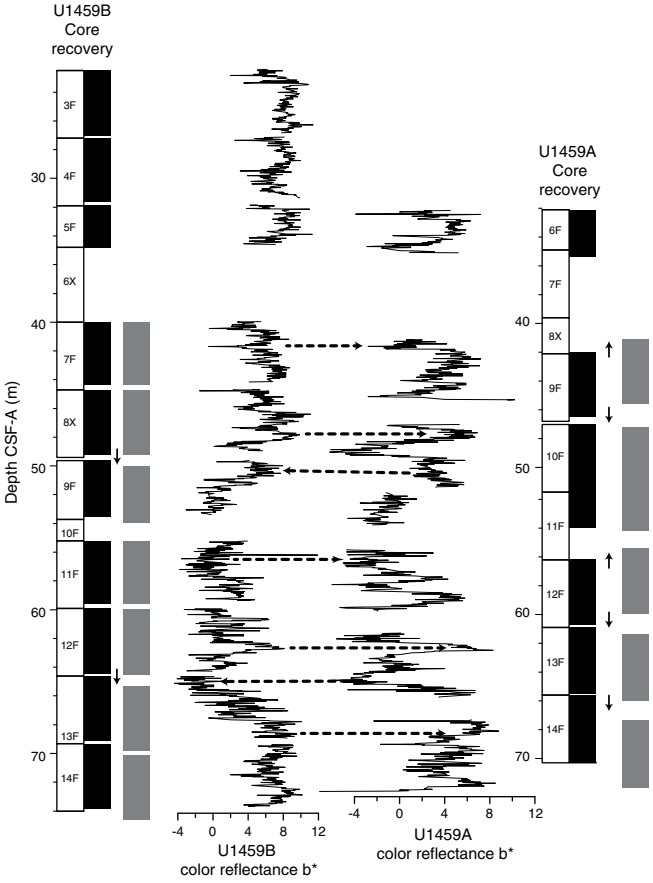

depths of the hard intervals were known and the HLAPC cores were strategically planned to increase core recovery. This strategy did increase core recovery, but the intervals cored with the XCB system still had low or no recovery. Although a correlation was made between Holes U1459B and U1459A using color reflectance b* data (Table **T16**; Figure **F44**), a detailed, complete composite depth scale could not be generated because of the many intervals of zero to very poor recovery. In addition, if the sediments were not completely indurated, some homogenization may have occurred during recovery and handling in those cores with less than full recovery. Therefore, the records presented may not accurately represent in situ lithology, especially in Hole U1459A and the deeper part of Hole U1459B (>170 m CSF-A). Hole U1459C was drilled down to overlap Hole U1459B at 208.6 m CSF-A. Recovery was also low and the dominant lithology recovered in Hole U1459C was chert. The discontinuous recovery in Hole U1459C hindered correlation of the core to the downhole logs.

Integration of physical properties records (b* and NGR) and wireline HSGR data with biostratigraphy and magnetostratigraphy (Figures **F45**, **F46**, **F47**) indicates that the oldest sediments recovered were of Eocene age. Hole U1459A (Cores 356-U1459A-1F

Figure F45. Hole U1459A summary with NGR and color reflectance b*. Age-depth model was produced from biostratigraphic datums (dashed lines = uncertainties in datum positions) (see **Biostratigraphy and micropaleontology**). The actual depth of datums determined in core catchers may be as deep as the maximum advance of the core barrel during drilling of that core or as shallow as the top of the core. See Figure **F7** in the Expedition 356 methods chapter (Gallagher et al., 2017) for lithology key. BF = benthic foraminifer, PF = planktonic foraminifer, NN = calcareous nannofossil. IS = inner shelf, MS = middle shelf.

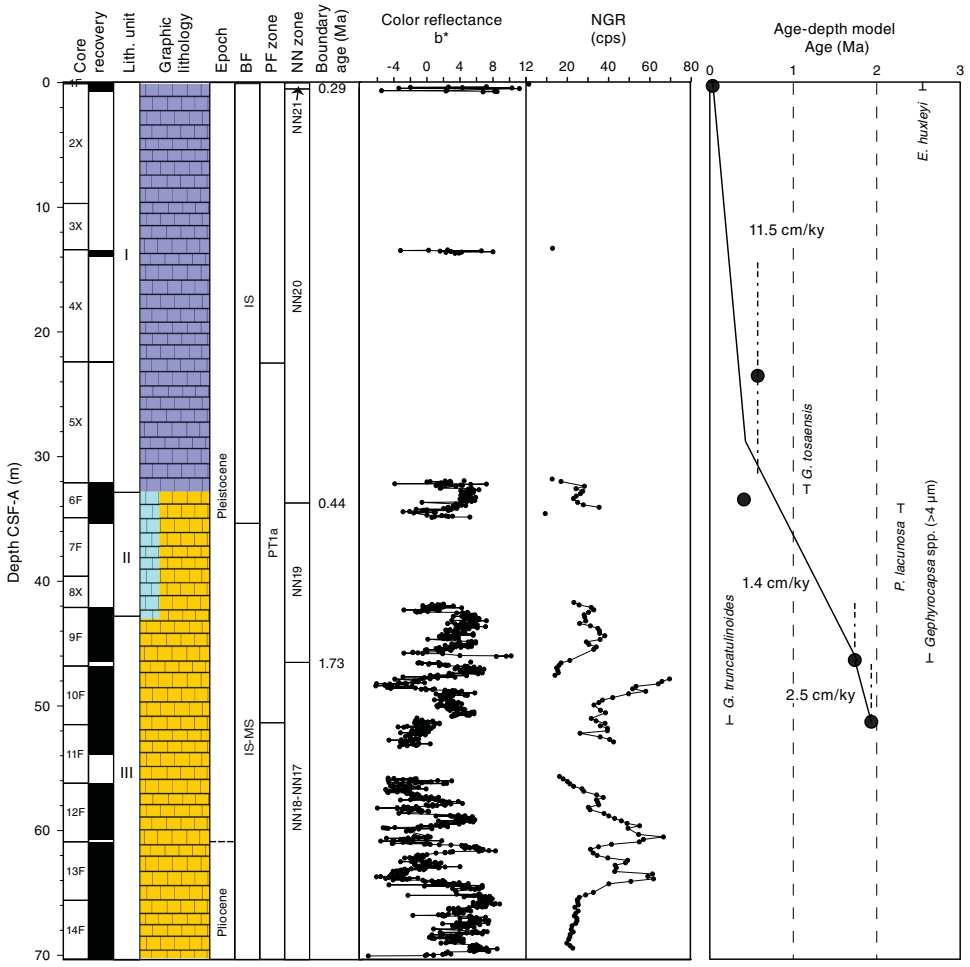

through 14F; 0–70.75 m CSF-A; Table **T2**) was deposited entirely within the Pliocene–Pleistocene, and Hole U1459B extended the record to the middle Miocene. Hole U1459C (Cores 356-U1459C-2R through 42R; 205.80–397.72 m CSF-A; Table **T2**) ranged from the Miocene into the early Eocene. Sedimentation rates are between 0.4 and 1.4 cm/ky in the Paleogene (Figures **F47**, **F48**). Sedimentation rates are relatively low in the Miocene (<1 cm/ky), very high during the middle Pliocene (nearly 15 cm/ky), and >1 cm/ky in the Pleistocene.

Figure F46. Hole U1459B summary with NGR and color reflectance b*. Age-depth model was produced from biostratigraphic datums (see **Biostratigraphy and micropaleontology**). See Figure **F7** in the Expedition 356 methods chapter (Gallagher et al., 2017) for lithology key. OS = outer shelf, UB = upper bathyal.

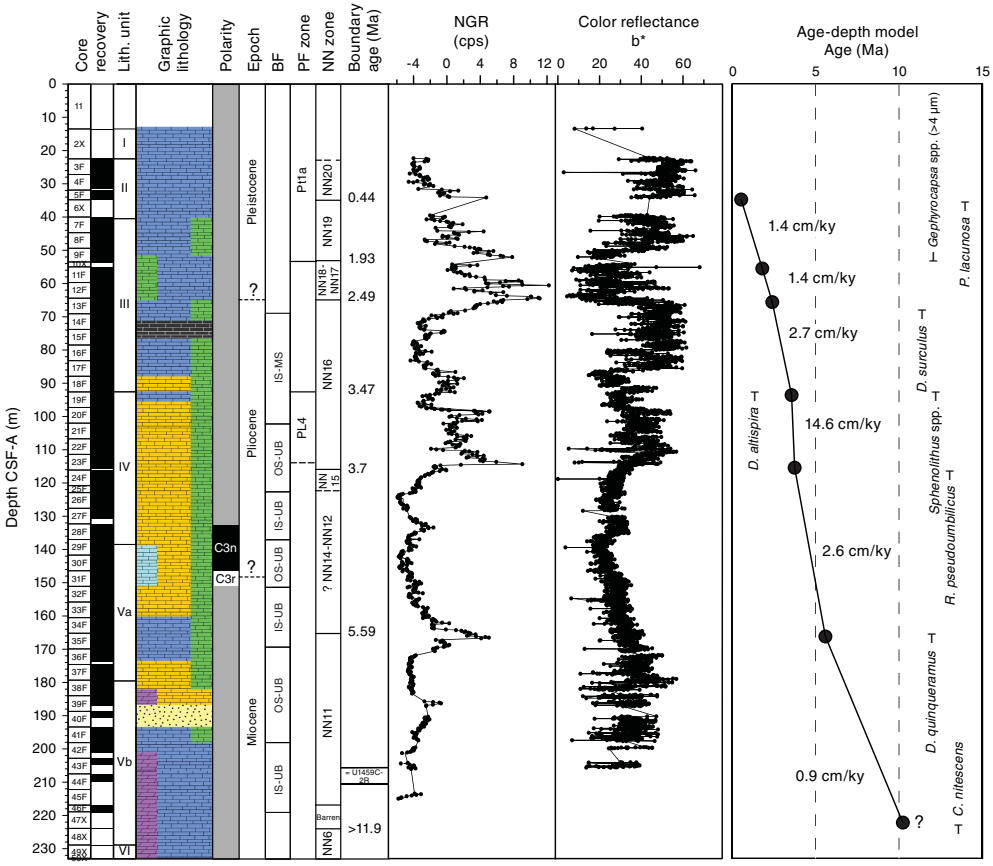

Figure F47. Hole U1459C summary with the HSGR wireline log (note the scale break in this plot). Age-depth model was produced from biostratigraphic datums (dashed lines = uncertainties in datum positions) (see **Biostratigraphy and micropaleontology**). The actual depth of datums determined in core catchers may be as deep as the distance the core barrel advanced while drilling that core or as shallow as the top of the core. See Figure **F7** in the Expedition 356 methods chapter (Gallagher et al., 2017) for lithology key.

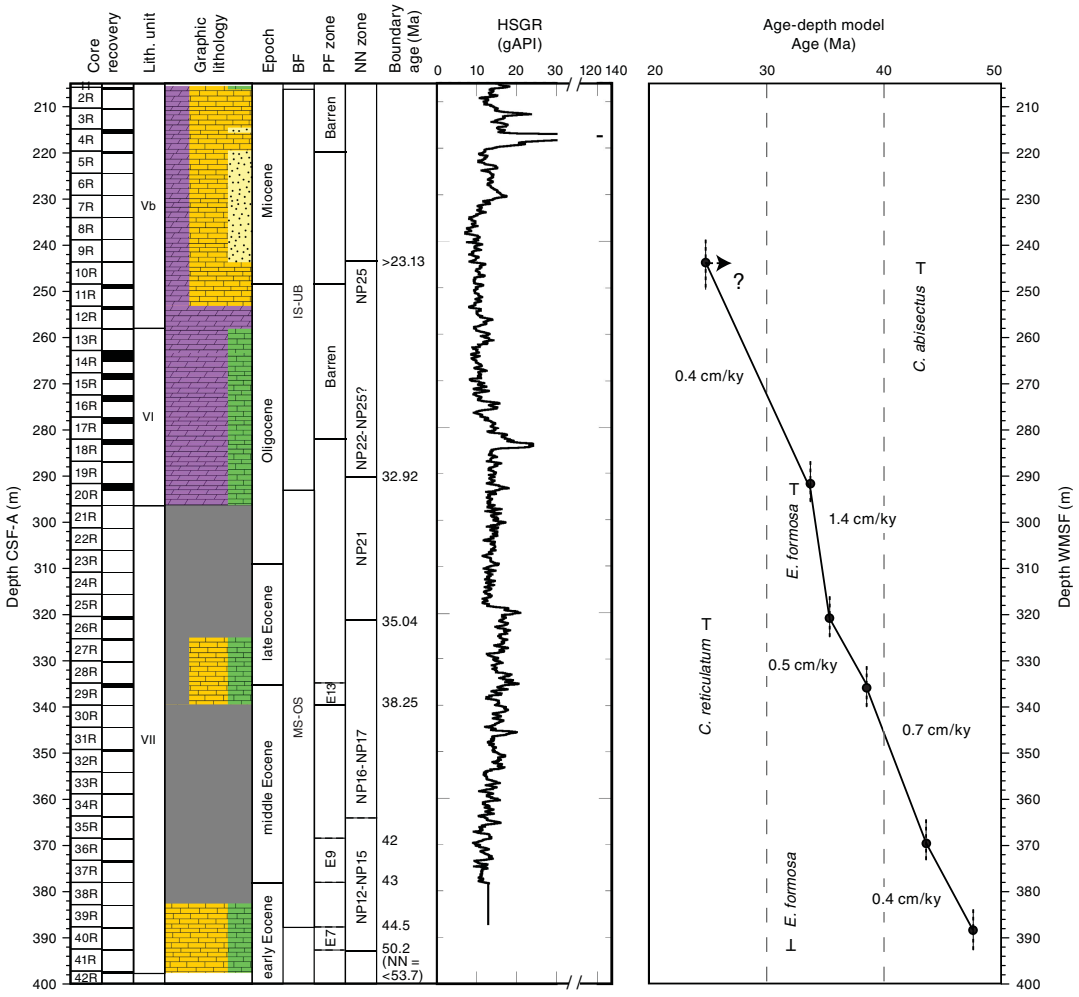

Figure F48. Site U1459 summary with NGR and the HSGR wireline log. Gray bar = approximate pipe depth in Hole U1459C; note the resulting dampened signal of the gamma log in the upper 72 m WMSF. Age-depth model was produced from biostratigraphic datums based on calcareous nannofossils (black = Hole U1459B, blue = Hole U1459C) (see **Biostratigraphy and micropaleontology**). Sedimentation rates are shown for Holes U1459A–U1459C. Basal sedimentation rate for Hole U1459B is extended and calculated based on the uppermost datum in Hole U1459C. See Figure **F7** in the Expedition 356 methods chapter (Gallagher et al., 2017) for lithology key. Benthic foraminiferal assemblages were smoothed to generate this synthesis, resulting in slight differences from data presented in hole summaries.

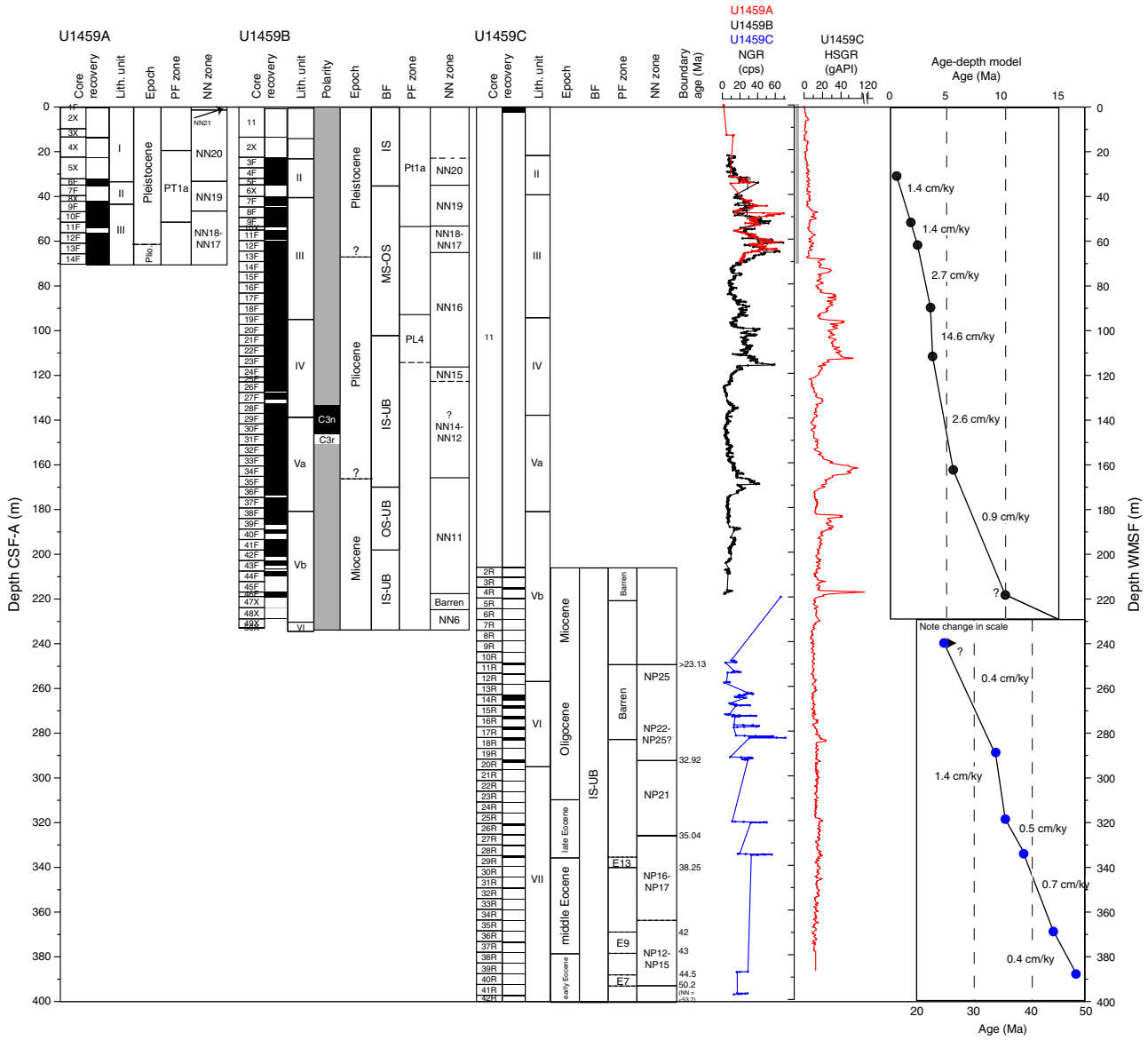

References

Agnini, C., Fornaciari, E. Raffi, I., Catanzariti., R., Pälike, H., Backman, J., and Rio, D., 2014. Biozonation and biochronology of Paleogene calcareous nannofossils from low and middle latitudes. *Newsletters on Stratigraphy,* 47(2):131–181. **http://dx.doi.org/10.1127/0078-0421/2014/0042**

Chaisson, W.P., 2003. Vicarious living: Pliocene menardellids between an isthmus and an ice sheet. *Geology,* 31(12):1085–1088. **http://dx.doi.org/10.1130/G19834.1**

Collins, L.B., James, N.P., and Bone, Y., 2014. Carbonate shelf sediments of the western continental margin of Australia. *In* Chiocci, F.L., and Chivas, A.R. (Eds.), *Continental Shelves of the World: Their Evolution During the Last Glacio-Eustatic Cycle.* Memoirs - Geological Society of London, 41:255–272. **http://dx.doi.org/10.1144/M41.19**

Collins, L.B., and Testa, V., 2010. Quaternary development of resilient reefs on the subsiding Kimberley continental margin, northwest Australia. *Brazilian Journal of Oceanography,* 58(SPE1):67–77. **http://dx.doi.org/10.1590/S1679-87592010000500007**

Gallagher, S.J., Fulthorpe, C.S., Bogus, K., Auer, G., Baranwal, S., Castañeda, I.S., Christensen, B.A., De Vleeschouwer, D., Franco, D.R., Groeneveld, J., Gurnis, M., Haller, C., He, Y., Henderiks, J., Himmler, T., Ishiwa, T., Iwatani, H., Jatiningrum, R.S., Kominz, M.A., Korpanty, C.A., Lee, E.Y., Levin, E., Mamo, B.L., McGregor, H.V., McHugh, C.M., Petrick, B.F., Potts, D.C., Rastegar Lari, A., Renema, W., Reuning, L., Takayanagi, H., and Zhang, W., 2017. Expedition 356 methods. *In* Gallagher, S.J., Fulthorpe, C.S., Bogus, K., and the Expedition 356 Scientists, *Indonesian Throughflow.* Proceedings of the International Ocean Discovery Program, 356: College Station, TX (International Ocean Discovery Program). **http://dx.doi.org/10.14379/iodp.proc.356.102.2017**

Gee, J., Staudigel, H., and Tauxe, L., 1989. Contribution of induced magnetization to magnetization of seamounts. *Nature,* 342(6246):170–173. **http://dx.doi.org/10.1038/342170a0**

Gradstein, F.M., Ogg, J.G., Schmitz, M.D., and Ogg, G.M. (Eds.), 2012. *The Geological Time Scale 2012:* Amsterdam (Elsevier).

James, N.P., Collins, L.B., Bone, Y., and Hallock, P., 1999. Subtropical carbonates in a temperate realm; modern sediments on the southwest Australian shelf. *Journal of Sedimentary Research,* 69(6):1297–1321. **http://dx.doi.org/10.2110/jsr.69.1297**

Kruiver, P.P., Dekkers, M.J., and Heslop, D., 2001. Quantification of magnetic coercivity components by the analysis of acquisition curves of isothermal remanent magnetization. *Earth and Planetary Science Letters,* 189(3–4):269–276. **http://dx.doi.org/10.1016/S0012-821X(01)00367-3**

Lumsden, D.N., 1979. Discrepancy between thin section and X-ray estimates of dolomite in limestone. *Journal of Sedimentary Petrology,* 49(2):429–436. **http://dx.doi.org/10.1306/212F7761-2B24-11D7-8648000102C1865D**

Moore, G.F., Billman, H.G., Hehanussa, P.E., and Karig, D.E., 1980. Sedimentology and paleobathymetry of Neogene trench-slope deposits, Nias Island, Indonesia. *Journal of Geology,* 88(2):161–180. **http://dx.doi.org/10.1086/628489**

Pearson, P.N., Olsson, R.K., Hemleben, C., Huber, B.T., and Berggren, W.A., 2006. Atlas of Eocene planktonic foraminifera. *Special Publication - Cushman Foundation for Foraminiferal Research,* 41.

Perch-Nielsen, K., 1985. Cenozoic calcareous nannofossils. *In* Bolli, H.M., Saunders, J.B., and Perch-Nielsen, K. (Eds.), *Plankton Stratigraphy:* Cambridge, United Kingdom (Cambridge University Press), 427–554.

Peters, C., and Thompson, R., 1998. Magnetic identification of selected natural iron oxides and sulphides. *Journal of Magnetism and Magnetic Materials,* 183(3):365–374. **http://dx.doi.org/10.1016/S0304-8853(97)01097-4**

Robertson, D.J., and France, D.E., 1994. Discrimination of remanence-carrying minerals in mixtures, using isothermal remanent magnetisation acquisition curves. *Physics of the Earth and Planetary Interiors,* 82(3–4):223–234. **http://dx.doi.org/10.1016/0031-9201(94)90074-4**

Shackleton, N.J., Baldauf, J.G., Flores, J.-A., Iwai, M., Moore, T.C., Jr., Raffi, I., and Vincent, E., 1995. Biostratigraphic summary for Leg 138. *In* Pisias, N.G., Mayer, L.A., Janecek, T.R., Palmer-Julson, A., and van Andel, T.H. (Eds.), *Proceedings of the Ocean Drilling Program, Scientific Results,* 138: College Station, TX (Ocean Drilling Program), 517–536. **http://dx.doi.org/10.2973/odp.proc.sr.138.127.1995**

van Hinsbergen, D.J.J., Kouwenhoven, T.J., and van der Zwaan, G.J., 2005. Paleobathymetry in the backstripping procedure: correction for oxygenation effects on depth estimates. *Palaeogeography, Palaeoclimatology, Palaeoecology,* 221(3–4):245–265. **http://dx.doi.org/10.1016/j.palaeo.2005.02.013**

Wade, B.S., Berggren, W.A., and Olsson, R.K., 2007. The biostratigraphy and paleobiology of Oligocene planktonic foraminifera from the equatorial Pacific Ocean (ODP Site 1218). *Marine Micropaleontology*, 62(3):167–179. **http://dx.doi.org/10.1016/j.marmicro.2006.08.005**